Structure/Function of Calmodulin Mutants bound to target peptides from Nitric Oxide Synthase

by

Michael Piazza

A thesis
presented to the University of Waterloo
in fulfillment of the
thesis requirement for the degree of
Master of Science
in
Chemistry

Waterloo, Ontario, Canada, 2011

AUTHOR'S DECLARATION

I hereby declare that I am the sole author of this thesis. This is a true copy of the thesis, including any required final revisions, as accepted by my examiners.

I understand that my thesis may be made electronically available to the public.

Michael Piazza

Abstract

Calmodulin (CaM) is a ubiquitous calcium binding protein that responds to intracellular Ca^{2+} and is proposed to be involved in the binding of over 300 functionally and structurally diverse proteins. It is a highly conserved eukaryotic protein comprised of an N- and C- terminal lobe separated by a highly flexible central linker region. Each of these lobes contains two EF hand motifs that are each capable of binding to one Ca^{2+}-ion. CaM is found to exist primarily in two states: the Ca^{2+} bound form, holo-CaM, or the Ca^{2+} free form, apo-CaM. Both forms of CaM are able to bind to target proteins. CaM also undergoes post translational modifications that play a role in its regulation of target proteins.

One of these important target proteins is nitric oxide synthase (NOS). NOS catalyzes the conversion of L-arginine to L-citrulline and nitric oxide ($\cdot$NO). There are three isoforms of NOS found in mammalian cells: endothelial (eNOS); neuronal (nNOS); and inducible (iNOS) nitric oxide synthases. All three isoforms of NOS are comprised of an N-terminal heme domain and a C-terminal flavin-binding domain containing FAD-, FMN-, and NADPH- binding sites, linked together by a CaM-binding region. The nNOS and eNOS isoforms are constitutively expressed and are Ca^{2+}-CaM-dependent. In contrast, iNOS is regulated at the transcriptional level and is classified as Ca^{2+}-independent. The exact mechanism of how CaM activates NOS is not fully understood. Studies have shown CaM to act like a switch that causes a conformational change in NOS to allow for the electron transfer between the reductase and oxygenase domains through a process that is thought to be highly dynamic.

This study is focused on the structure and function of CaM and CaM mutant constructs bound to the target peptides of the NOS CaM-binding region. The structural dynamics were monitored by nuclear magnetic resonance (NMR) spectroscopy. NMR spectroscopy is an efficient method for studying the dynamics and structures of protein-protein and protein-peptide complexes. The investigation of CaM bound to the CaM-binding region of the inducible nitric oxide synthase (iNOS)

isoform of NOS proved to be difficult due to the propensity of the iNOS CaM-binding domain to aggregate when not bound to CaM. In the present study, an isotopically labeled peptide of the CaM-binding region of iNOS has successfully been expressed, purified and characterized by NMR spectroscopy. These results demonstrate an efficient approach for the expression and purification of individually stable isotope labeled protein complexes for NMR analysis, even if one partner is prone to aggregation or has very low solubility.

The solution structures of CaM bound to the iNOS and eNOS CaM-binding region peptides were determined. In addition, the effect of CaM phosphorylation was investigated. The tyrosine 99 (Y99) residue of CaM is reported to be phosphorylated *in vivo*. In the present study, a phosphomimetic Y99E CaM was produced to investigate the structural and functional effects that the phosphorylation of this residue may have on nitric oxide production. All three mammalian NOS isoforms were included in the investigation. Our results show that a phosphomimetic Y99E CaM significantly reduces maximal synthase activity of eNOS by 40 % while having little effect on nNOS and iNOS activity. A comparative NMR study between phosphomimetic Y99E CaM and wild type CaM bound to the eNOS CaM-binding region peptide was performed. This investigation provides important insights into the effects that CaM phosphorylation has upon the binding and activation of the NOS enzymes.

Acknowledgements

I would like to thank my supervisors Dr. Thorsten Dieckmann and Dr. Guy Guillemette for all their guidance, support and encouragement during my studies at UW. I am grateful for the leadership and knowledge they provided me and for the experience to be able to work with them.

I would also like to thank my committee member, Dr. Elizabeth Meiering, for reading and reviewing my thesis, and for her input in my studies.

Great thanks go to my lab mates: Jason Da Costa, Valentina Taiakina, Kathryn Futrega, Malcolm Robb, and Erica Lee for making the lab a fun and enjoyable place to work. And thank you to my friends in the department, who have supported me through my studies and helped make this an amazing experience.

Special thanks go to my family and friends, who have been very supportive of me throughout my studies. Even though you guys would always regret asking me how my research was going, I appreciate you trying to understand what I have been doing.

Dedication

To my family,

for your love and support throughout my studies

Table of Contents

List of Figures

List of Tables

List of Abbreviations

AI loop	Autoinhibitory loop
apo-CaM	Calcium free calmodulin
BMRB	Biological Magnetic Resonance Bank
CaM	Calmodulin
CaM12	N-terminal Ca^{2+}-deficient CaM
CaM1234	Ca^{2+}-deficient CaM
CaM34	C-terminal Ca^{2+}-deficient CaM
CaM-eNOS	CaM-eNOS CaM binding domain peptide complex
CaM-iNOS	CaM-iNOS CaM binding domain peptide complex
CKII	Casein kinase II
cNOS	Constitutive nitric oxide synthase
eNOS	Endothelial nitric oxide synthase
FAD	Flavin adenine dinucleotide
FMN	Flavin mononucleotide
FRET	Fluorescence resonance energy transfer
H_4B	Tetrahydrobiopterin
holo-CaM	Calcium bound calmodulin
HSQC	Heteronuclear single quantum correlation
iNOS	Inducible nitric oxide synthase
mRNA	Messenger RNA
NMR	Nuclear magnetic resonance
·NO	Nitric oxide
nNOS	Neuronal nitric oxide synthase
NOE	Nuclear Overhauser enhancement
NOESY	Nuclear Overhauser effect spectroscopy
NOS	Nitric oxide synthase
RF	Radiofrequency
SPR	Surface plasmon resonance
TOCSY	Total Correlation Spectroscopy
TPK-III	Tyrosine protein kinase III

Chapter 1

Literature Review

1.1 Introduction

Calcium (Ca^{2+}) acts as an intracellular secondary messenger that relays information within cells to regulate their activity. Intracellular Ca^{2+} can be derived from external sources outside of the cell by passing through various channels spanning the plasma membrane, or from internal sources by being released from Ca^{2+} stores in the endoplasmic or sarcoplasmic reticulum. Intracellular Ca^{2+} concentrations regulate multiple cellular processes such as fertilization, cell proliferation, muscle contraction, neuron transmission, and cell death (Berridge *et al.*, 1998). These functions are regulated by a group of proteins that respond to increases in intracellular Ca^{2+}. Many of these proteins contain a Ca^{2+}-binding motif, called an EF hand (Figure 1.1), which consists of a helix-loop-helix structure with Ca^{2+} binding occurring in the loop region.

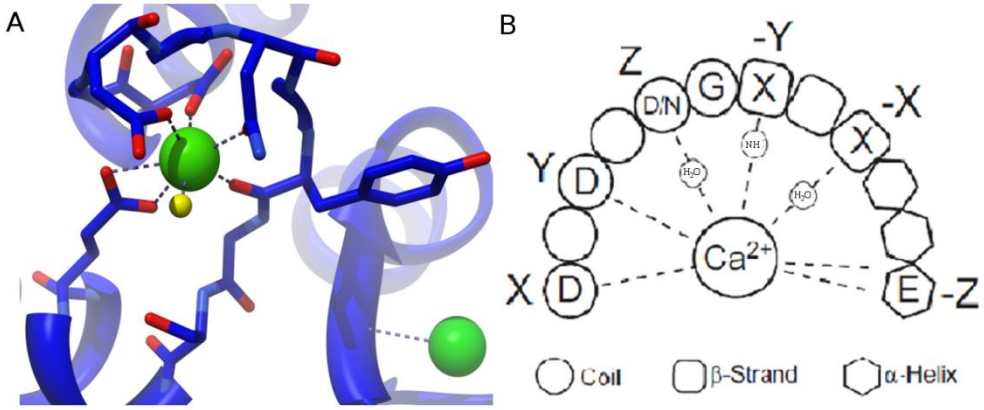

Figure 1.1Ca^{2+}-binding EF hand motif showing Ca^{2+} co-ordination.

(A) Stick representation of Ca^{2+} co-ordination by the EF hand III of CaM. The pentagonal bipyramidal co-ordination of the Ca^{2+} ion and oxygen atoms used to stabilize the ligand co-ordination of Ca^{2+} are represented by pink lines. The oxygen atoms, Ca^{2+} ion, and co-ordinating water are shown in red, green and yellow, respectively. (B) Consensus Ca^{2+}-binding loop for CaM's 4 EF hand motifs. This shows the 1-3-5-7-9-12 position pattern of the co-ordinating amino acids, *X*, *Y*, *Z*, -X, -Y and -Z, in the pentagonal bipyramdial co-ordination binding of Ca^{2+} (Xiong *et al.*, 2010). (A) Modified from PDB 3CLN (Babu *et al.*, 1988) using UCSF Chimera 1.5.3.

An important Ca^{2+}-binding protein that contains these EF hand motifs is calmodulin (CaM). Each EF hand motif of CaM consists of 12 amino acids, rich in aspartate residues, as shown in Figure 1.1B, which adopt a coil structure between positions 1-6, a short β strand between 7-9, and an α-helix between 10-12. Ca^{2+} is coordinated through 7 oxygen ligands from six residues in the 1-3-5-7-9-12 positions (Figure 1.1). This results in a pentagonal bipyramidal co-ordination of Ca^{2+} (Babu *et al.* 1988). EF hand motifs are also found in pairs, with the two loops interacting via two antiparallel β-sheet hydrogen bonds. They pack with their central core consisting of hydrophobic residues and their solvent-exposed faces consisting of charged, hydrophilic residues (Strynadka and James, 1989).

1.1.1 Overview of CaM

CaM is a ubiquitous, multifunctional protein, consisting of 148 amino acids and having a molecular weight of 16.7 kDa. It is a highly conserved protein that functions as a cytosolic Ca^{2+} receptor in response to varied intracellular signals in almost all eukaryotic cells. CaM is found to have 100% sequence homology in vertebrates, although it is coded for by three genes, CaM I, CaM II, and CaM III, which are transcribed into eight mRNAs (Chien and Dawid, 1983; Ikura and Ames, 2006). These different CaM mRNAs are targeted to different cellular domains where local protein synthesis occurs, indicating that mRNA translocation, not the CaM protein, is responsible for local CaM pools in the different intracellular compartments (Palfi *et al*., 2002; Kortvely and Gulya, 2004). CaM is also found in other organisms such as plants, fungi and protozoa and is found to be highly conserved (Friedberg, 1990).

1.1.2 Structure of CaM

CaM is a small, highly acidic protein (pI approximately 4.6), consisting of N- and C-terminal globular domains connected by a flexible central linker. Each of these two domains contains two EF hand motifs, resulting in the ability to bind a total of four Ca^{2+} ions (Crouch and Klee, 1980; Perret *et al.*,

1988). The EF hands of the C-terminal domain (K_d~10^{-6}M) have a 10-fold higher affinity for Ca^{2+} than the EF hands of the N-terminal domain (K_d~10^{-5}M), with cooperative binding within each domain (Crouch and Klee, 1980; Martin *et al.*, 1985). The order of Ca^{2+}-binding to CaM has been shown to be (1) EF hand III, (2) EF hand IV, (3) EF hand I, and (4) EF hand II, with the Ca^{2+} ions dissociating in the reverse order (Kilhoffer *et al.*, 1992). Even though CaM could potentially exist in various Ca^{2+} bound states, it is primarily found in two states: fully Ca^{2+}-free state, apo-CaM; and fully Ca^{2+}-bound state, holo-CaM. Examples of these conformational states can be seen in Figure 1.2.

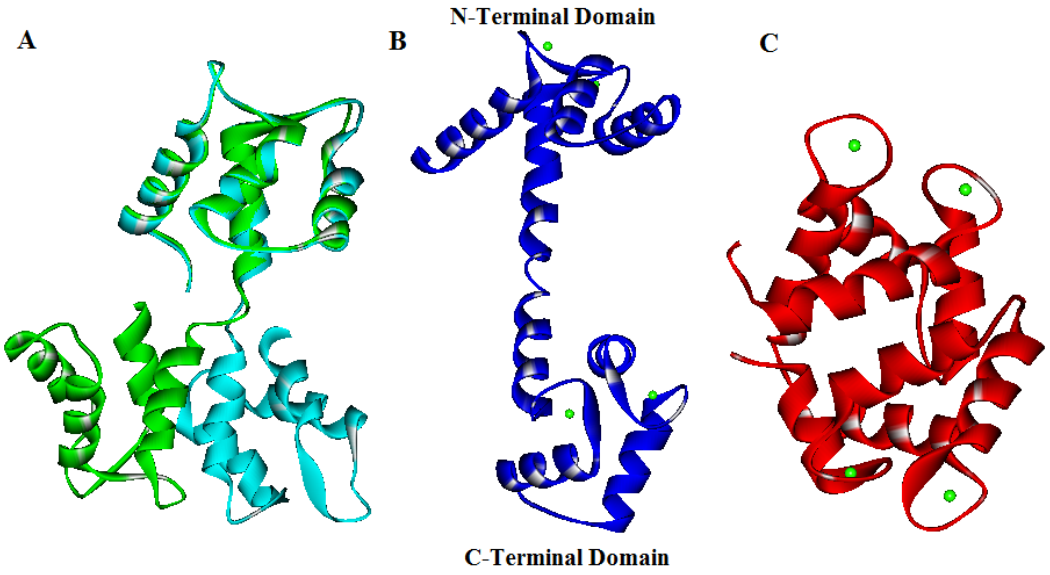

Figure 1.2:Structure comparison of CaM in it Ca^{2+}-free (apo) and Ca^{2+}-bound (holo) conformational states.

(A) Apo-CaM (Kuboniwa *et al.*, 1995), showing highly mobile C-terminal domain, (B) Holo-CaM (Babu *et al.*, 1988), and (C) holo-CaM in a compact conformation (Fallon and Quiocho, 2003). The structure for apo-CaM was solved by NMR, while the other two structures were solved using x-ray crystallography. The N- and C-terminal domains of CaM are indicated. Ca^{2+} ions are shown in green. Models were derived from PDB 1CFD and 1CFC (apo-CaM), 3CLN (holo-CaM), and 1PRW (compact holo-CaM), respectively, and were visualized using Accelrys DS visualize v2.5.5.

The N-terminal domain of CaM is comprised of residues 1-75 and the C-terminal domain is comprised of residues 82-148, with residues 76-81 corresponding to the flexible central linker. The secondary structure of CaM is essentially the same in the apo and holo-forms; however, there are

differences in helix packing. Apo-CaM has a more compact structure than holo-CaM, with each domain consisting of four tightly packed antiparallel α-helices. Also its C-terminal domain is much more dynamic than its N-terminal domain. Although these helices are packed tighter in the apo form compared to the holo form of CaM, they have been found to be much more mobile, with Ca^{2+} binding dramatically reducing their flexibility (Zhang *et al.*, 1995).

Upon Ca^{2+} binding, the two globular domains of CaM rotate outwards, increasing the distance between them, thus changing the more compact shape of apo-CaM to the more extended dumbbell shape of holo-CaM (Yamniuk and Vogel, 2004). The EF hands also undergo a structural rearrangement, consisting of the antiparallel packing of the α-helices shifting to a perpendicular packing. This allows the negatively charged side chains to coordinate the Ca^{2+} ion, resulting in a hydrophobic pocket being present on the surface of each domain, which is not present in the apo-CaM conformation (Kuboniwa *et al.*, 1995, Zhang *et al.*, 1995). These large hydrophobic patches exposed in holo-CaM are rich in methionine residues, with four being found in each domain and one in the central linker, contributing 46% of the total hydrophobic surface area (Zhang *et al.*, 1995). These 9 methionines comprise 6% of the amino acid content of CaM, which is much greater than the 1% methionine content average in known proteomes (Ikura and Ames, 2006). This high abundance of methionine residues is thought to play an important role in target recognition because of the high polarizability of the methionine sulphur atom and the ability of the long flexible side chains to allow them to be highly conformationally adaptable (Gellman, 1991). The central linker region of holo-CaM, which was thought to be a long rigid α-helix from crystal structures, is also found to be highly flexible and can be bent which allows for the orientation of the N- and C-terminal domains to change independently of each other to accommodate the binding of different target proteins (Persechini and Kretsinger, 1988).

1.1.3 CaM binding to Target Proteins

CaM has been proposed to bind to over 300 target proteins through the use of protein databases recognizing CaM binding motifs (Shen *et al.*, 2005; Ikura and Ames, 2006). This analysis involves the evaluation of a sequence on the basis of its electronic and hydrophobic properties and secondary-structure tendency to identify putative basic amphiphilic α-helical motifs (Yapp *et al.*, 2000). CaM has the ability to bind to target proteins in the apo or holo-forms, thus in a Ca^{2+}-independent or Ca^{2+}-dependent manner.

Target proteins that bind to CaM in a Ca^{2+}-dependent manner generally have a small binding domain of approximately 20 amino acids, which contain a hydrophobic face in contact with CaM and a basic face in contact with solvent and the negatively charged amino acids of CaM's linker region (O'Neil and Degrado, 1990). This basic face also has important electrostatic interactions that involve salt bridges with glutamate residues in CaM's terminal domains (Crivic and Ikura, 1995). These have the tendency to form basic amphiphilic α-helices, containing bulky hydrophobic amino acids (O'Neil and Degrado, 1990). These conserved bulky hydrophobic amino acids are arranged in a 1-8-14, 1-5-8-14 or 1-5-10 motif, where the outer numbers represent the anchoring residues (Rhoads and Friedberg, 1997). These are termed anchoring residues because they bind to the hydrophobic patches in the terminal domains of CaM, allowing the hydrophobic residues between them to interact with the linker region (Afshar et al., 1994).

Target proteins are also able to bind to CaM in a Ca^{2+}-independent manner. These target proteins include those that are only bound to apo-CaM, and those that are tightly bound to CaM in the presence and absence of Ca^{2+} (Rhoads and Friedberg, 1997). These proteins contain the consensus IQ motif which has the general form IQXXXRGXXXR, where X can be any amino acid (Rhoads and

Friedberg, 1997). However this consensus sequence is also found in some Ca^{2+}-dependent proteins (Jurado *et al*., 1999).

CaM is also able to bind to its target proteins in a variety of way (Figure 1.3). The most common binding interaction consists of the N- and C-terminal domains wrapping around the target protein. This binding can be in a parallel or anti-parallel conformation: parallel indicates that the N-terminal lobe of CaM binds towards the N-terminal lobe of the target protein and the C-terminal lobe of CaM binds towards the C-terminal lobe of the target protein; antiparallel indicates that the terminal lobes of CaM bind to the opposite terminal lobes of the target protein (Yamniuk and Vogel, 2004). CaM binding to target proteins can also involve the interaction where CaM itself is wrapped by the target protein or where more than one CaM subunit is required for target binding (Drum *et al.*, 2002; Houdusse *et al.*, 2006).

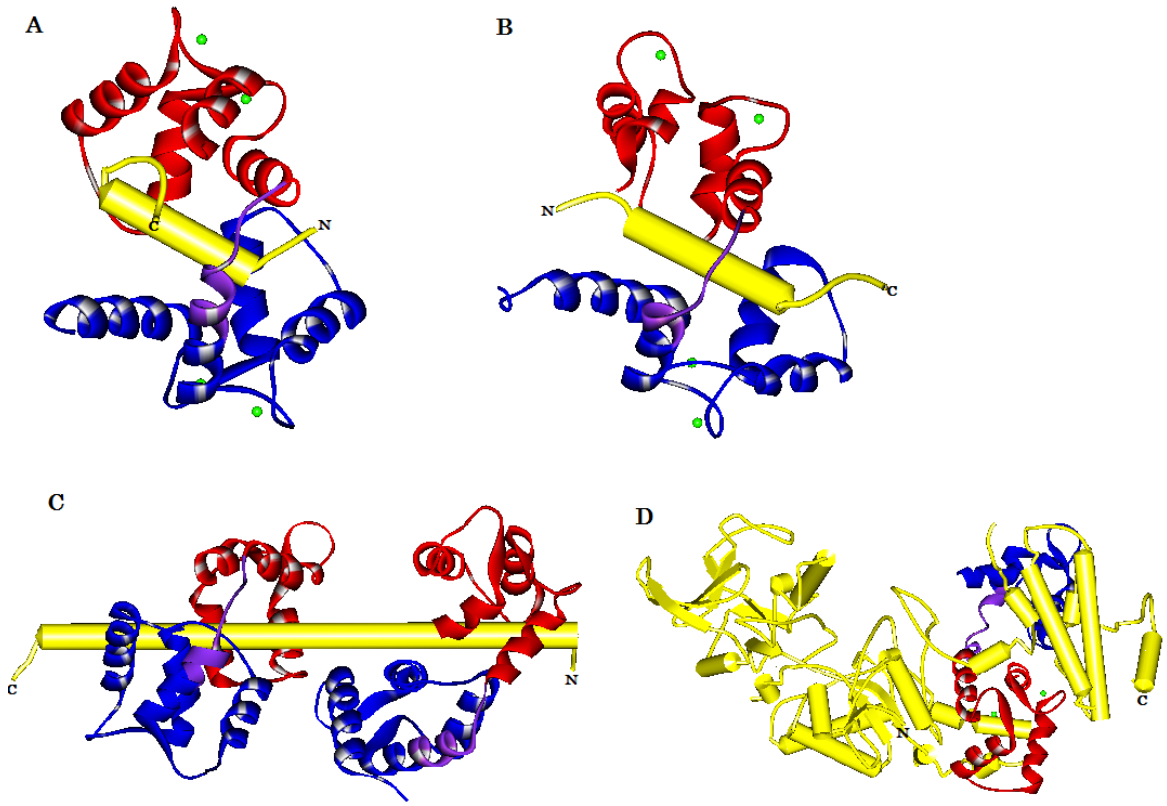

Figure 1.3:Structures of CaM bound to various target proteins in various conformations.

(A) CaM bound to CaM-dependent kinase kinase (CaMKK) in a parallel conformation (Kurokawa *et al.*, 2001). (B) CaM bound to myosin light chain kinase (MLCK) in an anti-parallel conformation (Ikura *et al.*, 1992), (C) two apo-CaMs bound to an unconventional myosin V IQ domain (Houdusse *et al.*, 2006), (D) CaM in complex with the edema factor of adenylyl cyclase of *B. anthracis* (Drum *et al.*, 2002). Models were derived from PDB 1IQ5, 2BBN, 2IX7 and 1K93, respectively, and were visualized using Accelrys DS visualize v2.5.5.

1.1.4 Post-Translational Modifications of CaM

CaM is also found to undergo post-translational modifications that play a role in regulating its activity with target proteins. These modifications include acetylation, trimethylation, carboxylmethylation, proteolytic cleavage, and phosphorylation (Benaim and Villalobo, 2002). The effect of these CaM modifications on different target proteins still remains unclear.

CaM has 18 putative phosphorylatable binding sites, including 4 serine, 12 threonine and 2 tyrosine, with 8 sites (Figure 1.4) being shown to be phosphorylated *in vitro* (Benaim and Villalobo,

2002). Furthermore three of these sites, Thr79, Ser81, and Ser101, have been found to be phosphorylated *in vivo* in rat liver (Quadroni *et al.*, 1994). All of these phosphorylation sites have been found to be phosphorylated by protein-serine/threonine kinases, such as casein kinase II and myosin light-chain kinase, and protein-tyrosine kinases, such as the insulin receptor and the epidermal growth factor receptor (Benaim and Villalobo, 2002).

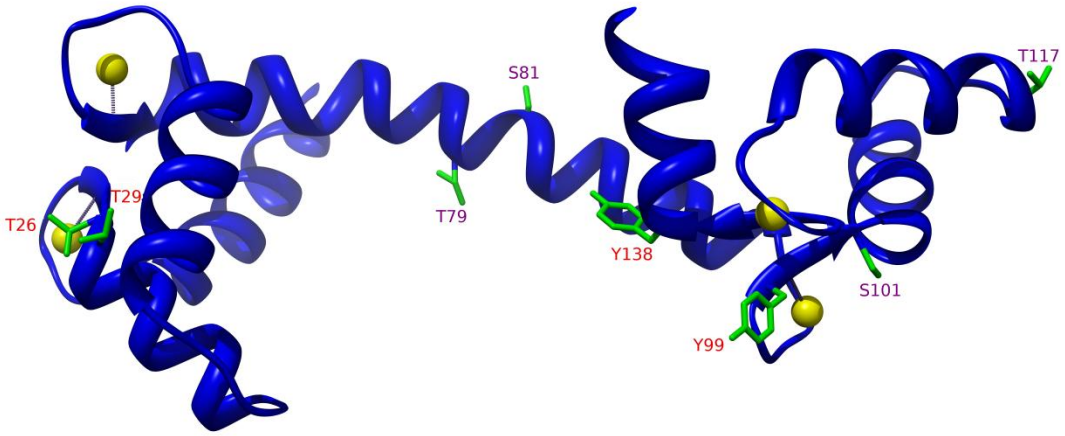

Figure 1.4: Structural representation of known phosphorylation sites in CaM.
There are 8 amino acid sites in CaM know to be phosphorylated by protein-serine/threonine kinases and protein-tyrosine kinases. These are labeled in red and purple. Residues labeled in purple have been found to be phosphorylated *in vivo*. Model was modified from PDB 3CLN and visualized using UCSF Chimera 1.5.3.

The effect of phosphorylated CaM on target proteins has been investigation. A study by Quadroni *et al.* (1998) found that CaM phosphorylated *in vitro* by Casein kinase II (CKII) increased the V_{max} of neuronal nitric oxide synthase (nNOS) 2.6-fold and its activity 2-fold. This group previously showed CK-II is able to phosphorylate CaM at residues Thr79, Ser81and Ser101, but did not determine which one was important for the increase in nNOS activity (Quadroni *et al.*, 1994; Quadroni *et al.*, 1998). A Study by Grief *et al.* (2004) showed that using a phosphomimetic CaM can faithfully mimic the effect of a phosphorylated CaM. Threonine/serine and tyrosine residues of CaM

are substituted with aspartate and glutamate residues, respectively, to create a phosphomimetic mutant. The negative charge of aspartate and glutamate's side chain mimics that of a phosphate ion. This study found that CaM phosphorylated at Ser101 attenuated endothelial NOS (eNOS) activity by 30% (Grief *et al.*, 2004).

Another study has involved the *in vitro* phosphorylation of CaM at Tyr99 by tyrosine protein kinase III (TPK-III) and its interaction with various target peptides. The study by Corti *et al.* (1999) determined that Tyr99-phosphorylated CaM increased the V_{max} of nNOS 3.45-fold and its activity 2.16-fold. They also determined that the binding affinity of Tyr99-phosphorylated CaM was 0.26 times less than that of holo-CaM. Mishra *et al.* (2010) hypothesized that hypoxia-induced phosphorylated CaM at Tyr99 by TPK-III has a higher affinity for nNOS than non-phosphorylated CaM, leading to increased activation of nNOS and increased production of nitric oxide (·NO). The increased tyrosine phosphorylation of CaM at Tyr99 in the cerebral cortex of newborn piglets resulting from hypoxia is mediated by the ·NO derived from nNOS (Mishra *et al.*, 2010).

CaM has been found to be phosphorylated *in vivo* through post-translational modification, and the interactions of phosphorylated CaMs with the NOS isoforms have been investigated. However, there is limited structural or dynamical data known about these CaM mutant interactions. This study provides structural and dynamic information on the interaction of a phosphomimetic CaM with a NOS target peptide.

1.2 Nitric Oxide Synthase (NOS)

Nitric oxide synthase (NOS) catalyzes the conversion of L-arginine to L-citrulline and nitric oxide (·NO) through two monooxygenase reactions. This reaction (Figure 1.5) uses reduced nicotinamide adenine dinucleotide phosphate (NADPH) as the electron donor in the presence of oxygen. ·NO is a

short-lived mediator, which can be induced in a variety of cell types and is essential in many biological functions (Nahrevanian and Dascombe, 2003).

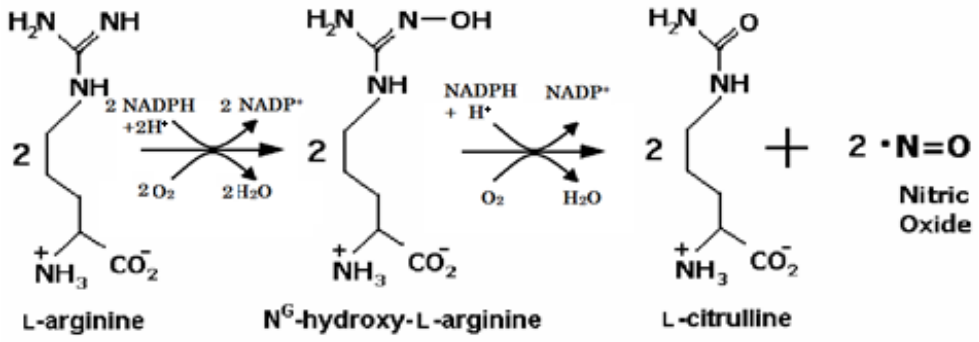

Figure 1.5: Reaction scheme of NOS-catalyzed conversion of L-arginine to L-citrulline and ·NO
Modified from (Alderton *et al.*, 2001).

1.2.1 Isoforms of mammalian NOS

There are three isoforms of NOS in mammals, all of which have different localization and cellular function. The three isoforms are neuronal NOS (nNOS, NOS I), inducible NOS (iNOS, NOS II), and endothelial NOS (eNOS, NOS III). These isoforms have 51-57% sequence homology in humans (Alderton *et al.*, 2001). Each NOS isoform varies in size, with nNOS, eNOS and iNOS having a molecular weight of 165, 133 and 130 kDa, respectively (Zhang *et al.*, 2001). The eNOS and nNOS enzymes have been found to be constitutively expressed and are thus referred to as the constitutive NOS (cNOS) isoforms. They are also found to be activated by increased cellular Ca^{2+}, through binding to holo-CaM and are thus Ca^{2+}-dependent (Roman *et al.*, 2002). In contrast iNOS is regulated at the transcriptional level *in vivo* by cytokines in macrophages and tightly binds CaM at basal levels of Ca^{2+}. Since iNOS binds to CaM regardless of Ca^{2+} concentration it is classified as Ca^{2+}-independent (Cho *et al.*, 1992; Roman *et al.*, 2002).

The NOS enzymes are found to be homo-dimeric proteins, with each monomer containing an N-terminal oxygenase domain and a multidomain C-terminal reductase domain (Figure 1.6). The

oxygenase domain contains binding sites for iron protoporphyrin IX (heme), (6*R*)-5,6,7,8-tetrahydrobiopterin (H_4B), and the substrates L-arginine and molecular oxygen (Alderton *et al.*, 2001). The reductase domain has an autoinhibitory region (only in cNOS isoforms) and binding sites for flavin mononucleotide (FMN), flavin adenine dinucleotide (FAD), and NADPH (Alderton *et al.*, 2001). The two domains are connected by a linker containing a CaM recognition site.

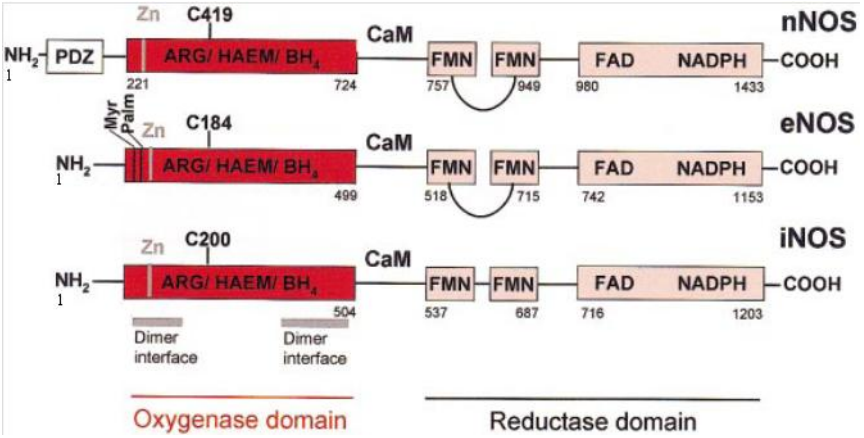

Figure 1.6: Domain structure of NOS isozymes.

The oxygenase and reductase domains are shown in red and pink, respectively. A CaM-binding domain separates the oxygenase and reductase domains. Numbers represent the amino acid residue at the start and end of the oxygenase, FMN, and FAD/NADPH domains. Figure is modified from Alderton *et al.*, 2001.

Currently there are no structures of any of the full isoforms available, however, crystal structures of the individual domains have been determined (Figure 1.7). These include the oxygenase domain of all three isoforms (Li *et al.*, 2001, Matter *et al.*, 2005, Fischmann *et al.*, 1999), the reductase domain of nNOS (Garcin *et al*., 2004), CaM bound to the CaM-binding region of eNOS (Aoyagi *et al*., 2003) and nNOS (Valentine *et al*., 2006), and most recently CaM bound to the CaM-binding region of iNOS (Ng *et al.*, PDB 3GOF) and CaM bound to the FMN domain with the CaM-binding region of iNOS (Xia *et al.*, 2009).

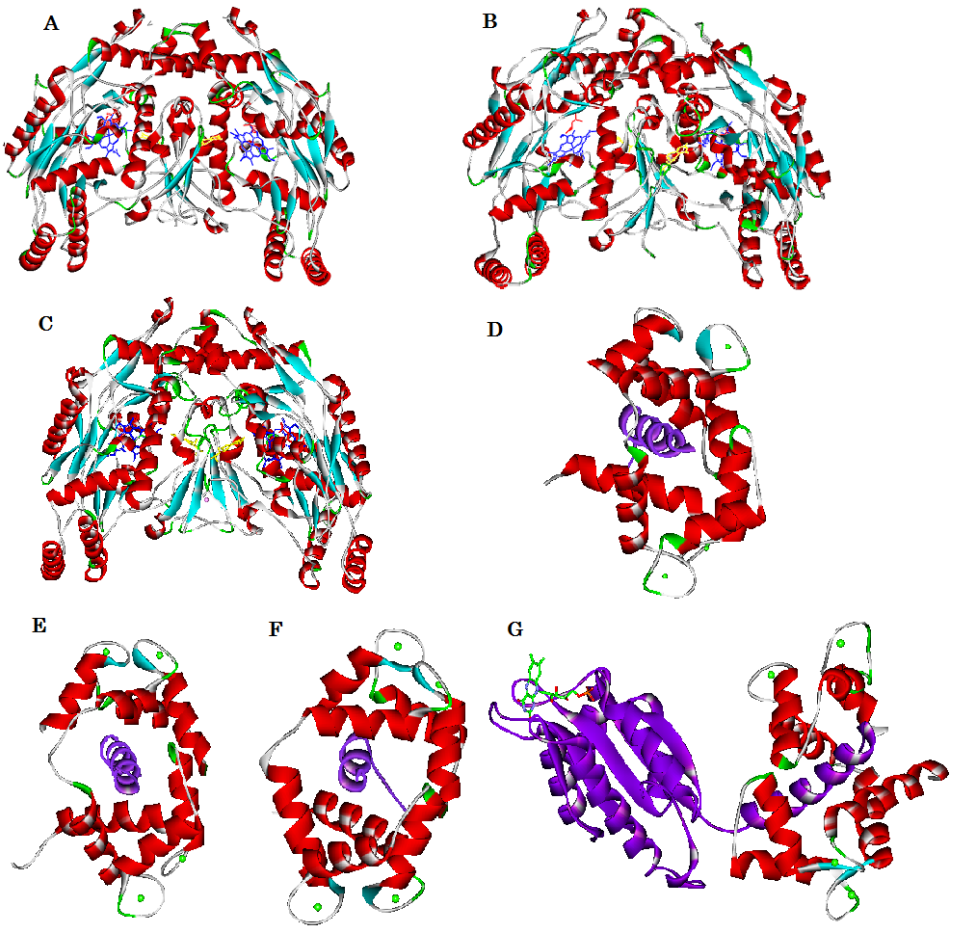

Figure 1.7: Structures of NOS oxygenase domains and NOS CaM-binding regions in complex with holo-CaM.

The crystal structure of (A) eNOS (Li *et al.*, 2001), (B) nNOS (Matter *et al.*, 2005) and (C) iNOS (Fischmann *et al.*, 1999) oxygenase domain dimer. Co-factors heme, H_4B, L-arginine and zinc, shown as blue, yellow and red line structures, and pink ball respectively. The crystal structures of CaM bound to (D) CaM-binding region peptide of eNOS (Aoyagi et al., 2003), (E) CaM-binding region peptide of nNOS (Valentine *et al*., 2006), (F) CaM-binding region peptide of iNOS (Ng *et al*., to be published) and (G) CaM-binding region peptide with FMN domain (Xia *et al.*, 2009). Peptide shown in purple, CaM shown in red and Ca^{2+} shown as green ball. Models were derived from PDB 1FOP, 1ZVL, 4NOS, 2O60, 3GOF and 3HR4, respectively, and were visualized using Accelrys DS visualize v2.5.5.

The crystal structures of the oxygenase domains show that all three isoforms have a similar fold and that the dimer interface contains the heme and a structural zinc ion coordinated by four conserved cysteine residues, two from each monomer, which are involved in dimer stability (Roman

et al., 2002). These structures have also shown the reductase domains of eNOS and nNOS form dimers, stabilized by salt bridges and hydrogen bonding in the interface, whereas iNOS has not been observed to form a dimer in the reductase domain (Roman *et al,*. 2002; Garcin *et al.*, 2004).

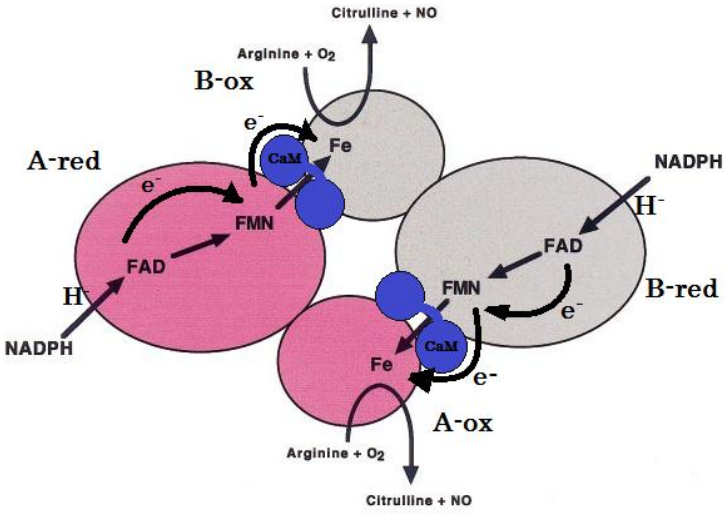

Figure 1.8: Electron transfer within NOS dimer.

The two NOS monomers A and B are shown in pink and grey, respectively. CaM is shown in blue. Electrons are transferred through NADPH-FAD-FMN of the reductase domain of monomer A to the heme (indicated by Fe) in the oxygenase domain of the opposite monomer B. Model is modified from Alderton *et al.*, 2001.

CaM binding to the CaM-recognition linker of the NOS enzymes is required to initiate the electron transfer reaction. This mechanism begins with the transfer of electrons from NADPH to FAD, then from FAD to FMN in the reductase domain, followed by transfer to the heme of the oxygenase domain of the opposite monomer, as shown in Figure 1.8 (Alderton *et al.*, 2001). This electron transfer from FMN to the heme of the opposite oxygenase domain cannot proceed without a subunit realignment and occurrence of conformational changes because the distance between them is 70Å (Garcin *et al.*, 2004). It is thought that CaM binding to the CaM-binding region causes a dynamic process where the FMN domain is allowed to swing back and forth between the FAD and heme, shown in Figure 1.9 (Garcin *et al.*, 2004).

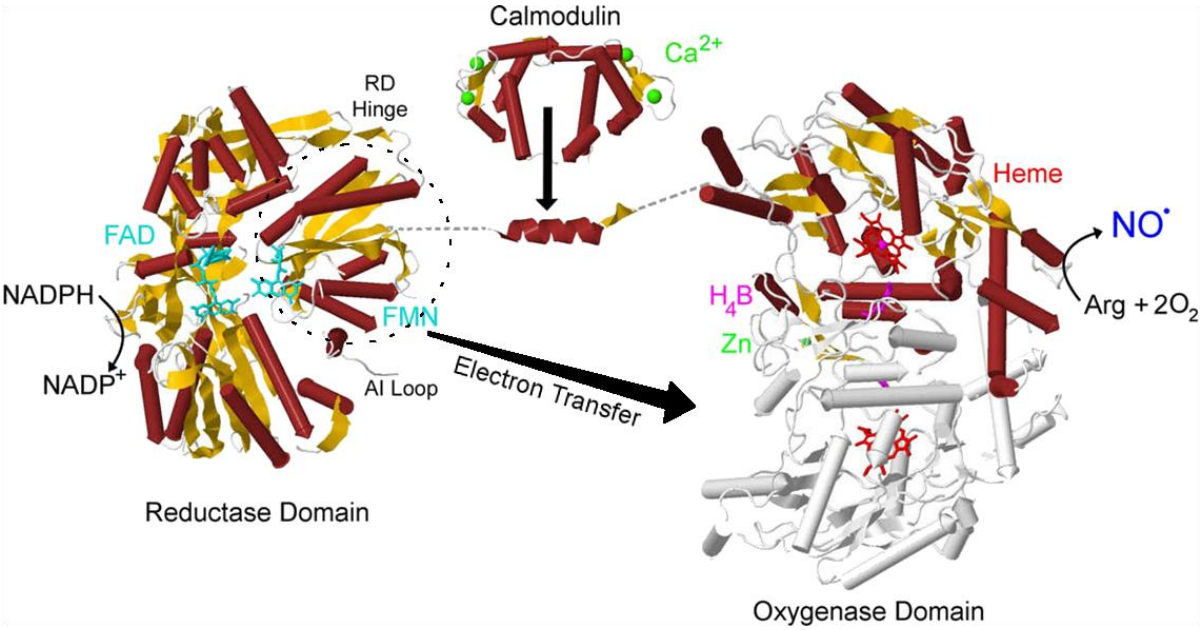

Figure 1.9: Structures of the domains of NOS aligned by amino acid sequence.

Shown is the reductase domain of nNOS (PDB 1TLL), CaM-binding region of eNOS bound with CaM (PDB 1NIW) and the dimeric oxygenase domain of nNOS (PDB 1ZVL). The FMN domain proposed to "swing" between the FAD and heme is circled in black. Figure modified from Daff, 2010.

1.2.2 Regulation of NOS

The cNOS isoforms contain an autoinhibitory (AI) loop and all NOS isoforms contain extended C-terminal tails that act in conjunction with CaM as elements to regulate NOS's activity. The AI loop found in the cNOS enzymes is positioned adjacent to the CaM-binding region and is thought to lock the FMN domain in its electron accepting position and is only displaced upon CaM binding (Salerno *et al.*, 1997; Garcin *et al.*, 2004). When this AI loop was removed from the cNOS isoforms, enzymatic activity increased by a factor of two compared to wild-type, and when it was inserted in the iNOS reductase domain, activity decreased by a third of wild-type (Montgomery *et al.*, 2000; Knudsen *et al.*, 2003). This implicates the AI loop in playing a role in the Ca^{2+} dependency of the cNOS isoforms perhaps by the direct interaction with CaM or the CaM binding site (Jones *et al.* 2004).

The C-terminal domain is thought to play a role in the electron transfer between the flavins, as well as protecting the NOS enzymes from becoming fully oxidized (Roman *et al.*, 2002). All three isoforms have this C-terminal tail, ranging from 21 to 42 amino acids, with nNOS being the longest and iNOS the shortest. Removal of this tail from the NOS isoforms resulted in a great increase in electron flow between the flavins; however, these truncated NOS enzymes became fully oxidized without exhibiting the one-electron semiquinone form of the wild-type enzyme (Roman *et al.*, 2002).

These regulatory elements are responsible for the control of the Ca^{2+} dependency of the NOS isoforms, and the control of electron flow, as well as providing a protective function for NOS. The binding of CaM to cNOS displaces these regulatory elements; however, the absence of this AI loop and the shorter C-terminal tail in iNOS along with the Ca^{2+}-independence of iNOS require further study.

1.2.3 CaM binding to NOS enzymes

CaM binds to NOS at a 1-5-8-14 CaM-binding motif, as shown in Figure 1.10 with the binding region consisting of residues 491-512 of eNOS, 731-752 of nNOS and 501-531 of iNOS (Aoyagi *et al.*, 2003).

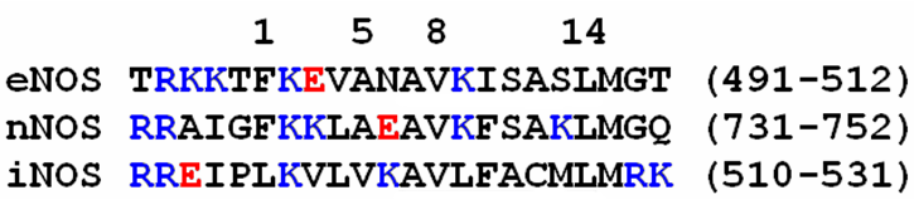

Figure 1.10: Sequence of CaM-binding domains of NOS.

Residues corresponding to the 1-5-8-14 CaM-binding motif are shown. The sequences are for human iNOS , rat nNOs and bovine eNOS. Acidic and basic residues are shown in red and blue, respectively. Figure modified from Aoyagi *et al.*, 2003.

A recent crystal structure shows that the CaM binding region of iNOS forms an α-helix that CaM wraps around, as shown in Figure 1.7 F and G (Xia *et al.*, 2009). Although iNOS displays Ca^{2+}-independent binding, it contains a 1-5-8-14 consensus binding motif of Ca^{2+}-dependent proteins, similar to cNOS, instead of containing the consensus IQ binding motif characteristic of Ca^{2+}-independent proteins, as described in section 1.1.3. However, its sequence differs from nNOS and eNOS by 42% and 30%, respectively, and has a much larger patch of hydrophobic residues in its α-helical conformation that binds with higher affinity to CaM (Aoyagi *et al.*, 2003). Spratt *et al.* (2007) have showed that an iNOS peptide containing the CaM binding region binds to CaM in an antiparallel orientation. Also another study of Spratt *et al.*(2008) using CaM mutants with truncated linker regions showed that the electrostatic interactions of residues 82-87 of CaM are important in binding this iNOS peptide.

The rate constants for the binding of CaM to the NOS target peptides have been determined using several methods and shows that CaM binds to the iNOS peptide with a higher affinity than the cNOS peptides. Vorherr *et al.* (1993) determined that binding of CaM to the nNOS peptide had a dissociation constant, K_d, of 1.8 nM using fluorescence measurements with dansylated CaM. There was no significant fluorescence enhancement found in the absence of Ca^{2+}.

Zoche *et al*, (1996) used surface plasmon resonance (SPR) to investigate the dynamics of CaM binding to the nNOS and iNOS peptides. They determined a K_d of 5.0 nM for nNOS, with an association rate constant, k_a, of 1.58 (+/- 0.44) x 10^5 M^{-1} s^{-1} and a dissociation rate constant, k_d, of 7.87 (+/- 0.64) x 10^{-4} s^{-1}. No binding was observed when excess EDTA was present in the buffer and complete dissociation was achieved by washing with EDTA, indicating Ca^{2+} dependent binding of CaM to the nNOS peptide. However, they found CaM binding to the iNOS peptide occurred in the presence or absence of Ca^{2+} and no dissociation occurred by washing with EDTA. They obtained a k_a

of 3 x 10^4 M^{-1} s^{-1} regardless of the presence or absence of Ca^{2+} and a rough estimate for the k_d of less than 10^{-6} s^{-1}, resulting in a K_d of < 0.1 nM.

Venema *et al*, (1996) used competition assays with nNOS to determine the K_D values of the binding of CaM to the eNOS and iNOS peptides. They estimated a K_d of 4.0 (+/- 1.2) nM for the eNOS peptide and CaM and a K_d of 1.5 (+/- 0.8) nM for the iNOS peptide and CaM.

Wu *et al.* (2011) determined the binding kinetics of Alexa 350 labelled T34C/T110W CaM to the NOS peptides using FRET and stopped-flow spectroscopy. They determined a K_d of 5.6 nM for nNOS, with a k_a of 6.6 (+/- 0.6) x 10^8 M^{-1} s^{-1} and a k_d of 3.7 (+/- 0.1) s^{-1}. The eNOS peptide gave a K_d of 1.6 nM, with a k_a of 2.9 (+/- 0.1) x 10^8 M^{-1} s^{-1} and a k_d of 4.5 (+/- 0.3) s^{-1}. The iNOS peptide gave a K_d of 0.1 nM, with a k_a of 6.1 (+/- 0.1) x 10^8 M^{-1} s^{-1} and a k_d of 0.063 (+/- 0.007) s^{-1}. They found that Ca^{2+} removal did not free CaM from the iNOS peptide, however, that the Ca^{2+}-depleted N- and C-lobes of CaM slowly separated from each other likely due to the conformational rearrangement of apo CaM.

These results show that the cNOS peptides reversibly bind to CaM with nanomolar affinities and suggest that the regulation of cellular Ca^{2+} concentrations modulates this dynamic interaction. However, CaM binding to the iNOS peptide is irreversible, Ca^{2+}-independent and occurs with a higher affinity.

1.3 Research Objectives

The overall research objectives of this study were to obtain a full nuclear magnetic resonance (NMR) assignment of holo-CaM bound to the 24 amino acid iNOS CaM-binding region for use in investigating the dynamic properties of CaM when bound to the three mammalian NOS isozymes. Recently there has been a crystal structure determined for holo-CaM bound to the FMN domain and the CaM-binding region of iNOS; however, obtaining the NMR structure of the CaM-iNOS CaM

binding region peptide complex allowed the investigation of the dynamic properties of this complex and those of other mutant CaM to be accomplished. The data obtained in this study was the crucial first step in using NMR for studying the structural dynamics of holo-CaM, and other mutant CaM, with the NOS peptides. The complete assignment of wild-type holo-CaM bound to the iNOS peptide was determined and used as a reference for obtaining the NMR assignment of other CaM and mutant CaM complexes and was used to determine any structural changes.

After the complete assignment of the wild-type holo-CaM-iNOS complex was finished, the complete assignment of the wild-type holo-CaM-eNOS complex was done, followed by an NMR investigation of a phosphomimetic Y99E CaM mutant. This study provides structural and dynamic information on the interaction of phosphomimetic CaM with the NOS peptides. To study this interaction, the phosphorylation of this residue was mimicked by substituting a negatively charged residue to imitate the phosphate ion.

The primary objectives of this study were:

1. Use NMR to determine the solution structures of holo-CaM bound to the iNOS and eNOS peptides
2. Use these assignments as a reference to examine structural changes in the phosphomimetic-CaM.
3. Determine backbone dynamics of the CaM-NOS complexes using ^{15}N longitudinal and transverse relaxation experiments, combined with $^{15}N(^{1}H)$ NOE measurements.

Chapter 2

Expression and purification of an isotopically labeled aggregation prone inducible nitric oxide synthase calmodulin-binding protein for use in nuclear magnetic resonance studies[*]

2.1 Introduction

One of the main methods to determine the 3D structure of a protein is through the use of NMR spectroscopy. NMR can be used to determine the 3D structure at resolution comparable to X-ray crystallography, and to monitor protein-ligand interactions and internal dynamics of a protein (Wüthrich, 1986). NMR is also used to determine structures of proteins and molecules that cannot be crystallized due to their high flexibility and mobility. However, the determination of large protein structures becomes increasingly difficult due to chemical shift overlap and lower sensitivity. Also, proteins require the incorporation of isotopes such as ^{15}N and ^{13}C, which are costly (Wüthrich, 1986). For NMR studies of complexes, both partner proteins must be available in stable isotopically (^{13}C, ^{15}N) labeled forms. The most common technique for isotopically labeling proteins is to clone and over express them in bacteria, most frequently using *E. coli*.

---

[*] The results presented in this chapter have been published as part of:

Piazza, M., Duangkham, Y., Spratt, D. E., Dieckmann, T., and Guillemette, J. G. (2011) Expression and purification of an isotopically labeled aggregation prone inducible nitric oxide synthase calmodulin-binding protein for use in nuclear magnetic resonance studies. *Journal of Labeled Compounds and Radiopharmaceuticals* 54, 657-663.

Unless otherwise stated, all of the work reported in this chapter was performed and analyzed by the candidate.

The NMR experiment consists of placing a solution of the protein of interest inside a static magnetic field and detecting the unique resonance frequencies of the NMR active nuclei when they are exposed to radiofrequency (RF) radiation (Wüthrich, 1986). The first step in this structure determination is to completely assign the ^{1}H spectrum of the protein, then assign as many nuclear Overhauser enhancement (NOE) interactions as possible (James and Oppenheimer, 1994).The principal information necessary for determining the 3D structure of a protein is derived from NOE measurements (James and Oppenheimer, 1994). NOEs are due to the dipolar coupling, through-space, between nuclei, in which the local field at one nucleus is influenced by the presence of the other (Wüthrich, 1986). The larger the number of NOE restraints, the higher the resolution of the structure.

The problem with the assignment of larger proteins is overlapping of resonances and increased line widths, due to the increasing rotational correlation time. The solutions to these problems are the isotopic labelling of the sample and the use of 2D and 3D heteronuclear NMR (Evans, 1995). 2D experiments are used to measure the correlation of two nuclei resonance frequencies through-bond or through-space (Wüthrich, 1986). The use of 3D experiments have aided in overcoming the problem of overlapping peaks by expanding the 2D spectrum into other dimensions, allowing these overlapping areas to be separated into layers.

One of the key spectra used in structure determination is the ^{15}N-heteronuclear single quantum correlation (HSQC) experiment. This experiment correlates each proton attached to a nitrogen atom in the protein, which include the backbone amides, with the exception of proline, and the side chain amides. This spectrum provides the “finger print” of the protein, typically giving rise to one peak for each amino acid in the protein. Assignment of these peaks to specific residues in the protein cannot be done using the ^{15}N-HSQC alone, and other 3D experiments must be performed.

These were used to assign the ^{1}H, ^{13}C, and ^{15}N chemical shifts for the protein and are shown in Figure 2.1.

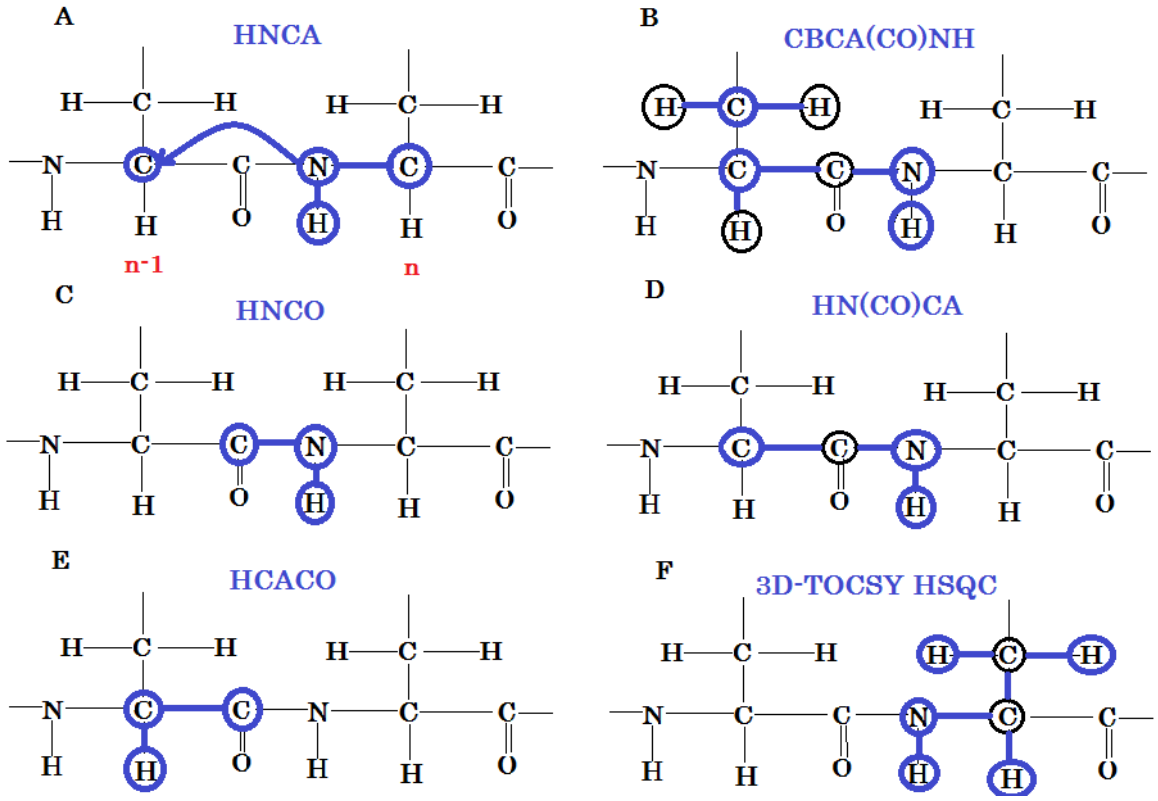

Figure 2.1: Heteronuclear multidimensional NMR experiments used for resonance assignments of proteins.

NMR experiments used to make resonance assignments for ^{1}H, ^{13}C and ^{15}N nuclei in a protein. This is done by the transfer of magnetization through bonds, shown by blue lines, to different nuclei, shown by blue circles. (A) HNCA-3D experiment which correlates the ^{15}N and NH chemical shifts with the intraresidue and preceding residue Cα shift. (B) CBCA(CO)NH-3D experiment which correlates the ^{15}N and NH chemical shifts with the preceding residue Cα and Cβ shift. (C) HNCO-3D experiment which correlates the ^{15}N and NH chemical shifts with the preceding residue carbonyl shift. (D) HN(CO)CA-3D experiment which correlates the ^{15}N and NH chemical shifts with the preceding residue Cα shift. (E) HCACO which correlate the carbonyl shift the intraresidue Cα and Hα shifts. (F) 3D-TOCSY (TOtal Correlation SpectroscopY) HSQC-3D experiment which correlates the ^{15}N and NH chemical shifts with the side chain ^{1}H shifts. (Evans, 1995).

Once all of the ^{1}H, ^{13}C, ^{15}N resonance assignments has been determined, the through-space nuclear Overhauser effect spectroscopy (NOESY) experiment can be used to determine

distance constraints. The NOESY shows NOE cross-peaks of nuclei that are close (within ~5Å) in the folded protein but may be far away in the primary sequence (Wüthrich, 1986).

There is considerable interest in understanding the structural basis of CaM's target protein interactions and diverse regulatory functions. It is well established that CaM is able to interact with its target enzymes in many different conformations, as previously mentioned. Furthermore, the effect that CaM binding has upon its target may involve important changes in the structural dynamic properties of the enzyme. For example, CaM binding is necessary for interdomain electron transfer (IET) and the activation of NOS enzymes. The kinetic regulation of the IET processes within the NOS enzymes by CaM binding has been proposed to be accomplished dynamically through controlling redox-linked conformational changes required for effective IET (Ghosh and Salerno, 2003). Only the inducible NOS (iNOS) isozyme is transcriptionally regulated and binds to CaM in the absence of Ca^{2+} (Roman *et al.*, 2002).

To obtain the NMR structure of the holo-CaM-iNOS peptide complex proposed in this study, one cannot simply isotopically label both holo-CaM and the iNOS peptide and perform NMR experiments on the two in complex. If this was undertaken it would not be possible to discern which resonance assignments belong to holo-CaM or the iNOS peptide. The process followed was to isotopically label one of the compounds, with the other being unlabeled and then determine the NMR resonance assignments of this isotopically labeled compound, and *vice versa* (Wüthrich, 1986). This study first determined the complete resonance assignment of the isotopically labeled iNOS peptide bound by the unlabeled wild-type holo-CaM, followed by the complete assignment of the isotopically labeled wild-type holo-CaM bound to the unlabeled iNOS peptide. Investigation of CaM bound to iNOS proved to be most difficult due to the propensity of the iNOS CaM binding domain to aggregate when not bound to CaM. Compared to the CaM-binding region of the cNOS isoforms, the

iNOS CaM-binding region has more hydrophobic amino acids and larger hydrophobic patches, which contribute to the peptide being insoluble (Matsubara et al., 1997, Spratt et al., 2006). This study reports on the development of a novel expression and purification system that allows for the production of individually stable isotope labeled aggregation prone proteins. This methodology is demonstrated on the iNOS peptide/CaM system and could potentially be used to label specific components found in other complexes involving insoluble proteins and peptides.

This project was originally started by Yay Duangkham (MSc. 2010, U of Waterloo) with her performing the initial expression and purification of the iNOS peptide. Subsequent to Yay's graduation, the candidate completed this study and performed all of the analyses reported in this chapter unless otherwise stated in the experimental procedures section (section 2.2).

2.2 Experimental Procedures

2.2.1 Materials

All oligonucleotides were 5'-phosphorylated and synthesized by Sigma-Genosys (Mississauga, ON, Canada). FastDigest restriction enzymes and T4 DNA ligase were purchased from Fermentas Life Sciences (Burlington, ON, Canada). All other chemicals were purchased from BioShop Canada (Burlington, ON, Canada). *E. coli* ER2566 cells and the pTYB12 plasmid were purchased from New England Biolabs (Markham, ON, Canada).

2.2.2 Expression of Recombinant CaM

The vector pET9d (NOVAGEN) used to express the rat calmodulin was made by Newman (2003) by cloning in the CaM sequence using restriction enzyme sites, *NcoI* and *BaMHI*. Calmodulin was expressed in *E. coli* BL21DE3 competent cells and then purified using phenyl-sepharose affinity chromatography as previously reported (Spratt *et al.*, 2008).

2.2.3 Plasmid Construction

The construction of the plasmids used in this study were performed by Yay Duangkham (MSc. 2010, U of Waterloo), a previous graduate student in our laboratory.

2.2.3.1 piNOSpep

The generation of the CaM-binding domain of human iNOS (residues 507-531; RPKRR EIPLK VLVKA VLFAC MLMRK) involved the use of three pairs of single-stranded complementary oligonucleotides using a similar methodology to a previously published study (Bisaglia *et al.*, 2005). These primers were designed to have complementary sticky ends for the facile ligation of the 5' and 3' ends of the open-reading frame (eg. For *Nco*I which recognizes and cuts C/CATGG, the 5' end of the first primer was 5' CATGG). The primers used to construct the CaM-binding domain of iNOS are summarized in Table 2.1. This construction also involved the incorporation of a 10-histidine tag followed by a thrombin cleavage site (LVPR/GS) upstream from the open-reading frame for the future cleavage and removal of the poly-histidine-tag.

Table 2.1:DNA primers used to construct phiNOSCBD.

Primer	Oligonucleotide sequence (5'-3')
iCBDp1fr	CATGGGCAGCAGCCATCATCATCATCACCATCATCATCATCACAGCAGCGGCCTGGTACCGCGGGGCAGCCA
iCBDp2fr	TATGCGCCCCAAGCGCCGCGAGATCCCCCTTAAGGTTCTTGTTAAGGCC
iCBDp3fr	GTTCTTTTCGCCTGCATGCTTATGCGCAAGTAATAGGGATCCGAATTCA
iCBDp1rv	CCGCGGTACCAGGCCGCTGCTGTGATGATGATGATGGTGATGATGATGATGGCTGCTGCC
iCBDp2rv	CAAGAACCTTAAGGGGGATCTCGCGGCGCTTGGGGCGCATATGGCTGCC
iCBDp3rv	AGCTTGAATTCGGATCCCTATTACTTGCGCATAAGCATGCAGGCGAAAAGAACGGCCTTAA

In preparation for the ligation of these primers, the six primers (iCBDp1fr, iCBDp2fr, iCBDp3fr, iCBDp1rv, iCBDp2rv, and iCBDp3rv) were mixed in equal portions, heated to 95^{o}C for 10 minutes and allowed to cool slowly to room temperature to facilitate annealing of the overlapping

sequences. The annealed DNA was then cloned into the kanamycin resistant pET28a (Novagen) plasmid using the unique flanking *Nco*I and *Hind*III restriction sites. The resulting vector that expressed the calmodulin binding domain of human iNOS (piNOSpep) was verified by DNA sequencing.

2.2.3.2 phiNOSCBD-intein

The intein mediated purification with an affinity chitin-binding tag (IMPACT) system (New England Biolabs) was also used to express the human iNOS peptide. The IMPACT system uses pTYB12, an ampicillin resistant vector coding for a chitin binding domain (CBD)-intein fusion protein with a multiple cloning site downstream at its 3' end. The coding region for the iNOS CaM-binding domain was amplified by PCR using piNOSpep as a template. Unique flanking *Nde*I and *PstI* restriction sites were introduced for subcloning into the 3' multiple cloning region of the pTYB12. The primers used were iCBDp1fr (Table 2.1) and NOSCBDrv 5'ATAA*CTGCAG*CCCGGGAAAACAGCATT-CCAGG 3'. The coding region of the iNOS CaM protein was then subcloned into the pTYB12 vector using the unique *Nde*I and *Pst*I restriction sites. The resulting vector, phiNOSCBD-intein (Figure 2.2) was verified by DNA sequencing to ensure that no spontaneous mutations had occurred. The iNOS peptide is attached to the fusion tag by its N-terminus. The CBD-intein protein has a molecular weight of 60.4 kDa while that of the CBD-intein-iNOS fusion protein is 61.8 kDa.

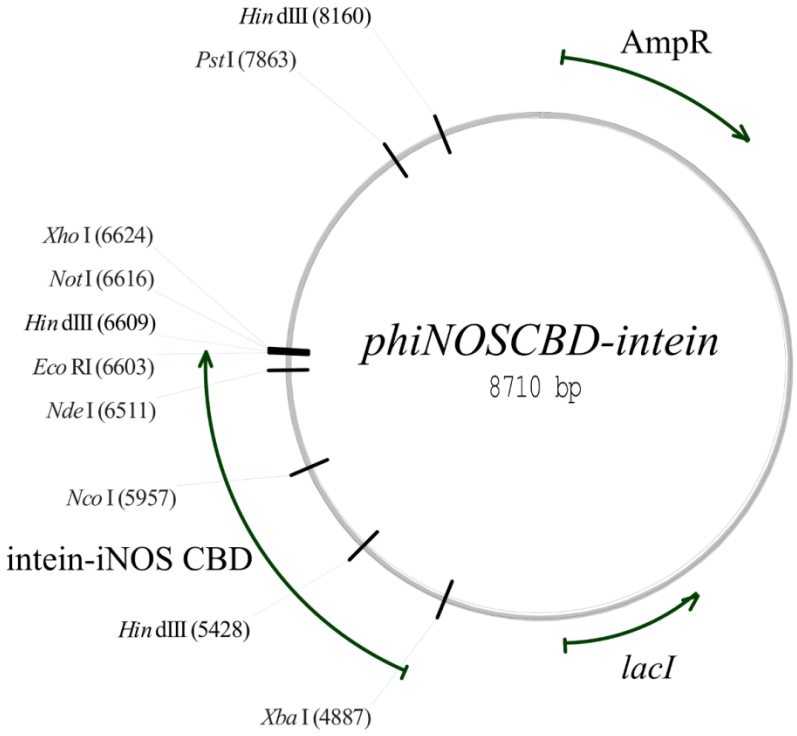

Figure 2.2: piNOSCBD-intein vector map showing restriction enzyme site for cloning iNOS CaM-binding region into pTYB12 (NEB).

The IMPACT pTBY12 vector contains an ampicillin resistance gene and an CBD-intein that was fused to the iNOS-CaM binding region by insertion at the *NdeI* and *PstI* sites. The piNOSCBD-intein in its circular form showing the location of the important ORFs are labeled. Please note that an extra ~1200 bp originating from the phiNOSCBD vector at the 3' end of the iNOS-CaM binding domain was required for cloning of this construct.

The cleavage process adds three extra amino acids to the N-terminus of the iNOS CaM-binding region peptide as shown by the underlined amino acids to produce a sequence of:

AGH *MR PK***RRE IPLKV LVKAV LFACM LMRK**.

The amino acids of the iNOS CaM-binding region are shown as a bold font. A few additional amino acids, shown in an italic font, were from the *NdeI* cut site. The peptide that is produced is 29 amino acids long with 22 amino acids from the human iNOS CaM-binding region (amino acids 510-531) and a molecular weight of 3.4 kDa. Since CaM interacts with target proteins between the

anchoring amino acids in a 1-5-8-14 motif, extra amino acids at the N-terminus of the peptide would not interfere with CaM binding (Aoyagi *et al.*, 2003).

2.2.4 Expression of intein-iNOS CaM-binding domain fusion protein

The expression of the protein used in this study was performed by Yay Duangkham (MSc. 2010, U of Waterloo), a previous graduate student in our laboratory. 500 μL of an overnight culture of *E. coli* ER2566 (DE3) transformed with phiNOSCBD-intein was used to inoculate 1 L of minimal media in 4 L flasks supplemented with 100 μg/ml of ampicillin. The ER2566 cells contain the T7 RNA polymerase that is under the control of a *lacI* repressor which is released after the addition of IPTG to allow for the production of the protein. It also lacks *lon* and *ompT* proteases, which can degrade foreign or short proteins. Minimal media contains M9 salts (refer to supplementary materials Table 2.2) ammonium chloride ($^{15}NH_4Cl$), glucose, magnesium sulfate ($MgSO_4$), thiamine and antibiotic in concentrations as given in table S1. The optimal conditions for protein expression were determined using a systematic approach of varying temperature and period used after the induction of protein synthesis. In general, the cultures were grown at 37ºC to an $O.D_{600}$ of 0.9 – 1.0, brought to the incubation temperature used during induction, induced with 500 μM IPTG, and then harvested several hours after induction. Cells were harvested by centrifugation at 6000 x g at 4^{o}C for 5 minutes, flash frozen on dry ice, and subsequently stored at –80ºC.

Table 2.2: Minimal Media Ingredients

Components[a]	50 mL Starter Culture in 250 mL Flask	1 L Growth Culture in 4 L Flask	Final Concentration
10X M9 Salts Stock Soln: 114 g $Na_2HPO_4 \cdot 7H_2O$ 30.0 g KH_2PO_4 5.0 g NaCl In 1 L	5 mL	100 mL	1X
20% N^b–NH_4Cl	250 µL	5 mL	0.1% or 0.001 g/mL
40% C^b-Glucose	250 µL	5 mL	0.2% or 0.002 g/mL
2 M $MgSO_4$	50 µL	1 mL	2 mM
0.05% Thiamine	50 µL	1 mL	0.00005% or 5 mg/mL
100 mg/mL Ampicillin	50 µL	1 mL	100 µg/mL
0.2 M $CaCl_2$	25 µL	500 µL	100 µg/mL
Starter Culture	500[c] µL	5 mL[d]	

[a]For sterilization of the components of the media, M9 solutions were sterilized by autoclave whereas all other solutions were filtered through a 0.2 µm pore sized filter. Method modified from Roberts (1993a).
[b]The ^{14}N- NH4Cl and ^{12}C-Glucose were used in the minimal media sample with the exception of 1 L growth cultures that were being prepared for NMR experiments where ^{15}N- NH4Cl and ^{13}C-Glucose were used
[c]Starter culture from 3 mL LB media culture
[d]Starter culture from 50 mL minimal media culture

2.2.5 Purification of soluble isotopically labeled iNOS peptides

The purification of the peptides used in this study were performed by Yay Duangkham (MSc. 2010, U of Waterloo), a previous graduate student in our laboratory. The pellet obtained from 4 L of minimal media culture growth was resuspended in the intein lysis buffer (20 mM Tris pH 7.5, 500 mM NaCl, 1 mM $CaCl_2$ and 0.01% Triton X-100) in a 1:10 (1 gram: 10 mL of buffer) ratio. When indicated, unlabeled CaM to a final concentration of 10 µM was added during cell lysis. The cells were lysed using an Avestin EmulsiFlex-C5 homogenizer (Ottawa, ON) and the suspension was

clarified by centrifugation. The supernatant was loaded onto the column with a 10 mL bed volume of chitin beads equilibrated with ten column volumes of wash buffer (20 mM Tris pH 7.5, 500 mM NaCl, 1 mM $CaCl_2$). Contaminating proteins were removed by washing the column with ten column volume of wash buffer at a rate of 2.0 mL/min. To elute the peptide, the column was incubated at room temperature in cleavage buffer (20 mM Tris pH 8.5, 500 mM NaCl, 1 mM $CaCl_2$, and 50 mM DTT) for 48 hours. Under these reducing conditions the Asn454 located at the C-terminus of the intein tag is induced to form a succinimide and break the bond between the iNOS CaM-binding domain peptide and the intein fusion tag. The eluted material was collected in 2 mL fractions by passing a pH 8.5 wash buffer through the column. 3 μL samples from each fraction were run on a Tris-tricine gel to determine which fractions contained the iNOS CaM-binding region. The appropriate fractions were pooled together, concentrated down to 1 mL using a Viva spin column with a 3 kDa cut off and then run through a Superdex 75 10/300 equilibrated with wash buffer. The fractions containing the desired protein were pooled, concentrated, and were quantified using the Lowry method with CaM as the standard. Protein purity was confirmed by SDS-PAGE and ESI mass spectrometry. The protein was flash frozen and stored at -80°C.

2.2.6 NMR Experiments

2.2.6.1 Sample preparation for NMR investigation

The isotopically labeled iNOS peptide bound to unlabeled CaM was purified in Tris buffer and required a buffer exchange prior to collecting NMR spectra. A 15 mL 3 kDa Viva spin column was loaded with the protein solution and concentrated to 500 μL. The flow through was discarded and 9.5 mL NMR buffer (100 mM KCl, 10 mM $CaCl_2$, 0.2 mM NaN_3, pH 6.0) was added. The sample was again concentrated to 500 μL. This process was repeated five times to ensure all traces of Tris buffer were removed. For the final spin, the sample was concentrated to 450 μL so that 50 μL of D_2O can be

added for a final 10% D_2O content. The final concentration of the 500 μL NMR sample was 1.4 mM protein-peptide complex. The sample was transferred into a NMR 5 mm, 7" NMR tube and stored at 4°C until required for NMR experiments.

2.2.6.2 NMR spectroscopy and data analysis

All NMR data were acquired at 25°C on Bruker 600 or 700 MHz DRX spectrometers equipped with $^{1}H/^{13}C/^{15}N$ triple-resonance probes with XYZ-gradients (Bruker, Billerica, MA, USA). All peptide NMR experiments were run by Dr. Thorsten Dieckmann. The peptide backbone resonances were assigned using standard 3D NMR techniques that included HNCA, HN(CO)CA, CBCANH, and CBCA(CO)NH experiments (Grzekiek and Bax, 1992, Muhandiram and Kay, 1994). Side-chain resonance assignments were obtained from a HCCH-total correlation spectroscopy (TOCSY) spectrum (Bax *et al.,* 1990). NOEs for structure determination were determined from ^{15}N-edited nuclear Overhauser effect spectroscopy (NOESY) experiments (Clore and Gronenborn, 1990, Fesik and Zuiderweg, 1990).

2.2.6.3 Strategy for NMR spectra assignment

The NMR spectra were visualized and assignments will be made using the Computer Aided Resonance Assignment (CARA) version 1.8.4 (Keller, 2004). The assignment of the protein starts with the ^{15}N-HSQC spectrum, which shows the backbone amide protons and nitrogen, as well as the amides in the side chains of the amino acids. The spectrum is opened in the main window of *SynchroScope* using CARA. Each observed peak is then given a peak number. In the strip window of *SynchroScope* the 3D experiments HNCA, HN(CO)CA and CBCA(CO)NH were each opened individually and used to correlate the H-N of amino acid "i" on the ^{15}N-HSQC to a Cα of amino acid "i", "i-1" and Cβ of "i-1".

After all possible peaks were assigned to H, N, $C\alpha_i$, $C\alpha_{i-1}$ and $C\beta_{i-1}$, the HNCA was opened in *StripScope* mode showing the $C\alpha_i$ and $C\alpha_{i-1}$ peaks, and the backbone assignment was started. The residues were connected by finding the best matches of $C\alpha_i$ and $C\alpha_{i-1}$ in different strips. This was done by aligning all best possible carbon chemical shifts for the preceding and subsequent amino acid, using the function of CARA *select strips* – *all best precursor* or – *all best successor*. Residues chosen as starting points for the backbone assignment were those that have unique carbon chemical shifts, such as threonine, alanine and glycine. The backbone was connected by confirming that the chemical shifts of the adjacent amino acids are in the correct range for the required amino acid in the sequence.

After a tentative backbone assignment was made using the HNCA spectrum, the ^{15}N-NOESY-HSQC spectrum was opened in *SystemScope* to aid in confirming the assignment. In the H_{NOE} plane of each NH in the ^{15}N-NOESY, cross peaks of the NH_{i-1} and NH_{i+1} should be present, which, if the backbone assignment is correct, will correspond to the NH of the adjacent amino acids in the sequence. Next, the intraresidue side chain carbon and proton peaks were assigned using various TOCSY experiments obtained. The side chain carbon assignments were made using the hCCH-$TOCSY_{ali}$ experiment, whereas, the side chain proton assignments were made using the HCcH-$TOCSY_{ali}$, ^{15}N-TOCSY-HSQC and HcccoNH experiments. After all possible spins were assigned to each amino acid by viewing these experiments in *SystemScope,* NOE cross peaks were assigned by analyzing the various NOESY experiments obtained. The ^{15}N-NOESY HSQC and $^{13}C_{ali}$-NOESY HSQC spectra were opened in *Polyscope, SystemScope* and *StripScope* and all cross peaks not assigned to intraresidue protons were assigned to interresidue protons.

2.3 Results

2.3.1 CaM protein expression and purification

The expressed and purified wild-type CaM produced high yields of 40mg/L. These purified CaM proteins were judged to be over 95% homogeneous by SDS-PAGE. Likewise, ESI-MS was used to confirm identity and homogeneity.

2.3.2 Expression of CaM binding domains

Difficulties were experienced when expressing the 10-histidine N-terminal tagged human iNOS CaM-binding domain peptide using the expression vector phiNOSpep in *E. coli* BL21 (DE3). These difficulties included dramatic cell density decreases upon induction and the grey to black cell discolouration, most likely due to the aggregation of the over-expressed hydrophobic iNOS peptide (Spratt *et al.*, 2006). Furthermore, since only one aromatic residue (Phe) is found in these peptides, it was difficult to monitor all three NOS peptides by absorbance during their purification. Numerous attempts were made to improve the yield of soluble peptide including lower induction temperatures accompanied by a prolonged incubation period since these have been shown to increase the solubility and yield of recombinant proteins. None of the modified procedures resulted in any significant amount of soluble peptide.

In order to circumvent these problems, the coding region for the iNOS CaM-binding domain was subcloned into pTYB12, a vector coding for a chitin binding domain-intein fusion protein with a multiple cloning site downstream at its 3' end (Figure 2.2). The intein-iNOS fusion protein showed a high level of expression (Figure 2.3). Several attempts were made to purify the iNOS CaM binding protein as an intein fusion protein. Variations in the induction temperatures and protein expression periods were tested to determine their effect on expression level and solubility. All attempts resulted in the production of proteins that accumulated as inclusion bodies. Another approach taken was to

extract the intein-iNOS fusion protein from the inclusion bodies using 8 M urea. Attempts were made to refold the intein protein using a variety of dialysis-based protocols both in the absence and presence of exogenous CaM. All failed to yield any significant quantity of soluble protein with a functional intein moiety that was needed for the self-cleavage of the fusion protein.

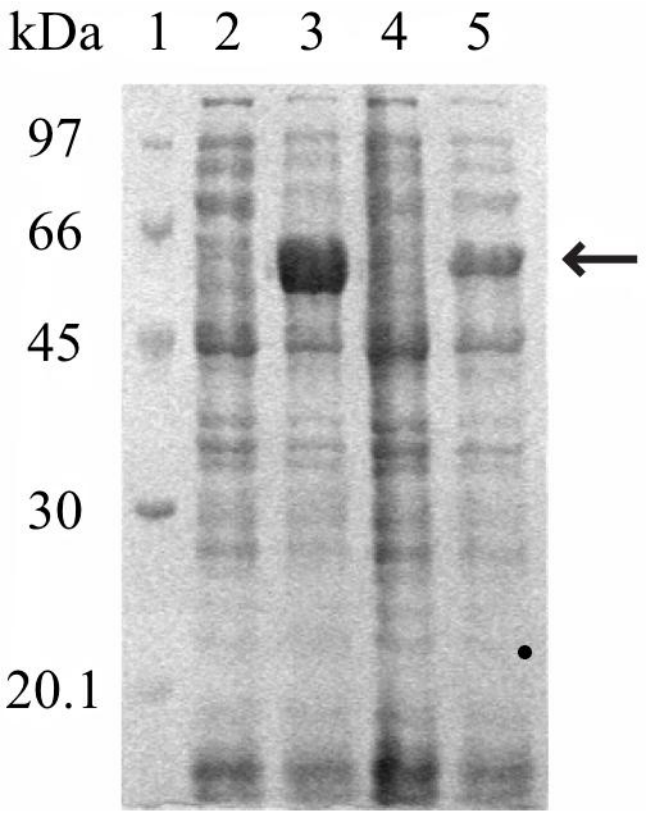

Figure 2.3: 12% SDS-PAGE of intein alone and intein-iNOS peptide time-course expression test in minimal medium.

Protein was loaded in a standard SDS-loading buffer. Samples consisted of ER 2566 (DE3) *E. coli* transformed with pTYB12 (intein alone) or phiNOSCBD-intein (intein-iNOS peptide) before and after 6 hours induction with 500 μM IPTG. *Lane 1*, low molecular mass protein standard (GE Healthcare Bio-sciences); *Lane 2*, intein alone at t = 0; *Lane 3*, intein alone at t = 6 hours; *Lane 4*, intein-iNOS peptide at t = 0; *Lane 5*, intein-iNOS peptide at t = 6 hours. Expected size of intein alone and intein-iNOS peptide fusion protein are 60.4 and 61.8 kDa, respectively.

The best results were obtained when expressing the fusion protein at low temperatures and extracting the protein in the presence of excess exogenous CaM (Table 2.3). The low temperature

conditions were used in an attempt to reduce the rate of aggregation. The CaM was added so that it could bind to the aggregation-prone iNOS CaM binding domain peptide immediately as the cells were lysed. The highest yields were obtained when *E. coli* ER2566 cells were transformed with the pTYB12-iNOS peptide vector and grown at 15^{o}C for extended periods of time in minimal media enriched with ^{15}N or ^{13}C isotopes (Table 2.3).

Table 2.3: Summary of expression and purification results of the iNOS CaM-binding domain peptide.

Purification Conditions	Growth Conditions in Minimal Media	Yield[a] from 2L of Minimal Media
Intein-iNOS peptide	37°C growth, 22°C induction for 6 hrs	~ 0.025 mM (750 μL)
Intein-iNOS peptide with CaM in lysis step	37°C growth, 22°C induction for 6 hrs	~ 0.03 mM (750 μL)
Refolding of intein-iNOS peptide drip-wise	37°C growth, 37°C induction for 6 hrs	None No self-cleavage
Intein-iNOS peptide with CaM in lysis step	37°C growth, 22°C induction for 12 hrs	~ 0.42 mM (500 μL)
Intein-iNOS peptide with CaM in lysis step	37°C growth, 15°C induction for 20 hrs	~ 0.84 mM (500 μL)

[a]Yield was determined using the Lowry method with wild-type CaM used as the standard.

A key part of the process of obtaining a soluble fusion protein was the lysing of the cells in a buffer that contained an excess of unlabeled wild type CaM. A major proportion of the CaM-bound iNOS fusion protein was isolated as a soluble complex in the supernatant after cell lysis. The chitin-binding domain of the fusion protein was tightly bound to the chitin beads since no intein-iNOS peptide was observed in the flow through or wash fractions (Figure 2.4). Excess CaM added during the lysis procedure can be seen in the flow through lane. Therefore, the CaM found in the subsequent steps of the purification process represents CaM that was tightly bound to the iNOS CaM-binding region of the fusion protein.

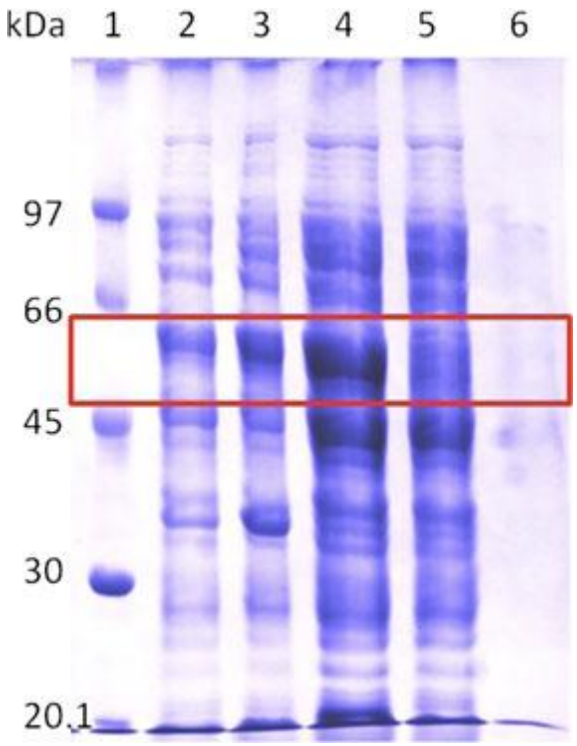

Figure 2.4: Monitoring of the soluble form of the CBD-intein-iNOS peptide during extraction in the presence of excess added calmodulin.

The protein composition was monitored using 10% SDS-PAGE during each step of the purification. 1) Low molecular marker. 2) A sample taken from the resuspended cell pellet that was lysed in the presence of added calmodulin. After centrifugation, samples were taken from 3) the pellet and 4) the supernatant to determine the solubility of the protein. 5) Sample taken from flow through when the supernatant was passed through the chitin column. 6) Sample from the flow through during the wash step of the column. The CBD-intein-iNOS peptide band is located at ~60 kDa, red box, and can be seen in the lanes 2,3, and 4.

The CaM-iNOS peptide complex was eluted by incubating the column in 50 mM DTT to initiate the intein-dependent self-cleavage. Each 2 mL fraction eluted from the column was analyzed using a 16.5% Tris-Tricine SDS-PAGE gel. The complex formed by the CaM and the iNOS peptide dissociates under the denaturing condition and is seen as two separate bands, 17 kDa for CaM and ~4 kDa for iNOS peptide (Figure 2.5). The fractions containing both CaM and the iNOS peptide were pooled and concentrated. Gel filtration chromatography was employed to remove the contaminating proteins as well as residual DTT that was not removed during the concentration step.

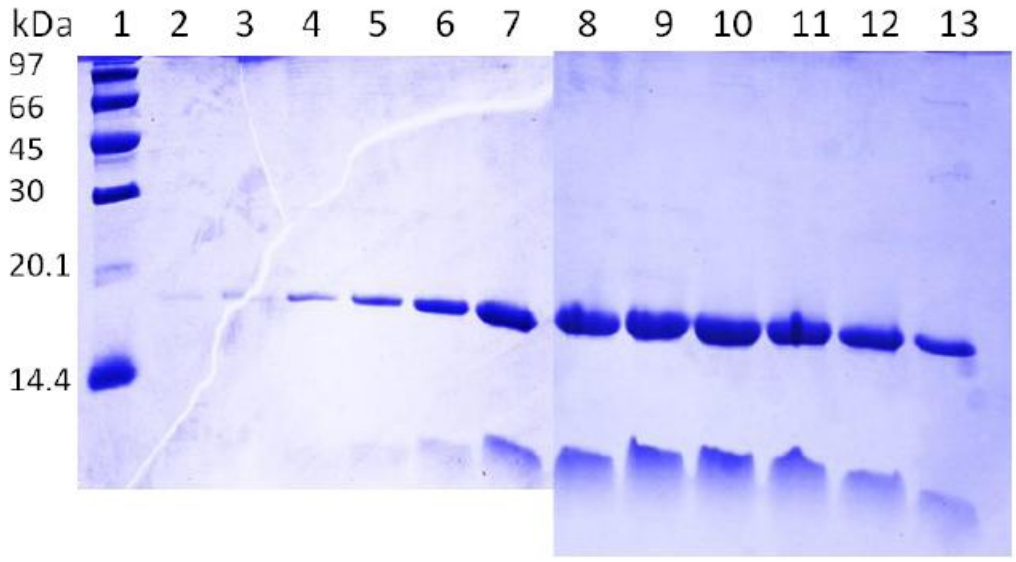

Figure 2.5: 16.5% Tris-tricine SDS-PAGE analysis of the eluted CaM-iNOS peptide fractions from the chitin column.

The fusion protein bound to the chitin resin was incubated for 48 hours in buffer containing 50 mM DTT. Lane 1 is the low molecular marker. Lane 2-13 represents fractions 1-12 respectively. All fractions contained some CaM-iNOS peptide, however, only fractions 2-12 (lanes 3-13) were pooled.

2.3.3 Characterization of the CaM-iNOS peptide complex

The expressed and copurified CaM-iNOS peptide complex produced a yield of 500 μL of 1.4 mM of iNOS CaM binding peptide from a 4L cell culture. ESI-MS was used to assess the homogeneity and confirm that the co-purification with wild-type CaM was successful (Table 2.4). Subsequent to the ESI-MS result, the co-purified CaM-iNOS peptide complex was tested using a gel shift mobility assay to ensure that the purified complex was pure, saturated and demonstrated the expected mobility shift when compared to wild-type CaM alone (Figure 2.6). The iNOS-peptide from the intein-fusion protein demonstrates a greater mobility shift which can be attributed to the extra histidine residue derived from the cleaved intein fusion protein at the N-terminus of the peptide (additional N-terminal of AGHM).

Table 2.4: Masses of unlabeled iNOS peptide co-purified with wild-type CaM.

Proteins/Peptides	Mass (Da)[a]	
	Observed	Theoretical[b]
iNOS peptide (from intein-fusion protein)[c]	3391.9	3393
Wild-type CaM (copurified)	16704.5	16706
iNOS peptide (synthesized by Sigma Genosys)	2995.5	2997

[a] Masses of deconvoluted ESI-MS spectra were determined with an accuracy of ± 4 Da.
[b] Calculated masses based upon amino acid sequence.
[c] Expected mass of intein-fusion-protein-derived iNOS peptide with additional N-terminal residues AG

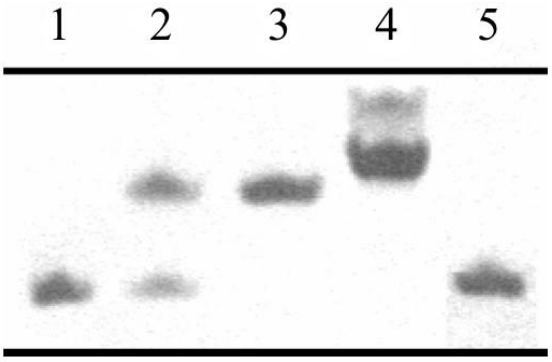

Figure 2.6: Gel Mobility Shift Assay of wild-type CaM with synthetic and recombinantly expressed iNOS peptides.

Wild-type CaM (20 μM) was incubated with synthetic iNOS peptide in the presence 0.2 mM CaCl2. CaM-iNOS peptide derived from intein-iNOS peptide fusion protein was loaded without any additional peptide added. The samples were then analyzed by PAGE (15% acrylamide) containing 0.375 M Tris, pH 8.8, 4 M urea, and 0.2 mM CaCl2 and visualized with Coomassie Blue R-250. *Lanes 1* & *5* – wild-type CaM alone; *Lane 2* – wild-type CaM with 0.5 molar equivalents of synthetic iNOS peptide; *Lane 3* – wild-type CaM with 2 molar equivalents of synthetic iNOS peptide; *Lane 4* – wild-CaM copurified with iNOS peptide derived from intein-iNOS peptide fusion protein.

2.3.4 NMR spectroscopy

The NMR analysis of the labeled iNOS peptide in complex with CaM (Figure 2.7A) followed routine procedures with the backbone resonance assignment based primarily on 3D triple resonance techniques. The HNCA experiment (Figure 2.7B) was supported by CBCA(CO)NH and HN(CO)CA experiments. This combination of the techniques resulted in complete backbone assignments for the region of the peptide interacting with CaM (Appendix B).

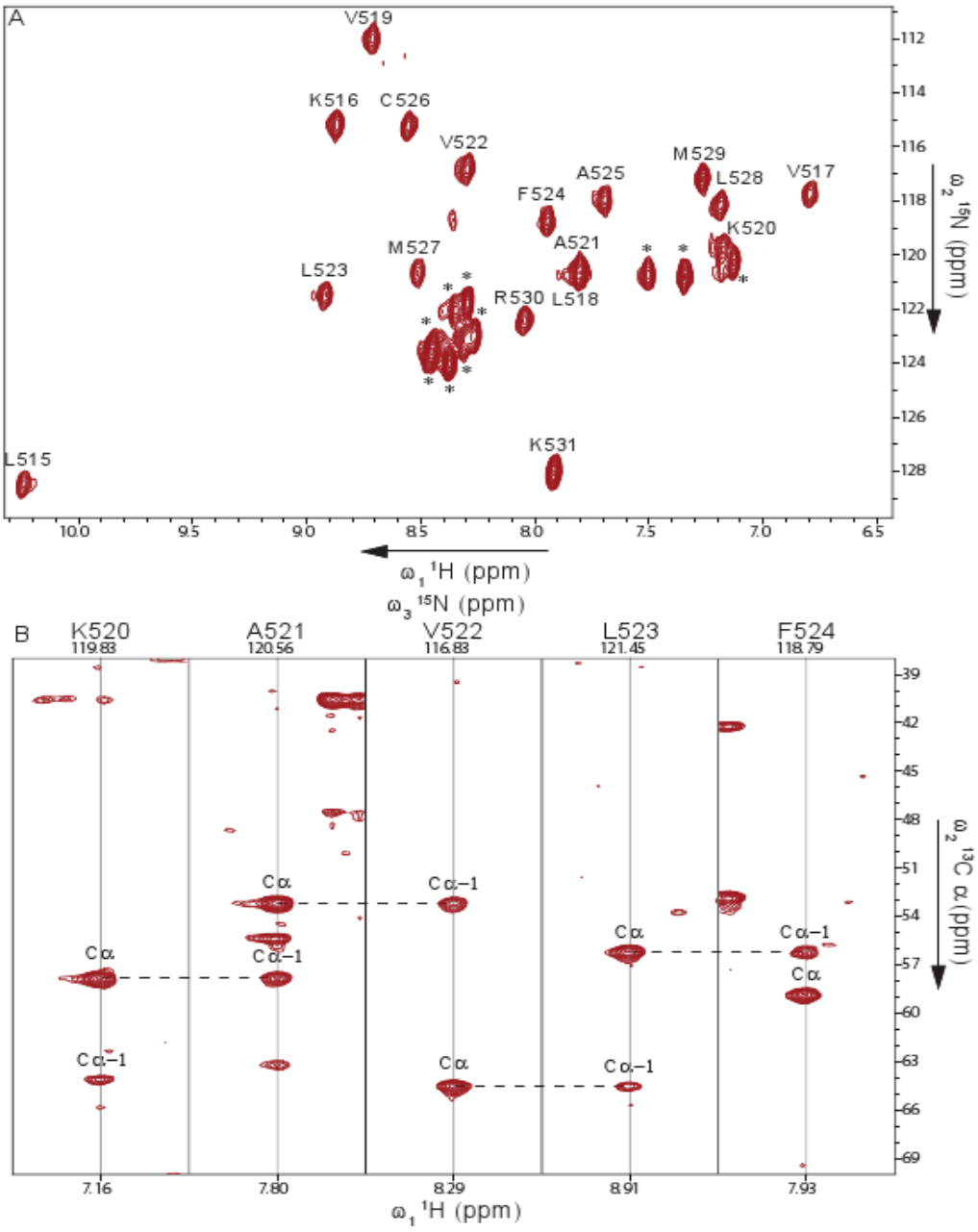

Figure 2.7: Composite figure of NMR structural data

(A) ^{1}H-^{15}N HSQC spectrum of the iNOS CaM-binding region peptide. The unlabeled peaks originate from N-terminal region of the peptide. (B) 3D HNCA strips of sequential amino acids Lys520 to Phe524 of the iNOS CaM-binding region peptide. The connection between the alpha carbon of the previous and successive residue are shown. The peaks are numbered as per residue number from full iNOS protein.

The N-terminal region (first 12 residues comprising the additional amino acids from cleavage, *NdeI* cut site and residues 510 – 514 of the iNOS peptide) is unstructured and highly mobile, resulting in weak, overlapped resonances that were not assigned. Subsequently, sidechain resonances were assigned using HCCH-TOCSY based techniques. NOEs for structure determination of the iNOS peptide bound to CaM were extracted from ^{15}N-edited NOESY experiments (Figure 2.8).

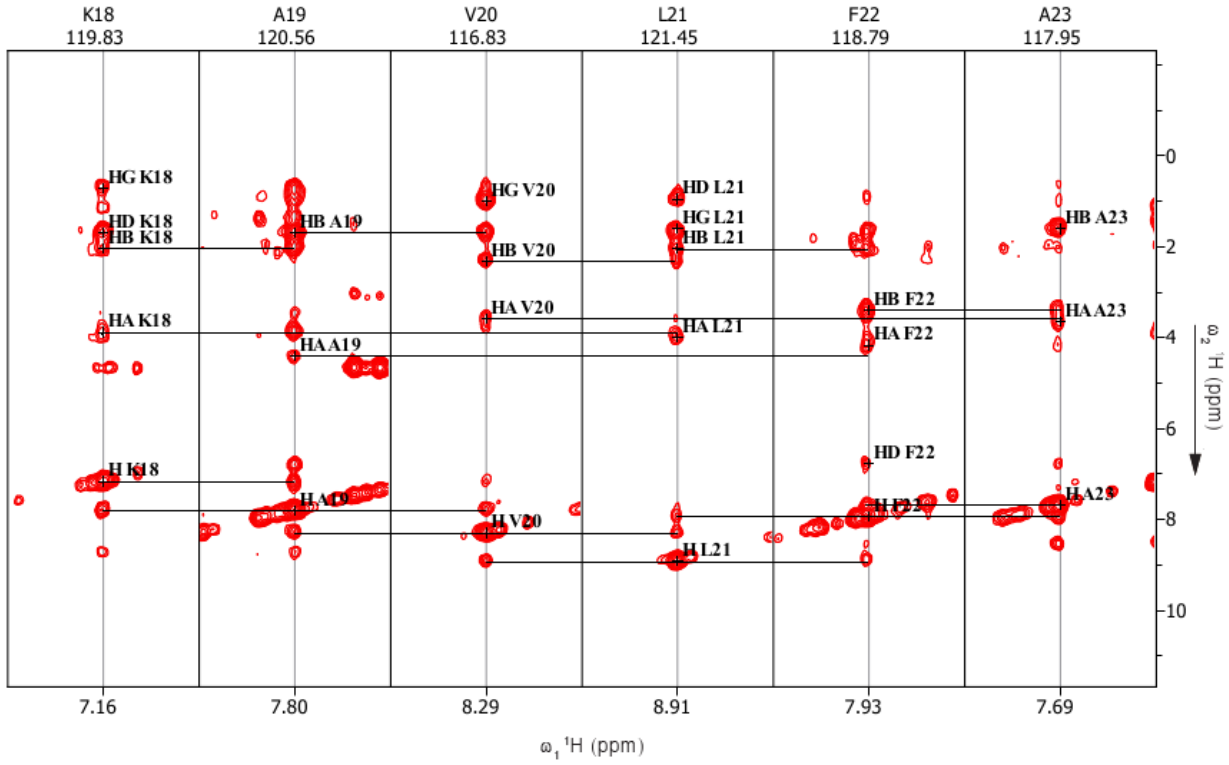

Figure 2.8: ^{15}N-NOESY of iNOS peptide.

3D ^{15}N-NOESY strips of sequential amino acids Lys18 to Ala23 (corresponding to residues Lys520 to Ala525 of the full iNOS protein) of the iNOS CaM-binding region peptide. The connection between: NH_i and NH_{i+1}; $H\alpha_i$ and NH_{i+1}; $H\alpha_i$ and NH_{i+3}; and $H\beta_i$ and NH_{i+1} can be seen. These NOE constraints are characteristic of α-helical secondary structure.

The three dimensional solution structures of human iNOS CaM binding domain peptide were determined using GeNMR: a web server for rapid NMR-based protein structure determination (Berjanskii *et al.*, 2009, http://www.genmr.ca/). The family of 20 final structures is shown in Figure 2.9A, and a ribbon diagram of the average structure is shown in Figure 2.9B. The determined solution

structures show that residues 13-29 (corresponding to residues Leu515 to Lys531 of the full iNOS protein) adopt an α-helical structure, and that residues 1-12 (comprising the additional amino acids from cleavage, *NdeI* cut site and residues 510 – 514 of the iNOS peptide) are unstructured.

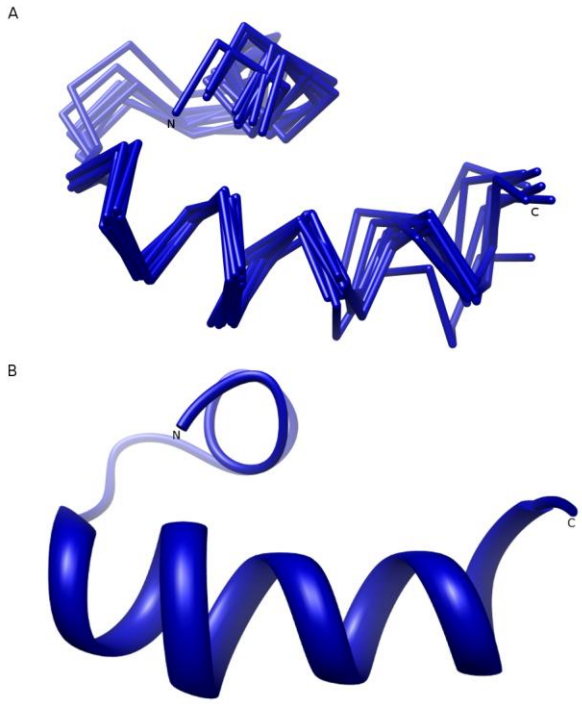

Figure 2.9: Determined solution structure of the iNOS CaM-binding domain peptide.
(A) Superposition of the ensemble of the 20 lowest energy calculated NMR solution structures of the iNOS peptide. (B) Ribbon diagram of the average structure of the iNOS peptide.

2.4 Discussion

In nature iNOS is found bound to CaM and the *in vitro* production of recombinant holo iNOS requires CaM to be co-expressed, indicating iNOS requires CaM for its activation as well as its stability (Guo *et al.*, 2004). Even though the iNOS CaM-binding region comprises just two percent of the whole iNOS protein (22 amino acids residues; 510-531), the extremely hydrophobic properties of the peptide make it unstable in solution and prone to aggregation. The expression in bacteria of protein peptide segments with stretches of highly hydrophobic sequences has proven to be

challenging. Attaching the hydrophobic peptide to a hydrophilic fusion protein can amplify expression of recombinant proteins, improve solubility and be used for affinity purification (Malhotra, 2009). In addition, growth temperature, the concentration of induction agents, different growth media and the *E. coli* strain employed for expression can be systematically optimized (Cunningham and Deber, 2007). All of our attempts to generate adequate quantities of the iNOS CaM-binding peptide using these practices failed to provide us with the material needed for the collection of structural data. For NMR spectroscopy labeling and assignment purposes, CaM and the iNOS CaM-binding region peptide could not be co-expressed since this would preclude selective isotope labeling when two proteins share the same growth medium. The addition of CaM during the lysis step resulted in higher yields of soluble iNOS peptide since the iNOS peptide portion of the recombinant fusion protein was bound to CaM reducing the amount of free iNOS peptide available for aggregation. The addition of CaM also facilitated iNOS peptide detection after the fusion tag was removed by cleavage.

The methodology outlined above allows for the asymmetric stable isotope labeling of protein-protein and protein-peptide complexes where one partner has very limited solubility. This technique greatly speeds up resonance assignment and structure calculation. In addition it allows for the analysis of larger complexes because the components can be analyzed separately, thereby reducing difficulties due to resonance overlap. If amino acid-deficient bacterial strains are employed during the production of one component (Hoffman and Spicer, 1991), this technique will also allow for the labeling of a specific amino acid type in one of the components for each of the protein or peptide binding partners.

Chapter 3

Solution NMR structures of CaM bound to NOS peptides: Effects of a phosphomimetic CaM mutation*

3.1 Introduction

CaM is a ubiquitous cytosolic Ca^{2+}-binding protein that is able to bind and regulate hundreds of different intracellular proteins (Ikura and Ames, 2006). CaM consists of two globular domains joined by a flexible central linker region. Two EF hand pairs that are capable of binding to $Ca^{2+}$are found in each globular domain. The binding of Ca^{2+} to CaM causes the exposure of hydrophobic patches that allow it to associate with its intracellular target proteins. The flexibility of CaM's central linker separating the *N*- and C-domains allows it to adapt its conformation to optimally associate with its intracellular target (Persechini and Kretsinger, 1988). There is considerable interest in obtaining a better understanding of the structural basis for CaM's ability to bind and recognize its numerous target proteins.

Among the target proteins bound and regulated by CaM are the nitric oxide synthase (NOS) enzymes (E.C. 1.14.13.39). These enzymes catalyze the production of nitric oxide (•NO) that acts as a secondary inter- and intracellular messenger involved in many physiological processes (Alderton *et al.*, 2001). There are three NOS isozymes found in mammals: neuronal NOS (nNOS, NOS I), endothelial NOS (eNOS, NOS III), and inducible (iNOS, NOS II). The NOS enzymes are homodimeric with each monomer containing an *N*-terminal oxygenase domain and a *C*-terminal reductase domain. The oxygenase and reductase domains are connected by a CaM binding domain that is required for efficient electron transfer from the reductase to the oxygenase domain for •NO

* The results in this section have been submitted for publication: JBC/2011/325035
Unless otherwise stated, all of the work reported in this chapter was performed and analysed by the candidate.

production (Alderton *et al.*, 2001, Daff 2010). CaM binds and activates the Ca^{2+}- dependent constitutive NOS (cNOS) enzymes, eNOS and nNOS, at elevated cellular Ca^{2+} concentrations. In contrast, iNOS is controlled at the transcriptional level *in vivo* by cytokines and binds to CaM in a Ca^{2+}-independent manner. A conformational change that is associated with CaM binding is required for electron transfer within NOS enzymes (Ghosh and Salerno, 2003). The large conformational change that CaM induces in the reductase domain of the NOS enzymes allows for the FMN domain to interact with both the FAD to accept electrons and pass the electrons on to the heme during catalysis (Welland and Daff, 2010). Clearly, these conformational changes caused by CaM are important in stimulating efficient electron transfer within the NOS enzymes.

There is considerable interest in understanding the structural basis of CaM's target protein interactions and diverse regulatory functions. It is well established that CaM is able to interact with its target enzymes in many different conformations (Ikura and Ames, 2006). For all three mammalian NOS isoforms, x-ray crystallographic and biophysical investigations indicate that CaM binds to peptides coding for their CaM-binding region in an anti-parallel orientation and a collapsed conformation (Spratt *et al*., 2011). While crystallographic studies provide considerable insight into CaM regulatory functions, further understanding of the process would come from solution structures of the CaM complexes.

This present investigation was designed to determine the NMR structures of CaM bound to peptides coding for the iNOS and eNOS CaM binding elements. This was then followed by a comparison of the dynamic properties of both complexes in solution to gain a better understanding of the different binding affinities exhibited between CaM and each NOS CaM binding domain. This approach was also used to investigate the structural consequences associated with the post-translational modification of a known phorphorylation site in the CaM protein. To accomplish this, a

phosphomimetic CaM Y99E mutant protein was used and an NMR comparison study was performed.

3.2 Experimental Procedures

3.2.1 Mutagenesis of CaM

The QuikChange site-directed mutagenesis procedure (Wang and Malcolm, 1999) was used to produce vectors coding for CaM Y99E and CaM Y99Q in the kanamycin resistant pET9dCaM plasmid (Spratt *et al.*, 2006). The primers used to construct CaM Y99E and CaM Y99Q are summarized in Table 3.1. The resulting vectors were confirmed by DNA sequencing.

Table 3.1: DNA oligonucleotides used to mutate CaM at residue Y99

Primer	Oligonucleotide sequence (5'-3')
CaMY99Efor	AAGGATGGCAATGGC**GAG**ATCAGTGCAGCA**GAGCTC**CGCCACGTGATGAC
CaMY99Erev	GTCATCACGTGGCG**GAGCTC**TGCTGCACTGAT**CTC**GCCATTGCCATCCTT
CaMY99Qfor	AAGGATGGCAATGGC**CAG**ATCAGTGCAGCA**GAGCTC**CGCCACGTGATGAC
CaMY99Qrev	GTCATCACGTGGCG**GAGCTC**TGCTGCACTGAT**CTG**GCCATTGCCATCCTT

3.2.2 CaM protein expression and purification

Wild-type CaM and mutant CaM proteins were expressed and purified using phenyl sepharose chromatography, as previously described in section 2.2.2. Isolation of the CaM proteins was confirmed by ESI-MS (Table 3.2) and purity was judged to be > 95% by SDS-PAGE. The human iNOS (residues 510-531) and eNOS (residues 491-512) peptides were synthesized and purchased from Sigma and their respective sequences are found in Figure 1.10.

Table 3.2: Masses of CaM proteins

CaM proteins	Mass (Da) [a]	
	Observed	Theoretical [b]
Wild-type CaM	16706	16706
CaM Y99E	16671	16672
CaM Y99Q	16671	16671

[a] Masses of deconvoluted ESI-MS spectra were determined with an accuracy of ± 5 Da.
[b] Calculated masses based upon amino acid sequence.

3.2.3 NOS expression and purification

The expression and purification of NOS in this study was performed by Kathryn Futrega, a previous graduate student in our laboratory. Rat nNOS and bovine eNOS were expressed as previously described (Montgomery *et al*., 2000, Newman *et al.*, 2004) with the exception that these constructs had an N-terminal polyhistidine tail cloned upstream from their respective start codons. Human iNOS carrying a deletion of the first 70 amino acids and an N-terminal polyhistidine tail was co-expressed with wild-type CaM or the mutant CaM protein in *E. coli* BL21 (DE3) as previously described (Spratt *et al.,* 2006). The purification of each NOS enzyme involved ammonium sulfate precipitation, metal chelation chromatography, and 2′5′-ADP sepharose chromatography (Spratt *et al.,* 2006).

3.2.4 Enzyme kinetics

The enzyme kinetics in this study was performed by Kathryn Futrega, a previous graduate student in our laboratory. Electron transfer rates in the NOS enzymes were monitored using the NADPH oxidation, cytochrome *c* reduction, and the oxyhemoglobin capture assays, as previously described (Spratt *et al.,* 2006, Montgomery *et al.,* 2000, Newman *et al.,* 2004). Assays were performed in 96-well microtitre plates in 100 μL total well volumes at 25 °C in a SpectraMax 384 Plus 96-well UV–visible spectrophotometer using Soft Max Pro software (Molecular Devices, Sunnyvale, CA). 200 μM $CaCl_2$ or 250 μM EDTA, as well as 3 μM wild-type CaM or CaM mutant proteins were added to the appropriate samples.

3.2.5 NMR Experiments

3.2.5.1 Sample preparation for NMR investigation

The expression and purification of isotopically labeled wild-type CaM produced for this study were performed by Don Spratt (PhD, 2008, U. of Waterloo), a previous graduate student in our laboratory.

Wild-type CaM and CaM Y99E for NMR experiments were expressed in M9 media

containing 2g/L ^{13}C-glucose and 1g/L $^{15}NH_4Cl$ (Table 2.2, except that kanamycin was used instead of ampicillin). ^{13}C-^{15}N wild-type CaM and ^{15}N CaM Y99E were purified as described above. The samples were prepared for NMR experiments via a buffer exchange into NMR buffer (100 mM KCl, 10 mM $CaCl_2$, 0.2 mM NaN_3, 90% H_2O/10% ^2H_2O) at pH 6.0 using Ym10 centrifugal filter devices (Millipore Corp., Billerica, USA). All NMR samples contained at least 1 mM ^{13}C-^{15}N-wild-type CaM or ^{15}N-CaM Y99E in a total volume of 500 µL. The samples were transferred into 5 mm 7" NMR sample tubes and stored at 4^{o}C until required for NMR experiments. NMR experiments on the complexes were conducted on samples titrated with either iNOS or eNOS peptide to saturation in a 1:1 CaM:peptide ratio. Complex formation was monitored after each addition by acquisition of a ^{15}N-HSQC spectrum. The isotope labeled iNOS peptide was prepared as described in section 2.2.

3.2.5.2 NMR spectroscopy and data analysis

Most of the NMR data were acquired prior to the start of this study by Dr. Thorsten Dieckmann. NMR spectra were recorded at 25^{o}C on Bruker 600 and 700 MHz DRX spectrometers equipped with ^{1}H/^{13}C/^{15}N triple-resonance probes with XYZ-gradients (Bruker, Billerica, MA, USA). Spectra were analyzed using the program CARA (Computer Aided Resonance Assignment) version 1.8.4 (Keller, 2005) as described in section 2.2.6.3.

The expression and purification of the various isotopically labeled CaM constructs produced peptide-free holo-CaM, unlike the expression of isotopically labeled iNOS peptide, which had CaM bound in a 1:1 ratio. However, we require CaM bound to the various NOS peptides we are determining the structure of. To obtain the complex, synthetically made iNOS or eNOS peptide (Sigma-Aldrich) was titrated into the CaM NMR solution. The synthetic NOS peptides were prepared by dissolving the powdered peptide in water to produce a concentration of 1 mM, aliquot into 200 µL and 100 µL fractions in 0.5 mL Eppendorf tubes and then lyophilized. To achieve the desired 1:1

binding ratio, aliquots of the lyophilized NOS peptides were titrated into the NMR solution of CaM and the ^{15}N-HSQC experiment was used to monitor the disappearance of the free CaM peaks and the appearance of the peaks of CaM in complex with the NOS peptides. The final saturated samples were used to run the rest of the NMR experiments using the Bruker 600 or 700 MHz NMR spectrophotometers.

Specific assignments of the backbone resonances were achieved using a combination of 3D triple resonance experiments including HNCA, HN(CO)CA, CBCA(CO)NH, and HNCO (Grzesiek and Bax, 1992, Muhandiram and Kay, 1994). Side-chain resonances were assigned using the TOCSY type experiments HC(C)H-TOCSY, (H)CCH-TOCSY and H(CCO)NH (Bax *et al.*, 1990).

3.2.5.3 Structure calculation

The ^{1}H, ^{13}C and ^{15}N resonance assignments were utilized to identify constraints for the structure calculations. For CaM and the iNOS peptide these were obtained from ^{15}N-NOESY-HSQC and ^{13}C-NOESY-HSQC spectra (Clore and Gronenborn, 1991, Fesik and Zuiderweg, 1990). In addition, dihedral angle restraints were derived from chemical shift analysis with TALOS+ (Shen *et al.*, 2009). CNSsolve (Brunger *et al.*, 1998) was used to perform the structure calculations using standard simulated annealing protocols. Constraints for the solution structure of CaM-eNOS peptide were derived from ^{15}N-NOESY-HSQC and ^{13}C- NOESY-HSQC spectra acquired on samples containing labeled CaM and unlabeled peptide. The peptide structure in this complex was modeled as an α-helix based on previous structure studies (Aoyagi *et al*., 2003) and positioned within the complex by the intermolecular NOEs identified in the NOESY spectra during the structure calculation. In addition dihedral angle restraints from chemical shift analysis with TALOS+ (Shen *et al.*, 2009) were used for CaM, along with secondary structure based helical dihedral angles for the eNOS peptide.

3.2.6 Model of CaM Y99E-eNOS peptide

The model of CaM Y99E-eNOS peptide was calculated similar to CaM-eNOS using CNSsolve (Brunger *et al.*, 1998). The calculation used the structural constraints input in the calculation of the CaM-eNOS peptide structure, except that the atoms of Glu were substituted for those of Tyr 99. All restraints involving the backbone atoms of Tyr99 were left in the input data as constraints for the backbone atoms of Glu, whereas, all constraints involving the side chain atoms of Tyr99 were removed. The average of the 20 lowest energy structures was used for the model of the structure of CaM Y99E-eNOS.

3.2.7 Delphi calculation of the CaM structures

Delphi electrostatic potentials of the CaM-eNOS and CaM Y99E-eNOS structures were calculated using the DelPhiController interface of UCSF Chimera 1.5.3 build 33475 (Pettersen *et al.*, 2004). The parseres atomic radii file and atomic charge file were used as the input files in the calculation. The electrostatic potential surface was viewed in Chimera.

3.3 Results and Discussion

The three dimensional structures of different regions of NOS enzymes, but not the holoenzyme, have been determined by x-ray crystallography (Daff, 2010). In several of the regions of interest, electron density was absent or weak, an indication of being crystallographically disordered and by inference, flexible. These studies were not able to give a direct measure of that flexibility. In contrast, NMR solution structure studies can provide information on the dynamic regions of proteins. Since cytoplasmic proteins function in solution, it is crucial to obtain detailed information about their structure in solution. Furthermore, although protein solution structures are often quite similar to their crystal structures, there are examples where they may be somewhat or completely different (Bertini *et al.*, 2009). The latter case has been reported when investigating the backboned dynamics of CaM in

solution (Barbato *et al.*, 1992).

In the present investigation, we have determined the three dimensional solution structure of CaM bound to the human iNOS CaM-binding element. This was made feasible by the development a novel expression and purification system that allows for the production of individually stable isotope labeled aggregation prone proteins described in chapter 2.

3.3.1 Structure of CaM-iNOS CaM binding peptide complex

The NMR assignment of the CaM-iNOS complex followed a similar procedure as that of the iNOS peptide in section 2.3.4. However, as mentioned above, the iNOS peptide had to be titrated into the ^{13}C-^{15}N CaM solution to achieve the 1:1 binding of CaM to iNOS peptide. This was done by acquiring a ^{15}N-HSQC after each titration of iNOS and monitoring the shift changes of the CaM amide peaks (shown in Figure 3.1). The titration of CaM with iNOS exhibited a slow exchange, where, as the titration proceeded, one could see that the intensity of the amide peak of the unbound CaM decreased as the intensity of the amide peak of the iNOS bound CaM increased. The sample was considered to be fully bound to the iNOS peptide when the peak of free CaM disappeared and only the peak of bound CaM was visible. This saturated sample was used for all other NMR experiments.

Using the results of these ^{15}N-HSQC spectra from the iNOS peptide titration (Figure 3.1), along with the NMR peak list of holo-CaM from Biological Magnetic Resonance Bank (BMRB) file 6541 (Ikura *et al.*, 1990), some amino acid residues were tentatively assigned and used as starting points in the backbone sequence assignment. The starting points used were the amide peaks of residues outside the middle cluster of peaks in Figure 3.1.

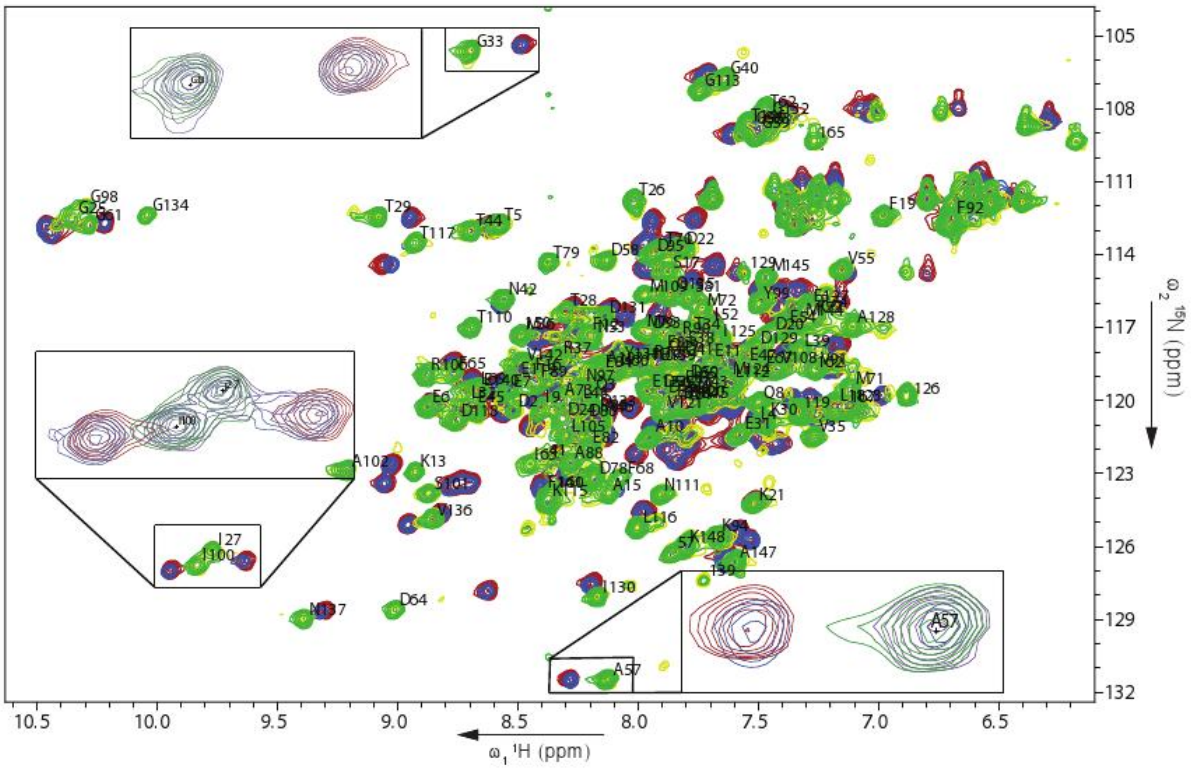

Figure 3.1: Overlay of 15N-HSQC spectra of holo-CaM being titrated with iNOS peptide.
The initial ^{15}N-HSQC spectrum of CaM (red) was overlaid with the spectra of different ratios of iNOS peptide to Ca^{2+}-CaM. The ratios are 1:3 ratio (blue), 2:3 ratio (purple) and 1:1 ratio (green). The HSQC spectra show amino acid residue assignments determined for the peptide-bound CaM

The NMR analysis of the labeled CaM with iNOS peptide (Figure 3.2A) followed routine procedures with the backbone resonance assignment based primarily on 3D triple resonance techniques. The HNCA experiment (Figure 3.2B) was supported by CBCA(CO)NH and HN(CO)CA experiments. This combination of techniques resulted in complete backbone assignments for CaM, with the exception of the prolines and the first two N-terminal amino acids (Appendix B). Subsequently, sidechain resonances were assigned using HC(C)H-TOCSY, (H)CCH-TOCSY and H(CCO)NH experiments. NOEs for structure determination of the iNOS peptide bound to CaM were extracted from ^{15}N-edited NOESY and $^{13}C_{ali}$-NOESY experiments (Figure 3.3).

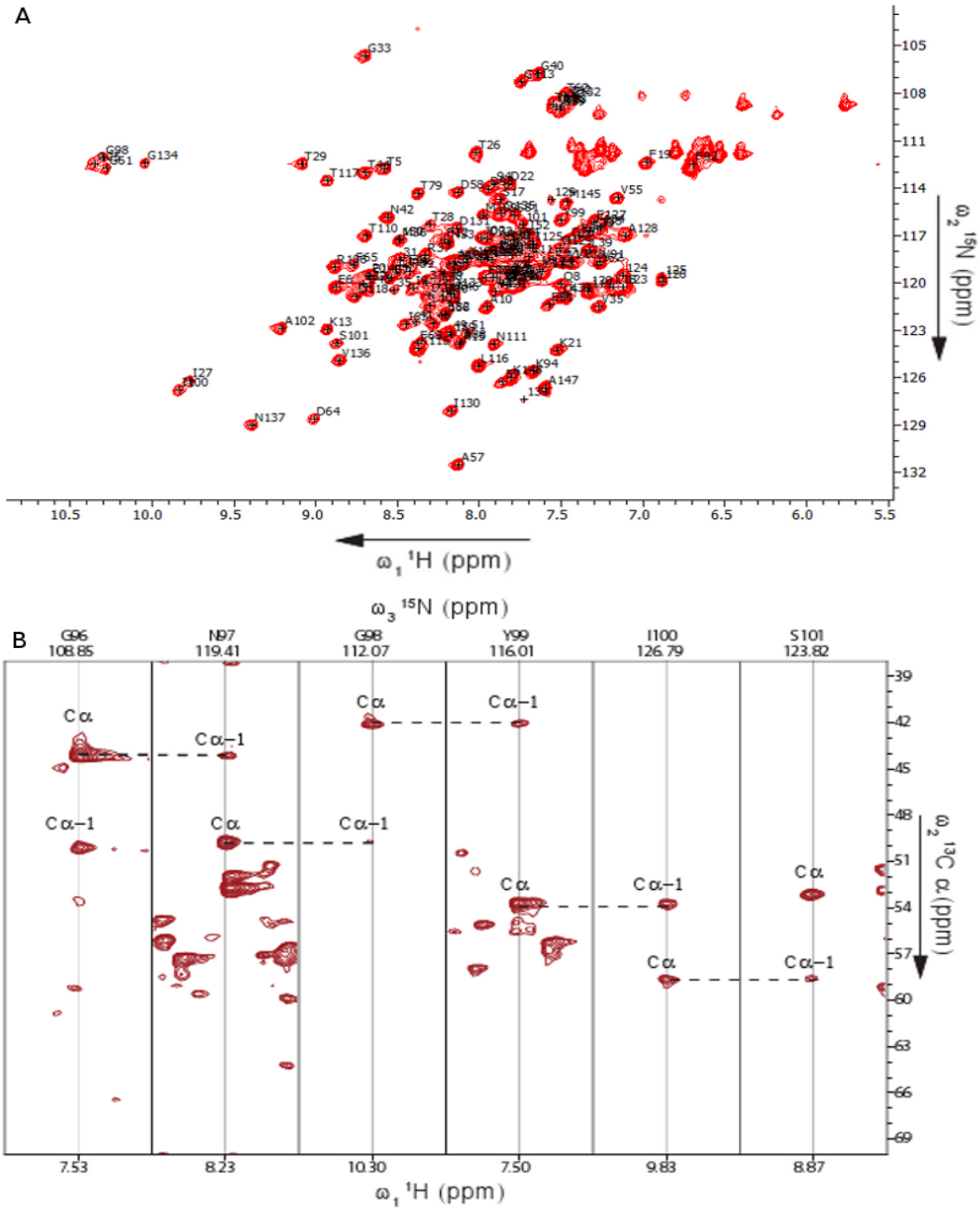

Figure 3.2: Composite figure of NMR structural data

(A) ^{1}H-^{15}N HSQC spectrum of the iNOS CaM-binding region peptide. The unlabeled peaks originate from N-terminal region of the peptide. (B) 3D HNCA strips of sequential amino acids Gly96 to Ser101 of the iNOS CaM-binding region peptide. The connection between the alpha carbon of the previous and successor residue are shown. The peaks are numbered as per residue number from full iNOS protein.

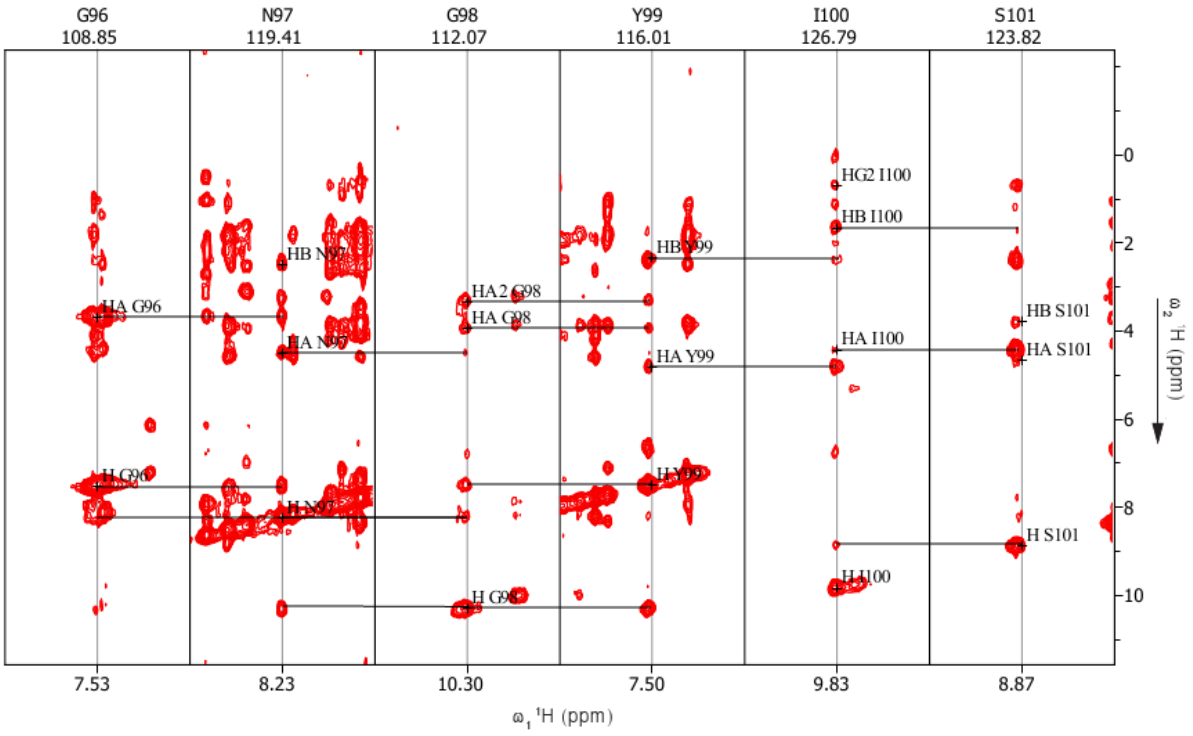

Figure 3.3: ^{15}N-NOESY-HSQC of CaM-iNOS peptide.

3D ^{15}N-NOESY-HSQC strips of sequential amino acids Gly96 to Ser101 of CaM from the CaM-iNOS complex. The connection between: NH_i and NH_{i+1}; $H\alpha_i$ and NH_{i+1}; and $H\beta_i$ and NH_{i+1} can be seen.

The three dimensional solution structure of CaM bound to the human iNOS CaM binding domain peptide (CaM-iNOS) was determined using multi-dimensional heteronuclear NMR spectroscopy. The structure of the complex is based on a large number of experimental constraints and is well defined. Structure statistics are summarized in Table 3.3. The family of 20 final structures is shown in Figure 3.4A. Residues 1-12 at the *N*-terminus of the iNOS CaM binding region peptide were not included in the structure calculation because they could not be unambiguously assigned. This is likely due to this region being highly mobile and unstructured as was seen previously in the crystal structure determined by Xia et al (2009). These residues include part of the intein cleavage site and restriction enzyme cutting site from the peptide production as well as residues 510-514 from the

iNOS peptide, as described in section 2.4.

Table 3.3: Statistics for the CaM-iNOS peptide structural ensemble

		CaM-iNOS Complex	
NMR-derived distance and dihedral angle restraints			
NOE constraints	Calmodulin	iNOS peptide	CaM-iNOS complex
Short-Range $\|i-j\| \leq 1$	714	52	N/A
Sequential	956	92	N/A
Medium-Range $1 \leq \|i-j\| < 4$	572	65	N/A
Long-Range $\|i-j\| > 4$	237	1	N/A
Total	2480	210	99
Dihedral angles from TALOS+	266	14	N/A
Total number of restraints		3069	
Structure statistics for the 20 lowest energy structures			
Mean deviation from ideal covalent geometry			
Bond lengths (Å)		0.009	
Bond angles (deg.)		1.0	
Average pairwise RMSD (Å) for all heavy atoms of the 20 lowest energy structures	All Residues	Ordered Residues[a]	Selected Residues[b]
Backbone Atoms	0.8	0.7	0.7
Heavy Atoms	1.2	1.2	1.2
Ramachandran statistics (%)			
Residues in most favored region		90.5	
Residues in additional allowed regions		7.9	
Residues in generously allowed region		1.7	
Residues in disallowed region		0.0	

[a]Ordered residue ranges: 3A-147A,150B-164B
[b] Selected residue ranges: 3A-147A,150B-164B

When the crystal (PDB 3HR4) and solution structures of the CaM-iNOS are superimposed (Figure 3.4B,C), the RMS difference between the two backbones was found to be 1.5 Å for CaM and 1.1 Å for the iNOS peptide. There is a slight reorientation between the two structures in helix B and C (see Figure 3.9 for helix nomenclature), with the crystal structure having a closer packing of the helices relative to the bound peptide. Overall, the solution structure is quite similar to the previously reported crystal structure of CaM-iNOS.

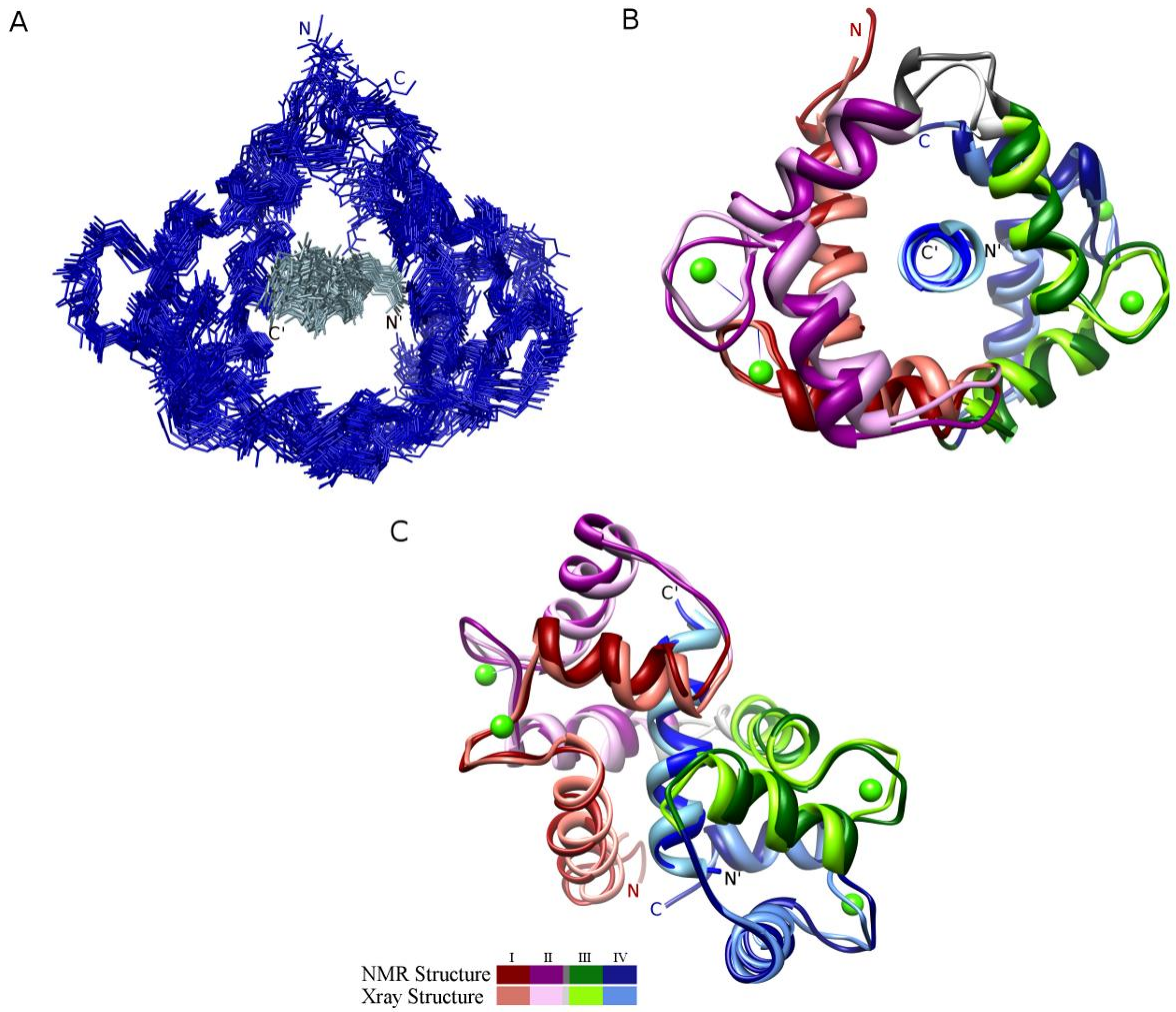

Figure 3.4: Solution structures of CaM bound to iNOS CaM binding peptides.

(A) Superposition of the ensemble of the 20 lowest energy calculated NMR solution structures of CaM bound to the iNOS peptide. Backbone atom traces of CaM are shown in dark blue and the iNOS peptide are shown in light blue. (B,C) Superpositions of the solution structures with the previously determined crystal structures for CaM-iNOS. Comparison of solution structure of CaM-iNOS peptide (dark colors) with the crystal structure (light colors) from PDB code 3HR4 by superimposing the two structures and viewing it along the bound peptide from its C-terminus (B) and rotated 90° with the C-terminus of the bound peptide on top (C). Residues 1-40 of CaM (EF Hand I) are colored red, 41-79 (EF Hand II) are purple, 80-114 (EF Hand III) are green, and 115-148 (EF Hand IV) are blue. The peptide is colored in a lighter blue. Calcium ions from the crystal structure are shown as green spheres.

3.3.2 Structure of CaM-eNOS CaM binding peptide complex

The NMR assignment of the CaM-eNOS complex followed the same procedure as that of the CaM-iNOS complex in section 3.3.1. The titration of CaM with eNOS also exhibited slow exchange, like the titration of CaM with iNOS. The sample was considered to be fully bound to the eNOS peptide when the peak of free CaM disappeared and only the peak of bound CaM was visible.

The NMR analysis of the labeled CaM with eNOS peptide followed routine procedures with the backbone resonance assignment based primarily on 3D triple resonance techniques. The HNCA experiment was supported by CBCA(CO)NH and HN(CO)CA experiments. This combination of techniques resulted in complete backbone assignments for CaM, with the exception of the prolines and the first two N-terminal amino acids (Appendix C). Subsequently, sidechain resonances were assigned using HC(C)H-TOCSY, (H)CCH-TOCSY and H(CCO)NH experiments. NOEs for structure determination of the eNOS peptide bound to CaM were extracted from ^{15}N-edited NOESY and $^{13}C_{ali}$-NOESY experiments. The three dimensional solution structure of CaM bound to the human eNOS CaM binding domain peptide (CaM-eNOS) was determined using multi-dimensional heteronuclear NMR spectroscopy. The structure is also well defined as shown by superimposing the final 20 structures (Figure 3.5A). Structure statistics are summarized in Table 3.4.

Table 3.4: Statistics for the CaM-eNOS peptide structural ensemble

		CaM-eNOS Complex	
NMR-derived distance and dihedral angle restraints			
NOE constraints	Calmodulin	eNOS peptide	CaM-eNOS complex
Short-Range $\|i-j\| \leq 1$	648	41[a]	N/A
Sequential	750	84[a]	N/A
Medium-Range $1 \leq \|i-j\| < 4$	341	60[a]	N/A
Long-Range $\|i-j\| > 4$	239	0	N/A
Total	1978	185[a]	43
Dihedral angles from TALOS+	270	14[a]	N/A
Total number of restraints		2491	
Structure statistics for the 20 lowest energy structures			
Mean deviation from ideal covalent geometry			
Bond lengths (Å)		0.009	
Bond angles (deg.)		0.9	
Average pairwise RMSD (Å) for all heavy atoms of the 20 lowest energy structures	All Residues	Ordered Residues[b]	Selected Residues[c]
Backbone Atoms	1.2	1.1	1.1
Heavy Atoms	1.7	1.6	1.6
Ramachandran statistics (%)			
Residues in most favored region		89.8	
Residues in additional allowed regions		10.0	
Residues in generously allowed region		0.1	
Residues in disallowed region		0.0	

[a] Modeled constraints
[d] Ordered residue ranges: 3A-41A,43A-55A,57A-78A,80A-114A,117A-147A,152B-164B
[e] Selected residue ranges: 3A-41A,43A-55A,57A-78A,80A-114A,117A-147A,152B-164B

The larger RMSD value for the family of CaM-eNOS structures compared to that of the CaM-iNOS structures is likely due to the smaller number of NOE constraints used in the structure calculation. This was due to the lack of a sample with stable isotope labeled eNOS peptide.

When the crystal (PDB 1NIW) and solution structures of the CaM-eNOS complex are aligned (Figure 3.5B,C) a RMSD of 2.3 Å for the backbone atoms of CaM was found. Each of the lobes of CaM and the peptide individually superimpose well on each other. However, the relative orientation

of the lobes to each other and the peptide is less well defined due to the smaller number of inter molecular NOEs. Nevertheless, the comparison with the crystal structure of CaM-eNOS showed that the solution structure adopts the same overall conformation

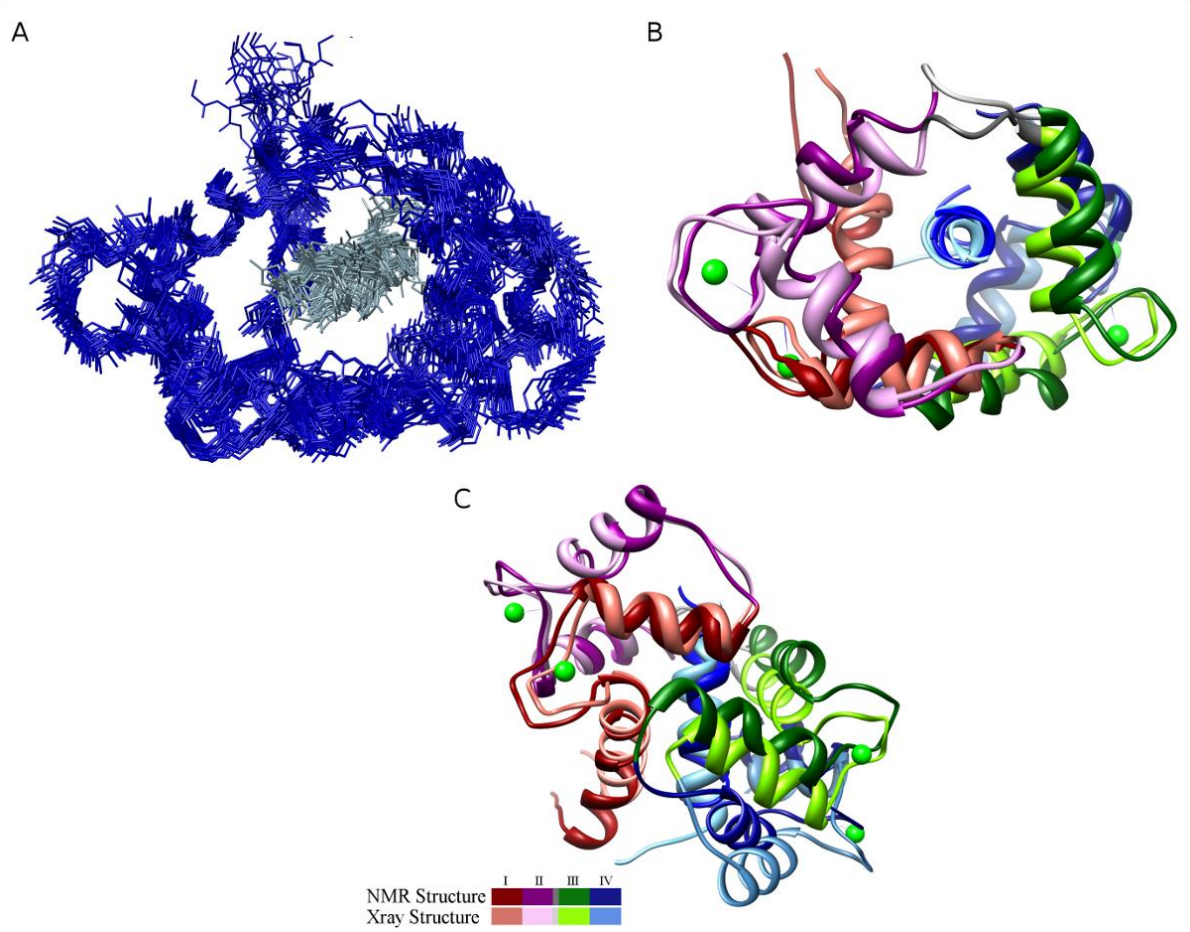

Figure 3.5: Solution structures of CaM bound to eNOS CaM binding peptides.

(A) Superposition of the ensemble of the 20 lowest energy calculated NMR solution structures of CaM bound to the the eNOS peptide. Backbone atom traces of CaM are shown in dark blue and the eNOS peptide are shown in light blue. (B,C) Superpositions of the solution structures with the previously determined crystal structures for CaM-eNOS**.** Comparison of solution structure of CaM-eNOS peptide (dark colors) with the crystal structure (light colors) from PDB code 1NIW by superimposing the two structures and viewing it along the bound peptide from its C-terminus (B) and rotated 90° with the C-terminus of the bound peptide on top (C). The color scheme is the same as in figure 3.4. Calcium ions from the crystal structure are shown as green spheres.

3.3.3 Comparison of the CaM-iNOS vs CaM-eNOS complexes

There are a number of studies indicating a stronger interaction exists between the iNOS peptide and CaM when compared to the association between the eNOS and CaM, including almost a threefold difference in their dissociation constants (Venema *et al.*, 1996).

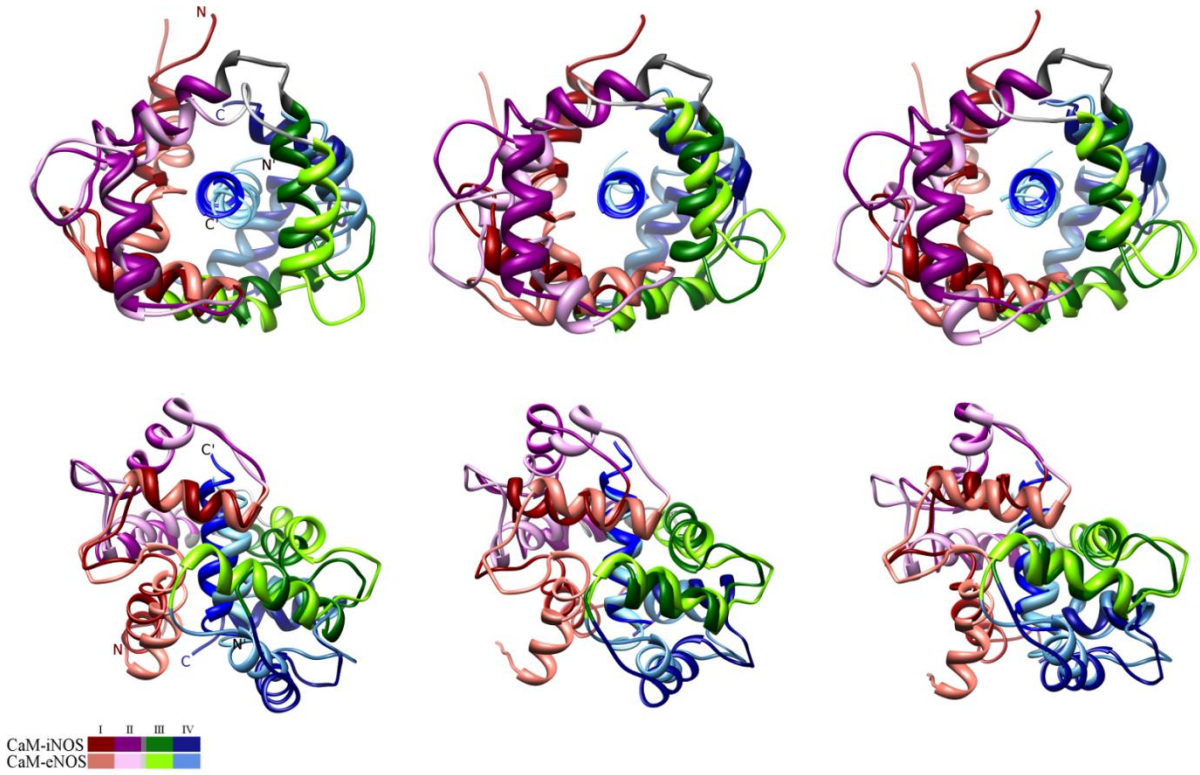

Figure 3.6: Superpositions of the CaM-iNOS peptide solution structure (dark colors) and the CaM-eNOS peptide solution structure (light colors).

The two structures are aligned by superimposing backbone atoms of the CaM *N*- lobe (left column), the bound peptides (middle column) and the CaM *C*- lobe (right column). The CaM-peptide complexes are viewed along the bound peptide helix from its C-terminus (C') to its N-terminus (N') in the top row, and rotated 90° around the horizontal axis with the C-terminus of the bound peptide on the top in the bottom row. The color scheme is the same as in figure 3.4.

When the solution structure of CaM-iNOS was superimposed onto that of the CaM-eNOS structure, there were apparent differences in the relative orientations of the lobes (Figure 3.6). When aligned with respect to the backbone atoms of the *N*-lobe, the iNOS peptide is shifted closer to the *N*-

lobe of CaM than the eNOS peptide, indicating that it is more tightly bound. This is consistent with results reported for the crystal structures of these two NOS isoforms (Aoyagi *et al.,* 2003, Xia *et al*., 2009). There is also a difference in the orientation of helix A of CaM between the two structures, with helix A of CaM-eNOS shifted towards the N-terminus of the eNOS peptide.

When the two structures are aligned with respect to the NOS peptide backbone atoms (Figure 3.6, middle structures) the *C*-lobes of the two CaM complexes are aligned closer to each other than the respective *N*-lobes. In comparison with the CaM-eNOS complex, the *C*-lobe of CaM-iNOS is rotated clockwise, by ~15°, around the peptide helix, and the *N*-lobe is rotated ~30°. This suggests that the eNOS *N*-lobe adopts a more open conformation thereby exposing larger surface areas of the protein for interaction with CaM and its target protein. Previous studies in our lab have shown that the *N*-lobe of CaM alone can activate iNOS to around 70% full activity while the *C*-lobe can only stimulate the enzyme about 10% of wild type CaM (Spratt *et al.,* 2006). Neither of these two lobes could stimulate the eNOS enzyme. In addition, repeated attempts failed to remove the *N*-lobe of CaM from the iNOS enzyme (Spratt *et al.,* 2006, Spratt *et al.,* 2007). The present results showing a closer association of the CaM *N*-lobe with the iNOS peptide when compared to the eNOS peptide further support the proposal that this lobe of CaM is principally responsible for the tighter binding of CaM. The CaM *N*-lobe forms a more stable structure with the iNOS peptide due to hydrophobic interactions. Several NOEs are found from helix C residues (Met51 and Val55) to Leu 523 and helix D residues (Met72, Lys75 and Met76) to Met 522 in the iNOS peptide. In contrast, the *N*-lobe has significantly less NOEs for helix C and D residues to the eNOS peptide.

When aligned with respect to the backbone atoms of the *C*-lobe of CaM, helix E and F of the two CaM complexes are in slightly different conformation with respect to each other. In addition one

can see the same degree of rotation as observed when aligning the structures via the NOS peptide backbone atoms.

In all three views from Figure 3.6, the central linker regions (residues 77-81) of the two complexes are in different loop conformations. The CaM-eNOS linker region loop is more unfolded and resides closer to the helical peptide than the CaM-iNOS loop. This could in part account for the more open structure of the eNOS complex. The central linker of the CaM-eNOS structure is elongated when compared to that of the CaM-iNOS structure, having residues 75 and 76 being unwound from helix D. The linker region of CaM-iNOS also has a higher pitch than that of CaM-eNOS, due to the large hydrophobic interactions of helix C and D with the iNOS peptide.

3.3.4 Conformational dynamics of CaM-iNOS and CaM-eNOS peptide complexes

The difference in the relative strength of the interactions between CaM and the two target peptides used in this study was investigated by measuring the relaxation properties of the backbone ^{15}N nuclei in CaM. T_1, T_2, and ^{1}H-^{15}N NOE values were measured (Figure 3.7 and Appendix E-G). The standard model free approach (Lipari and Szabo, 1982) was used to determine order parameters (S^2) for each of the CaM-peptide complexes and summarized in Figure 3.7 and shown as a worm structure in Figure 3.9. The two complexes have similar overall characteristics. The binding of CaM to the peptide causes the linker region to adopt a more rigid conformation compared to free CaM (Figure 3.8) as illustrated by the higher S^2 values. This has also been seen in other relaxation studies of CaM complexes (Wang *et al.*, 2005). Both the *N*-lobes and central linker regions of the two complexes show similar moderate order parameters. In contrast, when compared to the iNOS complex, the CaM *C*-lobe in the eNOS complex has a higher degree of mobility (smaller S^2 values), especially for the residues in EF hand III. This is consistent with the weaker association of the eNOS peptide.

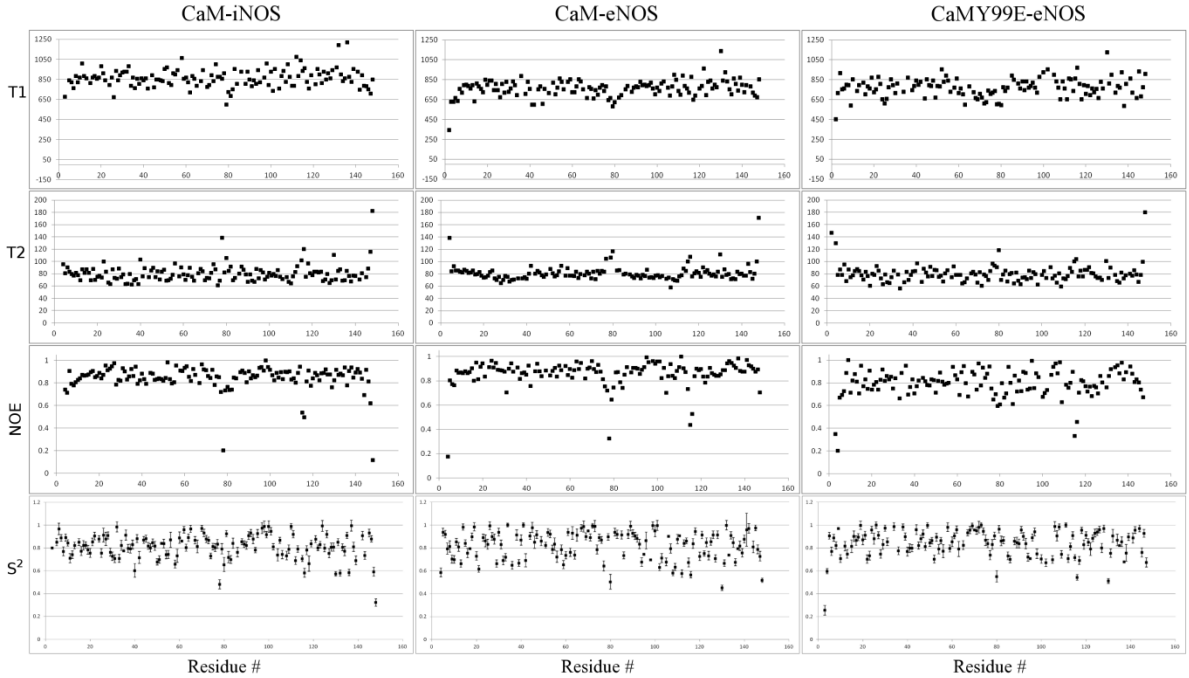

Figure 3.7: Relaxation data for CaM complexes.

Plots as a function of residue number of the measured T1 and T2 values (in ms), the ^{15}N NOE, and the order parameter, S^2. Only residues for which the ^{15}N-^{1}H correlation is sufficiently well resolved to permit accurate measurement of its intensity are included.

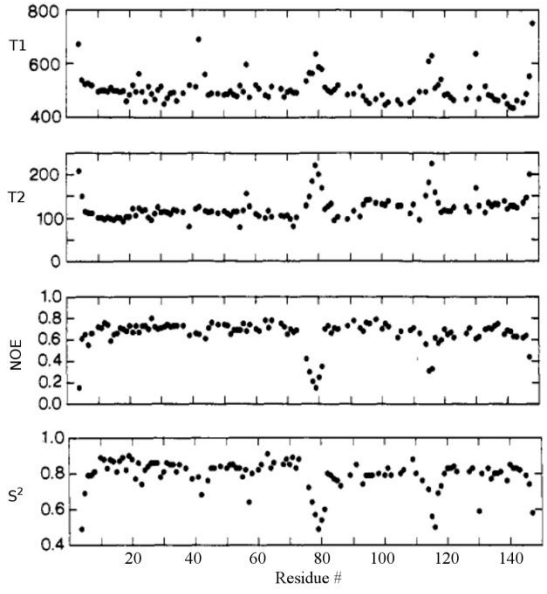

Figure 3.8: Relaxtion data for free CaM.

Plots as a function of residue number of the measured T1 and T2 values, the ^{15}N NOE, and the order parameter, S^2. Data modified from Barbato *et al.*, 1992.

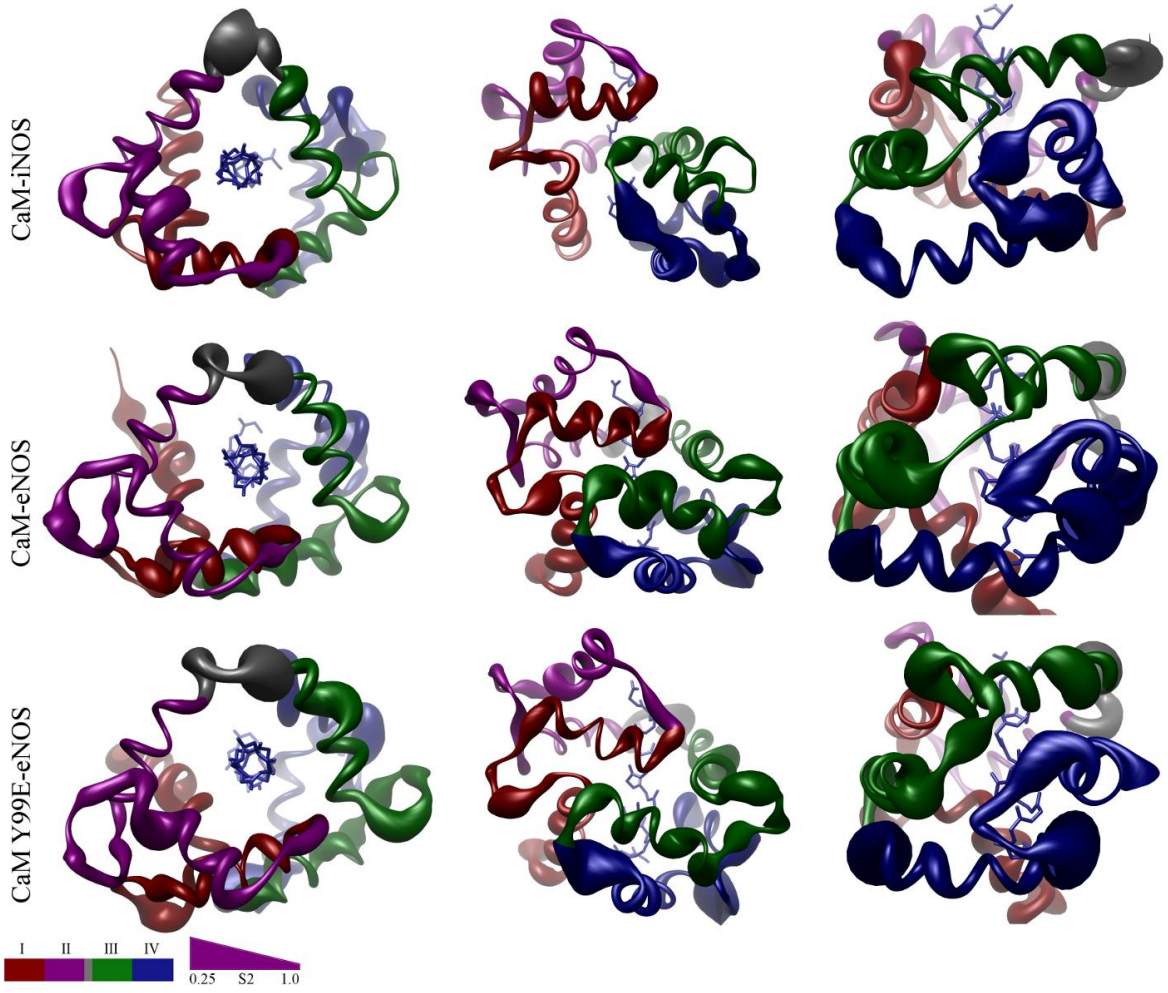

Figure 3.9: Worm models of CaM-iNOS peptide, CaM-eNOS peptide and CaM Y99E-eNOS peptide complexes illustrating the intramolecular dynamics.

The worm models were prepared using UCSF Chimera with the render by attribute function. The worm radius ranges from 0.25, corresponding to a S^2 value of 1, to 4, corresponding to a S^2 value of 0.25. The CaM-peptide complexes are viewed along the bound peptide helix from its C-terminus in the left column, rotated 90° around the horizontal axis with the C-terminus of the bound peptide on the top in the middle column and looking at the interface of EF Hand II and IV) in the right column. The color scheme is the same as in figure 3.4.

3.3.5 Phosphomimetic mutation of CaM Y99 residue

NMR spectroscopy has been shown to be a good method for investigating the structural effects of protein modification (Igumenova *et al.*, 2005). The interaction of CaM with its target proteins is

modified by a number of post-translation modifications including phosphorylation (Jang *et al.*, 2007). For example, of the 18 amino acid residues in CaM that have been proposed as candidates for phosphorylation, only 8 have been verified to undergo this process by known kinases (Benaim and Villalobo, 2002). Four tyrosine kinases are known to phosphorylate tyrosine 99 in CaM. Phosphorylation of CaM residue Y99 has been reported to affect the CaM-dependent activity of a number of enzymes including the NOS enzymes (Corti *et al.*, 1999, Mishra *et al.*, 2009). To assess the potential of NMR structural studies when investigating post translational modifications of proteins, we decided to study the consequences of the phosphorylation of CaM Y99. A comparative investigation was performed on the effect that phosphorylation of this residue has upon the function of all three mammalian NOS isozymes. In order to allow for the structural studies to be performed, a phosphomimetic form of CaM carrying a glutamate residue at position 99 (CaM Y99E) was used in the investigation. Phosphomimetic mutants have been used extensively for the investigation of protein phosphorylation (Greif *et al.*, 2004). The use of the phosphomimetic mutant in our investigation allowed for the straightforward generation of isotopically labeled CaM for structural characterization without the difficulty of producing a specifically phosphorylated, isotope labeled CaM. A second mutant in which tyrosine was replaced by glutamine (Y99Q) was also generated as a control.

CaM binding to NOS enzymes modulates electron transfer within the enzyme and this process can be monitored using NADPH oxidation, cytochrome *c* and oxyhemoglobin capture assays as previously described (Spratt *et al.*, 2008). The effect of the mutations on CaM-dependent activation of all three isoforms of nitric oxide synthase was investigated (Tables 3.5 and 3.6). Both iNOS and nNOS enzymes demonstrate only a small increase in nitric oxide production rates when bound by either of the two mutant CaM proteins. Both enzymes also showed small changes in the rate of

NADPH oxidation and cytochrome *c* reduction. These results indicated that the mutation had little effect on the apparent properties of these enzymes.

Table 3.5: Mutant CaM Protein Activation of iNOS[a]

CaM protein	NADPH oxidation		Cyt *c* reduction		•NO synthesis		
	200 µM $CaCl_2$ %	250 µM EDTA %	200 µM $CaCl_2$ %	250 µM EDTA %	200 µM $CaCl_2$ %	250 µM EDTA %	250 µM EDTA with 3 µM CaM %
CaM	100 ± 2	86 ± 4	100 ± 4	84 ± 5	100 ± 4	87 ± 2	82 ± 2
CaM Y99E	112 ± 7	92 ± 3	120 ± 4	108 ± 5	116 ± 4	90 ± 3	121 ± 3
CaM Y99Q	104 ± 4	90 ± 4	110 ± 4	102 ± 5	108 ± 4	91 ± 2	109 ± 4

[a] •NO synthesis, cytochrome *c* reduction and NADPH oxidation rates were measured with no exogenous CaM added to the assay. Each assay was performed in the presence of either 200 µM $CaCl_2$ or 250 µM EDTA as indicated. The activities obtained for iNOS coexpressed with CaM and assayed in the presence of 200 µM $CaCl_2$ at 25°C were all set to 100% and were 52 min^{-1} (•NO synthesis), 83 min^{-1} (NADPH oxidation) and 1490 min^{-1} (cytochrome *c* reduction).

Table 3.6: Mutant CaM Protein Activation of cNOS Enzymes[a]

	Neuronal NOS			Endothelial NOS		
CaM protein	NADPH Oxidation %	Cyt *c* Reduction %	•NO Production %	NADPH Oxidation %	Cyt *c* Reduction %	•NO Synthesis %
CaM	100 ± 4	100 ± 3	100 ± 2	100 ± 1	100 ± 4	100 ± 2
CaM Y99E	101 ± 5	98 ± 3	104± 3	81± 5	104 ± 4	60 ± 3
CaM Y99Q	93 ± 5	95 ± 5	110 ± 4	91 ± 3	94 ± 5	82 ± 4

[a] The oxyhemoglobin capture assay used to measure the rate of CaM-activated •NO production, the cytochrome *c* assay and the NADPH oxidation assay were performed in the presence of either 3 µM wild-type or mutant CaM protein and either 200 µM $CaCl_2$ or 250 µM EDTA, as indicated. The activities obtained with the respective enzyme bound to wild-type CaM at 25°C in the presence of 200 µM $CaCl_2$ were all set to 100%. The activities for nNOS bound to CaM were 35 min^{-1} (•NO synthesis), 130 min^{-1} (NADPH oxidation) and 1240 min^{-1} (cytochrome *c* reduction). The activities for eNOS bound to CaM were 8 min^{-1} (•NO synthesis), 25 min^{-1} (NADPH oxidation) and 68 min^{-1} (cytochrome *c* reduction).

The eNOS enzyme function was more susceptible to the phosphomimetic mutation showing a decrease of 40% in nitric oxide production while still maintaining full capacity to reduce cytochrome *c*. This suggests that the transfer of electrons from the reductase to the oxidase domain of eNOS was most affected by the mutation. For this reason, it was decided to further investigate the effect of the mutation by obtaining a model of the solution structure of the Y99E CaM bound to the eNOS peptide.

3.3.6 NMR Spectra Indicate altered structure of EF Hands III and IV in CaM Y99E-eNOS

NMR spectroscopy was used to assess changes to the CaM-eNOS complex due to the mutation of Tyr99 to Glu. The complete resonance assignments of CaM-iNOS and CaM-eNOS were used as a reference for investigating the structural dynamics of the Y99E CaM mutant. The process began with obtaining a ^{15}N-HSQC spectrum of the labeled Y99E CaM bound to the eNOS peptide and then overlapping it with the ^{15}N-HSQC obtained for CaM-eNOS, as was done for the iNOS titration in Figure 3.1. Figure 3.10 shows the overlay of the ^{15}N-HSQC spectra of CaM Y99E-eNOS with that of CaM-eNOS. Cross peaks for amides in the N-domain of CaM Y99E overlap with those of CaM, but amides in the *C*-domain, specifically the amides of residues in EF hand III and IV, do not overlap with those of CaM Y99E due to differences in chemical shifts. Almost all of the residues that participate in coordinating the Ca^{2+} ion in EF hands III and IV are affected by changing Tyr99 to Glu.

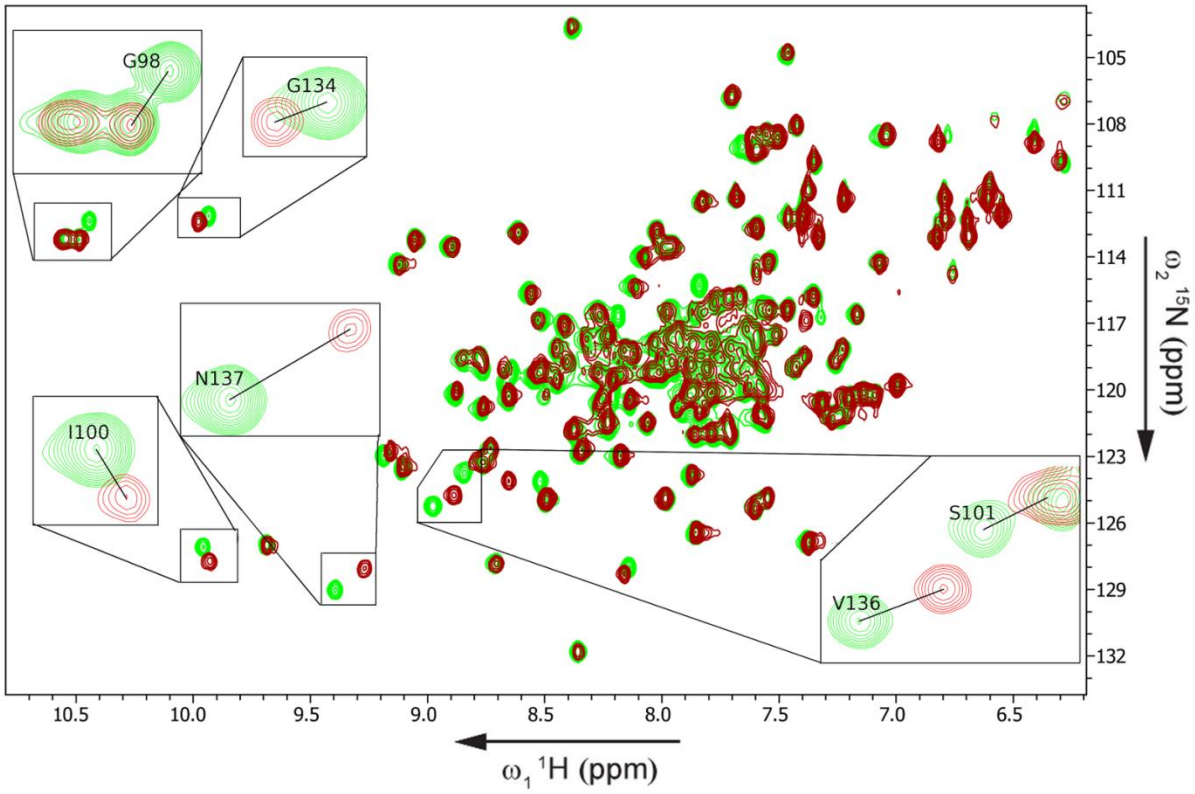

Figure 3.10: Overlay of ^{1}H-^{15}N HSQC spectra of CaM-eNOS peptide complex (green) and CaM-Y99E-eNOS peptide complex (red).

The insets of the overlay of the spectra show representative amide resonances for residues in EF hands III and IV that are affected by the mutation of Tyr99.

Figure 3.11B shows why the mutation of Tyr99 to Glu would result in the chemical shift differences seen in Figure 3.10 and 3.11D. Tyr99 contributes its carbonyl oxygen to the hydrogen bonding network used to stabilize the pentagonal bipyramidal coordination of the Ca^{2+} ion in EF Hand III and is also part of a β-strand that interacts with the β-strand of the EF hand IV loop. A substitution of Tyr99 to Glu would introduce a charge that could cause an electrostatic repulsion between the side chain of Glu and the carbonyl oxygen of Val 136 or Asn 137. These residues are also involved in coordinating the Ca^{2+} ion in EF hand IV, therefore, any shift in their positioning should cause a perturbation in the other Ca^{2+} coordinating residues of EF hand IV. This electrostatic

repulsion should also cause the backbone of Tyr99 to be affected, which should perturb the tertiary geometry of the residues involved in coordinating the Ca^{2+} ion in EF hand III. This would account for the chemical shift changes observed in the overlaying of the ^{15}N-HSQC spectra for the Ca^{2+} coordinating residues of EF hand III and IV.

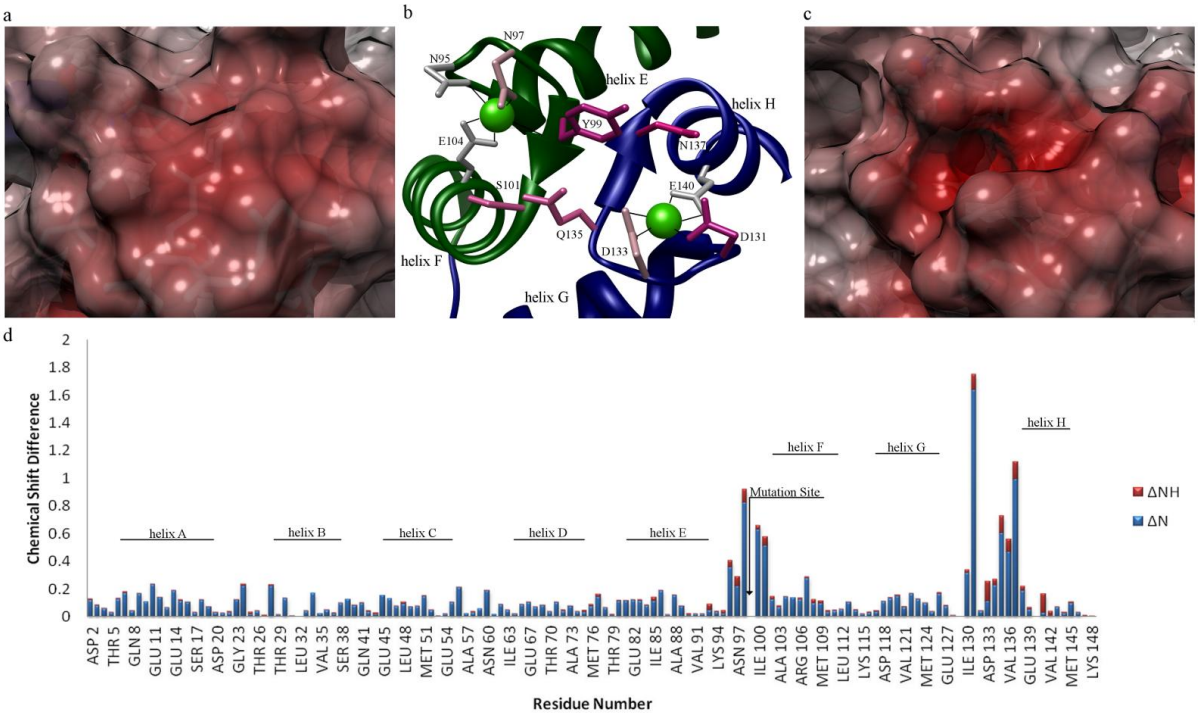

Figure 3.11: Mutation of Tyr99 affects the conformation of EF Hand III and IV.

The Delphi-calculated electrostatic potential maps are projected on the surface of the solution structure of the CaM-eNOS peptide complex (A) and the calculated model of the CaM-Y99E-eNOS peptide complex structure (C). B displays the residues of CaM-eNOS complex that have amide chemical shift differences greater than 0.25. The side chains of these residues are colored from light pink to dark pink corresponding to the increase in the chemical shift difference. The color scheme is the same as in Figure 3.4. D compares the chemical shift differences between CaM-eNOS versus CaM Y99E -eNOS. The greatest differences are localized to Ca^{2+} binding loops of EF hand III (green) and IV (blue).

The introduction of a negative charge in this region due to the mutation would be expected to have structural effects on not only EF hand III but also EF hand IV. This is seen in the chemical shift differences between the wild type and mutant form of CaM bound to the eNOS peptide in Figure

3.11B and D. The analysis of our CaM Y99E model structure with DelPhi illustrates that the mutation causes a more negative potential on the surface of EF hand III (Figure 3.9A,C). This substitution causes a cleft to be formed on the surface of EF hand III. This is most likely due to the large aromatic group of Tyr99 being replaced with the less bulky side chain of Glu. This would likely not be present in the physiology observed phosphorylated Tyr99. This change in the electrostatics on the surface of the protein would have a major effect upon the binding of CaM to its target proteins.

3.3.7 Consequences of the CaM Y99E substitution on conformational dynamics of the complex

The order parameters (S^2) were determined for the CaM Y99E-eNOS peptide complex from ^{15}N relaxation data and compared with the native CaM complex as shown in Figures 3.7 - 3.9. The substitution results in an increase in the dynamic motion of the central linker region. Residue 78 has the lowest S^2 value, thus demonstrating the highest internal dynamics in the linker region in CaM-iNOS, whereas it is residue 80 in CaM-eNOS and CaM Y99E-eNOS that show the highest degree of internal dynamics (Figure 3.7 and 3.9).

The Y99E substitution perturbs both EF hands III and IV resulting in higher mobility for most of the residues that are involved in Ca^{2+} coordination in both regions of the C lobe of CaM. In EF hand III, this perturbation is especially high for residue 100 and other residues surrounding the bound calcium ion including residues in helix E, but the dynamics of residues in helix F are lower (Figure 3.7 and 3.9). The dynamic changes in EF IV associated with the substitution Y99E are mainly found in the linker region between helices G and H and residing closest to the mutation site in the three dimensional structure of the protein (Figure 3.11B).

3.4 Conclusion

From the analysis of the NMR solution structures of both NOS peptides bound to CaM, the overall structures are very similar to the previously reported X-ray crystallographic complexes. A direct comparison of the solution structures indicates that the CaM-eNOS *N*-lobe adopts a more open conformation and a greater surface area for interactions with its target protein. The structural studies indicate that iNOS peptide forms a more stable complex with the *N*-lobe due to hydrophobic interactions. The conformational dynamics results show that the CaM *C*-lobe in the eNOS-CaM complex has a higher degree of mobility. These results are consistent with the significantly higher affinity that exists between CaM and the iNOS CaM binding peptide.

The posttranslational modification of CaM mimicked by replacing a tyrosine by a glutamic acid residue within EF hand III showed only a significant decrease in activity of the eNOS enzyme. The change in activity was associated with alterations in the structure and dynamics of the residues that coordinate the Ca^{2+} ions in both EF hands in the *C*-lobe of CaM. These observations provide important insights into our understanding of why eNOS enzymes require both the lobes of CaM for activation while the iNOS enzyme is active when bound only by the *N*-lobe of CaM.

Chapter 4
Future Work

4.1 Recommendations for Future Studies

4.1.1 NMR structure determination of CaM mutants with NOS peptides

There are a few CaM mutants of interest currently being studied in the lab, including CaM_{12}, CaM_{34} and CaM_{1234}. The CaM_{12} mutant has two mutations in the N domain, consisting of an aspartate residue mutated to an alanine in each of the N-lobe EF hand motifs, that plays a key role in coordinating the Ca^{2+} ion. These mutations make this mutant CaM incapable of binding calcium in the N lobe of the protein. CaM_{34} is similar, however, it is unable to bind calcium in the C-lobe EF hands. And CaM_{1234} has an aspartate mutation in all 4 EF hands making it unable to bind calcium at all.

A recent study by Xiong *et al.* (2010) showed NMR data that indicated this aspartate mutation in each EF hand caused potential structural alterations in the rest of the structure. They showed that the CaM_{34} mutation, which is situated in the C-lobe, caused amide chemical shift differences for residues from the unmodified N-lobe from the analysis of ^{15}N-HSQC spectra. This study was performed with CaM bound to the IQ motif protein PEP-19. These CaM mutants are frequently used in studying if there is a Ca^{2+}-independent association of CaM to its target proteins. CaM_{12} and CaM_{34} are used to determine if there is Ca^{2+}-independent association of CaM to the target enzymes. More specifically, is the association between binding and/or activation of the target enzyme solely due to the Ca^{2+}-free N- or C-terminal lobe of CaM.

In order to provide further evidence of this potential structural change the solution structure determination of these CaM mutants with the NOS peptides should be performed. The NMR

assignments of the determined structures in our previous studies would be used as reference in the determination of the CaM mutant structures.

Appendix A

NMR Pulse Programs

^{15}N-HSQC:

```
# 1 "/opt/xwinnmr/exp/stan/nmr/lists/pp/hsqcetf3gpsi"
;hsqcetf3gpsi
;avance-version (02/07/15)
;HSQC
;2D H-1/X correlation via double inept transfer
; using sensitivity improvement
;phase sensitive using Echo/Antiecho-TPPI gradient selection
;with decoupling during acquisition
;using trim pulses in inept transfer
;using f3 - channel
;
;A.G. Palmer III, J. Cavanagh, P.E. Wright & M. Rance, J. Magn.
; Reson. 93, 151-170 (1991)
;L.E. Kay, P. Keifer & T. Saarinen, J. Am. Chem. Soc. 114,
; 10663-5 (1992)
;J. Schleucher, M. Schwendinger, M. Sattler, P. Schmidt, O. Schedletzky,
; S.J. Glaser, O.W. Sorensen & C. Griesinger, J. Biomol. NMR 4,
; 301-306 (1994)
```

HNCA:

```
# 1 "/opt/xwinnmr/exp/stan/nmr/lists/pp/hncagp3d"
;hncagp3d
;avance-version (02/05/31)
;HNCA
;3D sequence with
; inverse correlation for triple resonance using multiple
; inept transfer steps
;
; F1(H) -> F3(N) -> F2(Ca,t1) -> F3(N,t2) -> F1(H,t3)
;
;on/off resonance Ca and C=O pulses using shaped pulse
;phase sensitive (t1)
;phase sensitive using Echo/Antiecho gradient selection (t2)
;using constant time in t2
;(use parameterset HNCAGP3D)
;
;S. Grzesiek & A. Bax, J. Magn. Reson. 96, 432 - 440 (1992)
;(J. Schleucher, M. Sattler & C. Griesinger, Angew. Chem. Int. Ed. 32,
; 1489-1491 (1993))
;(L.E. Kay, G.Y. Xu & T. Yamazaki, J. Magn. Reson. A109, 129-133 (1994))
prosol relations=<triple>
```

HNcoCA:

```
# 1 "/opt/xwinnmr/exp/stan/nmr/lists/pp/hncocagp3d"
;hncocagp3d
;avance-version (03/08/05)
;HN(CO)CA
;3D sequence with
; inverse correlation for triple resonance using multiple
; inept transfer steps
;
; F1(H) -> F3(N) -> F2(C=O) -> F2(Ca,t1)
; -> F2(C=O) -> F3(N,t2) -> F1(H,t3)
```

;
;on/off resonance Ca and C=O pulses using shaped pulse
;phase sensitive (t1)
;phase sensitive using Echo/Antiecho gradient selection (t2)
;using constant time in t2
;(use parameterset HNCOCAGP3D)
;
;S. Grzesiek & A. Bax, J. Magn. Reson. 96, 432 - 440 (1992)
;(L.E. Kay, G.Y. Xu & T. Yamazaki, J. Magn. Reson. A109, 129-133 (1994))
prosol relations=<triple>

CBCAcoNH:
1 "C:/Bruker/XWIN-NMR/exp/stan/nmr/lists/pp/cbcaconhgpwg3d"
;cbcaconhgpwg3d
;avance-version (02/05/31)
;CBCACONH
;3D sequence with
; inverse correlation for triple resonance using inept transfer steps
;
; F1(H) -> F2(Caliph.,t1 -> Ca) -> F2(C=O) -> F3(N,t2) -> F1(H,t3)
;
;on/off resonance Ca and C=O pulses using shaped pulse
;phase sensitive (t1)
;phase sensitive (t2)
;using constant time in t1
;using constant time in t2
;water suppression using watergate sequence
;(use parameterset CBCACONHGPWG3D)
;
;S. Grzesiek & A. Bax, J. Biomol. NMR 3, 185-204 (1993)
;(D.R. Muhandiram & L.E. Kay, J. Magn. Reson. B 103, 203-216 (1994))
prosol relations=<triple>

^{13}C-NOESY HSQC:
#1 "C:/Bruker/XWIN-NMR/exp/stan/nmr/lists/pp/noesyhsqcetgp3d"
;noesyhsqcetgp3d
;avance-version (02/07/15)
;NOESY-HSQC
;3D sequence with
; homonuclear correlation via dipolar coupling
; dipolar coupling may be due to noe or chemical exchange.
; H-1/X correlation via double inept transfer
; using sensitivity improvement
;phase sensitive (t1)
;phase sensitive using Echo/Antiecho-TPPI gradient selection (t2)
;using trim pulses in inept transfer
;with decoupling during acquisition
;using shaped pulses for inversion on f2 - channel
;(use parameterset NOESYHSQCETGP3D)
;
;A.L. Davis, J. Keeler, E.D. Laue & D. Moskau, J. Magn. Reson. 98,
; 207-216 (1992)
;A.G. Palmer III, J. Cavanagh, P.E. Wright & M. Rance, J. Magn.
; Reson. 93, 151-170 (1991)
;L.E. Kay, P. Keifer & T. Saarinen, J. Am. Chem. Soc. 114,
; 10663-5 (1992)
;J. Schleucher et al., Angew. Chem. 114(10), 1518 (1993)

^{15}N-NOESY HSQC:

```
# 1 "C:/Bruker/XWIN-NMR/exp/stan/nmr/lists/pp/noesyhsqcfpf3gpsi3d"
;noesyhsqcfpf3gpsi3d
;avance-version (03/06/18)
;NOESY-HSQC
;3D sequence with
; homonuclear correlation via dipolar coupling
; dipolar coupling may be due to noe or chemical exchange
; H-1/X correlation via double inept transfer
; using sensitivity improvement
;phase sensitive (t1)
;phase sensitive using Echo/Antiecho-TPPI gradient selection (t2)
;with decoupling during acquisition
;using flip-back pulse
;using f3 - channel
;(use parameterset NOESYHSQCFPF3GPSI3D)
;
;O. Zhang, L.E. Kay, J.P. Olivier & J.D. Forman-Kay,
; J. Biomol. NMR 4, 845 - 858 (1994)
;A.G. Palmer III, J. Cavanagh, P.E. Wright & M. Rance, J. Magn.
; Reson. 93, 151-170 (1991)
;L.E. Kay, P. Keifer & T. Saarinen, J. Am. Chem. Soc. 114,
; 10663-5 (1992)
;J. Schleucher, M. Schwendinger, M. Sattler, P. Schmidt, O. Schedletzky,
; S.J. Glaser, O.W. Sorensen & C. Griesinger, J. Biomol. NMR 4,
; 301-306 (1994)
prosol relations=<triple>
```

HCCH-TOCSY:

```
# 1 "C:/Bruker/XWIN-NMR/exp/stan/nmr/lists/pp/hcchdigp3d"
;hcchdigp3d
;avance-version (03/01/17)
;HCCH-TOCSY
;3D sequence with
; inverse correlation using multiple inept transfer and
; C-C DIPSI3 spinlock
;
; F1(H,t1) -> F2(C,t2) -> F2(C') -> F1(H',t3)
;
;off resonance C=O pulse using shaped pulse
;phase sensitive (t1)
;phase sensitive (t2)
;spinlock during z-filter
;(use parameterset HCCHDIGP3D)
;
;(L.E. Kay, G.Y. Xu, A.U. Singer, D.R. Muhandiram & J. D. Forman-Kay
; J. Magn. Reson. B 101, 333 - 337 (1993))
prosol relations=<triple>
```

Appendix B

CaM-iNOS Peptide Assigned Chemical Shifts

_Atom_shift_assign_ID
_Residue_seq_code
_Residue_label
_Atom_name
_Atom_type
_Chem_shift_value
_Chem_shift_value_error
_Chem_shift_ambiguity_code

1	2	ASP	CA	C	51.929	
2	2	ASP	CB	C	38.505	
3	2	ASP	H	H	8.521	
4	2	ASP	HA	H	4.453	
5	2	ASP	HB2	H	2.507	
6	2	ASP	HB3	H	2.507	
7	2	ASP	N	N	120.442	
8	3	GLN	CA	C	52.686	
9	3	GLN	H	H	8.199	
10	3	GLN	HA	H	4.218	
11	3	GLN	N	N	119.769	
12	4	LEU	CA	C	51.584	
13	4	LEU	CB	C	40.561	
14	4	LEU	CG	C	23.770	
15	4	LEU	CD1	C	20.686	
16	4	LEU	H	H	7.510	
17	4	LEU	HA	H	4.483	
18	4	LEU	HB2	H	1.669	
19	4	LEU	HB3	H	1.353	
20	4	LEU	HG	H	1.534	
21	4	LEU	HD1	H	0.733	
22	4	LEU	HD2	H	0.680	
23	4	LEU	N	N	120.939	
24	5	THR	CA	C	57.873	
25	5	THR	CB	C	68.203	
26	5	THR	CG2	C	18.858	
27	5	THR	H	H	8.576	
28	5	THR	HA	H	4.253	
29	5	THR	N	N	112.777	
30	6	GLU	CA	C	57.645	
31	6	GLU	CB	C	26.286	
32	6	GLU	CG	C	33.810	
33	6	GLU	H	H	8.874	
34	6	GLU	HA	H	3.794	
35	6	GLU	HB2	H	1.876	
36	6	GLU	HB3	H	1.876	
37	6	GLU	HG2	H	2.213	
38	6	GLU	HG3	H	2.213	
39	6	GLU	N	N	120.254	
40	7	GLU	CA	C	57.176	
41	7	GLU	CB	C	26.054	
42	7	GLU	CG	C	33.593	
43	7	GLU	H	H	8.536	
44	7	GLU	HA	H	3.896	
45	7	GLU	HB2	H	1.878	
46	7	GLU	HB3	H	1.878	
47	7	GLU	HG2	H	2.166	
48	7	GLU	HG3	H	2.166	
49	7	GLU	N	N	119.637	
50	8	GLN	CA	C	56.411	
51	8	GLN	CB	C	26.625	
52	8	GLN	CG	C	33.022	
53	8	GLN	H	H	7.499	
54	8	GLN	HA	H	3.838	
55	8	GLN	HB2	H	1.759	
56	8	GLN	HB3	H	1.887	
57	8	GLN	HG2	H	2.175	
58	8	GLN	HG3	H	2.175	
59	8	GLN	N	N	120.086	
60	9	ILE	CA	C	64.046	
61	9	ILE	CG1	C	27.539	
62	9	ILE	CG2	C	14.518	
63	9	ILE	CD1	C	10.291	
64	9	ILE	H	H	8.405	
65	9	ILE	HA	H	3.667	
66	9	ILE	HB	H	1.804	
67	9	ILE	HG12	H	0.883	
68	9	ILE	HG13	H	0.883	
69	9	ILE	HG2	H	0.936	
70	9	ILE	HD1	H	0.690	
71	9	ILE	N	N	120.295	
72	10	ALA	CA	C	52.657	
73	10	ALA	CB	C	14.975	
74	10	ALA	H	H	7.949	
75	10	ALA	HA	H	3.911	
76	10	ALA	HB	H	1.364	
77	10	ALA	N	N	121.503	
78	11	GLU	CA	C	56.673	
79	11	GLU	CB	C	26.968	
80	11	GLU	CG	C	33.250	
81	11	GLU	H	H	7.700	
82	11	GLU	HA	H	3.838	
83	11	GLU	HB2	H	1.761	

84	11	GLU	HB3	H	1.900
85	11	GLU	HG2	H	2.177
86	11	GLU	HG3	H	2.177
87	11	GLU	N	N	118.352
88	12	PHE	CA	C	59.655
89	12	PHE	CB	C	35.535
90	12	PHE	H	H	8.211
91	12	PHE	HA	H	4.477
92	12	PHE	HB2	H	3.252
93	12	PHE	HB3	H	3.401
94	12	PHE	N	N	117.277
95	13	LYS	CA	C	57.154
96	13	LYS	CB	C	26.169
97	13	LYS	CG	C	24.455
98	13	LYS	CD	C	29.824
99	13	LYS	CE	C	39.419
100	13	LYS	H	H	8.925
101	13	LYS	HA	H	3.925
102	13	LYS	HB2	H	1.889
103	13	LYS	HB3	H	1.889
104	13	LYS	HG2	H	1.527
105	13	LYS	HG3	H	1.527
106	13	LYS	HD2	H	1.761
107	13	LYS	HD3	H	1.761
108	13	LYS	HE2	H	2.517
109	13	LYS	HE3	H	2.517
110	13	LYS	N	N	122.928
111	14	GLU	CA	C	56.336
112	14	GLU	CB	C	26.283
113	14	GLU	CG	C	33.479
114	14	GLU	H	H	7.824
115	14	GLU	HA	H	3.858
116	14	GLU	HB2	H	1.759
117	14	GLU	HB3	H	1.919
118	14	GLU	HG2	H	2.175
119	14	GLU	HG3	H	2.175
120	14	GLU	N	N	119.706
121	15	ALA	CA	C	52.835
122	15	ALA	CB	C	15.203
123	15	ALA	H	H	8.124
124	15	ALA	HA	H	3.867
125	15	ALA	HB	H	1.652
126	15	ALA	N	N	123.880
127	16	PHE	CA	C	58.983
128	16	PHE	CB	C	36.449
129	16	PHE	H	H	8.446
130	16	PHE	HA	H	3.132
131	16	PHE	HB2	H	2.177
132	16	PHE	HB3	H	2.517
133	16	PHE	HZ	H	6.791
134	16	PHE	N	N	118.972
135	17	SER	CA	C	58.999
136	17	SER	CB	C	60.436
137	17	SER	H	H	7.874
138	17	SER	HA	H	3.902
139	17	SER	HB2	H	3.902
140	17	SER	HB3	H	3.902
141	17	SER	N	N	114.737
142	18	LEU	CA	C	54.729
143	18	LEU	CB	C	38.162
144	18	LEU	CG	C	23.998
145	18	LEU	CD1	C	20.686
146	18	LEU	CD2	C	22.399
147	18	LEU	H	H	7.183
148	18	LEU	HA	H	3.785
149	18	LEU	HB2	H	1.580
150	18	LEU	HB3	H	1.580
151	18	LEU	HG	H	1.516
152	18	LEU	HD1	H	0.472
153	18	LEU	HD2	H	0.611
154	18	LEU	N	N	120.225
155	19	PHE	CA	C	56.424
156	19	PHE	H	H	6.977
157	19	PHE	N	N	112.357
158	20	ASP	CA	C	49.512
159	20	ASP	CB	C	36.677
160	20	ASP	H	H	7.446
161	20	ASP	HA	H	4.432
162	20	ASP	HB2	H	2.485
163	20	ASP	HB3	H	2.485
164	20	ASP	N	N	117.274
165	21	LYS	CA	C	55.679
166	21	LYS	CB	C	29.595
167	21	LYS	CG	C	21.714
168	21	LYS	CD	C	25.712
169	21	LYS	CE	C	39.190
170	21	LYS	H	H	7.520
171	21	LYS	HA	H	3.838
172	21	LYS	HB2	H	1.662
173	21	LYS	HB3	H	1.662
174	21	LYS	HG2	H	1.331
175	21	LYS	HG3	H	1.246
176	21	LYS	HD2	H	1.491
177	21	LYS	HD3	H	1.491
178	21	LYS	HE2	H	2.816
179	21	LYS	HE3	H	2.816
180	21	LYS	N	N	124.296
181	22	ASP	CA	C	50.061
182	22	ASP	CB	C	36.563
183	22	ASP	H	H	7.819
184	22	ASP	HA	H	4.434
185	22	ASP	HB2	H	2.485

186 22 ASP HB3 H 2.890
187 22 ASP N N 113.761
188 23 GLY CA C 44.305
189 23 GLY H H 7.497
190 23 GLY HA2 H 3.667
191 23 GLY HA3 H 3.667
192 23 GLY N N 108.838
193 24 ASP CA C 50.853
194 24 ASP CB C 37.363
195 24 ASP H H 8.312
196 24 ASP HA H 4.350
197 24 ASP HB2 H 2.496
198 24 ASP HB3 H 2.891
199 24 ASP N N 120.790
200 25 GLY CA C 42.420
201 25 GLY H H 10.352
202 25 GLY HA2 H 4.098
203 25 GLY HA3 H 3.549
204 25 GLY N N 112.499
205 26 THR CA C 56.878
206 26 THR CB C 70.031
207 26 THR CG2 C 18.972
208 26 THR H H 8.018
209 26 THR HA H 5.316
210 26 THR HB H 3.668
211 26 THR HG2 H 0.867
212 26 THR N N 111.781
213 27 ILE CA C 58.477
214 27 ILE CB C 37.572
215 27 ILE CG1 C 15.456
216 27 ILE CG2 C 24.348
217 27 ILE CD1 C 11.352
218 27 ILE H H 9.769
219 27 ILE HA H 4.658
220 27 ILE N N 126.162
221 28 THR CA C 56.878
222 28 THR CB C 69.688
223 28 THR CG2 C 19.543
224 28 THR H H 8.302
225 28 THR HA H 4.669
226 28 THR HB H 3.838
227 28 THR HG2 H 0.952
228 28 THR N N 116.311
229 29 THR CA C 63.820
230 29 THR CB C 65.160
231 29 THR CG2 C 20.586
232 29 THR H H 9.078
233 29 THR HA H 3.633
234 29 THR HB H 4.054
235 29 THR HG2 H 1.128
236 29 THR N N 112.465
237 30 LYS CA C 56.569
238 30 LYS CB C 29.595
239 30 LYS CG C 22.171
240 30 LYS CD C 26.397
241 30 LYS CE C 39.304
242 30 LYS H H 7.467
243 30 LYS HA H 3.955
244 30 LYS HB2 H 1.684
245 30 LYS HB3 H 1.684
246 30 LYS HG2 H 1.256
247 30 LYS HG3 H 1.331
248 30 LYS HD3 H 1.502
249 30 LYS HE2 H 2.827
250 30 LYS N N 120.792
251 31 GLU CA C 56.677
252 31 GLU CB C 27.082
253 31 GLU CG C 33.593
254 31 GLU H H 7.574
255 31 GLU HA H 3.906
256 31 GLU HB2 H 1.897
257 31 GLU HB3 H 1.897
258 31 GLU HG2 H 2.229
259 31 GLU HG3 H 2.164
260 31 GLU N N 121.359
261 32 LEU CA C 55.572
262 32 LEU CB C 39.852
263 32 LEU CG C 23.892
264 32 LEU CD1 C 20.814
265 32 LEU H H 8.712
266 32 LEU HA H 4.057
267 32 LEU HB2 H 1.772
268 32 LEU HB3 H 1.772
269 32 LEU HG H 1.530
270 32 LEU HD1 H 1.291
271 32 LEU HD2 H 1.291
272 32 LEU N N 120.087
273 33 GLY CA C 45.637
274 33 GLY H H 8.696
275 33 GLY HA2 H 3.855
276 33 GLY HA3 H 3.395
277 33 GLY N N 105.634
278 34 THR CA C 64.259
279 34 THR CB C 66.033
280 34 THR CG2 C 18.515
281 34 THR H H 7.785
282 34 THR HA H 3.810
283 34 THR HB H 4.162
284 34 THR HG2 H 1.128
285 34 THR N N 117.265
286 35 VAL CA C 64.308
287 35 VAL CB C 28.796

288	35	VAL	CG1	C	17.487
289	35	VAL	CG2	C	20.115
290	35	VAL	H	H	7.268
291	35	VAL	HA	H	3.401
292	35	VAL	HB	H	1.932
293	35	VAL	HG1	H	0.419
294	35	VAL	HG2	H	0.739
295	35	VAL	N	N	121.498
296	36	MET	CA	C	56.606
297	36	MET	CB	C	28.453
298	36	MET	CG	C	31.188
299	36	MET	H	H	8.487
300	36	MET	HA	H	3.842
301	36	MET	HB2	H	1.761
302	36	MET	HB3	H	1.761
303	36	MET	HG2	H	2.177
304	36	MET	HG3	H	2.177
305	36	MET	N	N	117.302
306	37	ARG	CA	C	56.480
307	37	ARG	CB	C	26.740
308	37	ARG	CG	C	25.597
309	37	ARG	CD	C	40.904
310	37	ARG	H	H	8.330
311	37	ARG	HA	H	4.657
312	37	ARG	HB2	H	1.759
313	37	ARG	HB3	H	1.759
314	37	ARG	HG2	H	1.887
315	37	ARG	HG3	H	1.887
316	37	ARG	HD2	H	3.040
317	37	ARG	HD3	H	3.040
318	37	ARG	N	N	118.262
319	38	SER	H	H	7.815
320	38	SER	N	N	117.873
321	39	LEU	CA	C	51.438
322	39	LEU	CB	C	38.162
323	39	LEU	CG	C	23.313
324	39	LEU	CD1	C	18.744
325	39	LEU	CD2	C	17.031
326	39	LEU	H	H	7.326
327	39	LEU	HA	H	4.072
328	39	LEU	HB2	H	1.644
329	39	LEU	HB3	H	1.644
330	39	LEU	HG	H	1.516
331	39	LEU	HD1	H	0.398
332	39	LEU	N	N	117.970
333	40	GLY	CA	C	42.664
334	40	GLY	H	H	7.636
335	40	GLY	HA2	H	4.071
336	40	GLY	HA3	H	4.071
337	40	GLY	N	N	106.755
338	41	GLN	CA	C	50.853
339	41	GLN	CB	C	27.311
340	41	GLN	CG	C	30.395
341	41	GLN	H	H	7.827
342	41	GLN	HA	H	4.285
343	41	GLN	HB2	H	1.474
344	41	GLN	HB3	H	1.474
345	41	GLN	HG2	H	1.782
346	41	GLN	HG3	H	1.782
347	41	GLN	N	N	118.316
348	42	ASN	CA	C	48.562
349	42	ASN	CB	C	36.318
350	42	ASN	H	H	8.557
351	42	ASN	HA	H	5.013
352	42	ASN	HB2	H	2.606
353	42	ASN	HB3	H	2.329
354	42	ASN	N	N	115.866
355	44	THR	CA	C	57.922
356	44	THR	CB	C	68.317
357	44	THR	CG2	C	18.858
358	44	THR	H	H	8.694
359	44	THR	HA	H	4.296
360	44	THR	HB	H	4.669
361	44	THR	HG2	H	1.154
362	44	THR	N	N	113.035
363	45	GLU	CA	C	57.356
364	45	GLU	CB	C	25.716
365	45	GLU	CG	C	33.582
366	45	GLU	H	H	8.687
367	45	GLU	HA	H	3.896
368	45	GLU	HB2	H	1.847
369	45	GLU	HB3	H	1.847
370	45	GLU	HG2	H	2.213
371	45	GLU	HG3	H	2.213
372	45	GLU	N	N	120.283
373	46	ALA	CA	C	52.316
374	46	ALA	CB	C	15.089
375	46	ALA	H	H	8.153
376	46	ALA	HA	H	3.870
377	46	ALA	HB	H	1.244
378	46	ALA	N	N	120.685
379	47	GLU	CA	C	56.508
380	47	GLU	CB	C	26.740
381	47	GLU	CG	C	33.707
382	47	GLU	H	H	7.554
383	47	GLU	HA	H	3.859
384	47	GLU	HB2	H	1.878
385	47	GLU	HB3	H	1.772
386	47	GLU	HG2	H	2.113
387	47	GLU	HG3	H	2.208
388	47	GLU	N	N	118.546
389	48	LEU	CA	C	55.368

390 48 LEU CB C 39.419
391 48 LEU CG C 26.397
392 48 LEU CD1 C 23.656
393 48 LEU CD2 C 21.942
394 48 LEU H H 8.247
395 48 LEU HA H 3.940
396 48 LEU HB2 H 1.523
397 48 LEU HB3 H 1.523
398 48 LEU HG H 1.481
399 48 LEU HD1 H 0.551
400 48 LEU HD2 H 1.224
401 48 LEU N N 120.085
402 49 GLN CA C 56.703
403 49 GLN CB C 26.397
404 49 GLN CG C 33.479
405 49 GLN H H 7.891
406 49 GLN HA H 3.913
407 49 GLN HB2 H 1.889
408 49 GLN HB3 H 1.889
409 49 GLN HG2 H 2.166
410 49 GLN HG3 H 2.166
411 49 GLN N N 118.119
412 50 ASP CA C 54.876
413 50 ASP CB C 37.248
414 50 ASP H H 7.803
415 50 ASP HA H 4.179
416 50 ASP HB2 H 2.604
417 50 ASP HB3 H 2.485
418 50 ASP N N 119.263
419 51 MET CA C 57.074
420 51 MET CB C 29.975
421 51 MET CG C 30.211
422 51 MET H H 7.831
423 51 MET HA H 3.838
424 51 MET HB2 H 1.665
425 51 MET HB3 H 1.665
426 51 MET HG2 H 1.804
427 51 MET HG3 H 1.804
428 51 MET N N 120.178
429 52 ILE CA C 61.675
430 52 ILE CB C 33.822
431 52 ILE CG1 C 13.604
432 52 ILE CG2 C 26.054
433 52 ILE CD1 C 8.921
434 52 ILE H H 7.703
435 52 ILE HA H 3.348
436 52 ILE HB H 1.868
437 52 ILE HG12 H 0.568
438 52 ILE HG13 H 0.515
439 52 ILE HG2 H 1.101
440 52 ILE HD1 H 0.547
441 52 ILE N N 116.856
442 53 ASN CA C 53.041
443 53 ASN CB C 35.078
444 53 ASN H H 8.187
445 53 ASN HA H 4.253
446 53 ASN HB2 H 2.826
447 53 ASN HB3 H 2.730
448 53 ASN N N 117.417
449 54 GLU CA C 55.874
450 54 GLU CB C 26.397
451 54 GLU CG C 33.479
452 54 GLU H H 7.391
453 54 GLU HA H 3.859
454 54 GLU HB2 H 1.889
455 54 GLU HB3 H 1.751
456 54 GLU HG2 H 2.208
457 54 GLU HG3 H 2.208
458 54 GLU N N 116.996
459 55 VAL CA C 58.945
460 55 VAL CB C 30.738
461 55 VAL CG1 C 20.343
462 55 VAL CG2 C 19.886
463 55 VAL H H 7.151
464 55 VAL HA H 3.987
465 55 VAL HB H 1.910
466 55 VAL HG1 H 0.909
467 55 VAL HG2 H 0.920
468 55 VAL N N 114.596
469 56 ASP CA C 51.356
470 56 ASP CB C 37.591
471 56 ASP H H 7.913
472 56 ASP HA H 4.317
473 56 ASP HB2 H 2.506
474 56 ASP HB3 H 2.326
475 56 ASP N N 119.670
476 57 ALA CA C 51.183
477 57 ALA H H 8.126
478 57 ALA HA H 4.101
479 57 ALA HB H 1.364
480 57 ALA N N 131.491
481 58 ASP CA C 49.960
482 58 ASP CB C 36.563
483 58 ASP H H 8.130
484 58 ASP HA H 4.434
485 58 ASP HB2 H 2.890
486 58 ASP HB3 H 2.485
487 58 ASP N N 114.255
488 59 GLY CA C 44.296
489 59 GLY H H 7.504
490 59 GLY HA2 H 3.688
491 59 GLY HA3 H 3.688

492 59 GLY N N 108.987
493 60 ASN CA C 49.859
494 60 ASN CB C 34.507
495 60 ASN H H 8.095
496 60 ASN HA H 4.429
497 60 ASN HB2 H 2.474
498 60 ASN HB3 H 2.474
499 60 ASN N N 118.770
500 61 GLY CA C 42.712
501 61 GLY H H 10.280
502 61 GLY HA2 H 3.344
503 61 GLY HA3 H 4.087
504 61 GLY N N 112.773
505 62 THR CA C 56.878
506 62 THR CB C 69.688
507 62 THR CG2 C 19.543
508 62 THR H H 7.475
509 62 THR HA H 4.672
510 62 THR HB H 3.838
511 62 THR HG2 H 0.952
512 62 THR N N 108.117
513 63 ILE CA C 57.812
514 63 ILE CB C 37.363
515 63 ILE CG1 C 24.341
516 63 ILE CG2 C 15.431
517 63 ILE CD1 C 11.319
518 63 ILE H H 8.449
519 63 ILE HA H 4.796
520 63 ILE HB H 1.855
521 63 ILE HG2 H 1.096
522 63 ILE HD1 H 0.765
523 63 ILE N N 122.642
524 64 ASP CA C 49.280
525 64 ASP CB C 39.761
526 64 ASP H H 9.011
527 64 ASP HA H 5.316
528 64 ASP HB2 H 2.666
529 64 ASP HB3 H 2.826
530 64 ASP N N 128.633
531 65 PHE CA C 60.213
532 65 PHE H H 8.766
533 65 PHE HA H 3.767
534 65 PHE HB2 H 1.812
535 65 PHE HB3 H 1.812
536 65 PHE N N 118.892
537 67 GLU CA C 56.605
538 67 GLU CB C 26.397
539 67 GLU CG C 33.250
540 67 GLU H H 7.487
541 67 GLU HA H 3.837
542 67 GLU HB2 H 1.889
543 67 GLU HB3 H 1.761
544 67 GLU HG2 H 2.155
545 67 GLU HG3 H 2.155
546 67 GLU N N 118.675
547 68 PHE CA C 58.429
548 68 PHE CB C 37.591
549 68 PHE H H 8.066
550 68 PHE HA H 3.668
551 68 PHE HB2 H 3.265
552 68 PHE HB3 H 3.265
553 68 PHE HD1 H 6.154
554 68 PHE HD2 H 6.154
555 68 PHE N N 123.182
556 69 LEU CA C 54.774
557 69 LEU CB C 39.419
558 69 LEU CG C 26.169
559 69 LEU CD1 C 21.828
560 69 LEU H H 8.672
561 69 LEU HA H 3.955
562 69 LEU HB3 H 1.523
563 69 LEU HG H 1.481
564 69 LEU HD1 H 1.224
565 69 LEU HD2 H 1.224
566 69 LEU N N 119.530
567 70 THR CA C 63.861
568 70 THR CB C 66.147
569 70 THR CG2 C 18.515
570 70 THR H H 7.909
571 70 THR HA H 3.806
572 70 THR HB H 4.157
573 70 THR HG2 H 1.122
574 70 THR N N 113.765
575 71 MET CA C 56.106
576 71 MET CB C 29.595
577 71 MET CG C 29.481
578 71 MET H H 7.120
579 71 MET HA H 3.881
580 71 MET HB2 H 1.676
581 71 MET HB3 H 1.676
582 71 MET HG2 H 2.219
583 71 MET HG3 H 2.219
584 71 MET HE H 2.110
585 71 MET N N 119.518
586 72 MET CA C 55.111
587 72 MET CB C 27.892
588 72 MET CG C 29.595
589 72 MET H H 7.737
590 72 MET HA H 3.817
591 72 MET HB2 H 1.878
592 72 MET HB3 H 1.878
593 72 MET HG2 H 2.177

594	72	MET	HG3	H	2.177
595	72	MET	N	N	116.280
596	73	ALA	CA	C	51.812
597	73	ALA	CB	C	15.203
598	73	ALA	H	H	8.322
599	73	ALA	HA	H	3.838
600	73	ALA	HB	H	1.128
601	73	ALA	N	N	119.984
602	74	ARG	CA	C	55.957
603	74	ARG	CB	C	25.255
604	74	ARG	CG	C	27.425
605	74	ARG	CD	C	40.675
606	74	ARG	H	H	7.264
607	74	ARG	HA	H	3.838
608	74	ARG	HB2	H	1.942
609	74	ARG	HB3	H	1.527
610	74	ARG	HG2	H	1.740
611	74	ARG	HG3	H	1.740
612	74	ARG	HD2	H	3.039
613	74	ARG	HD3	H	3.039
614	74	ARG	N	N	116.354
615	75	LYS	CA	C	54.859
616	75	LYS	CB	C	28.681
617	75	LYS	CG	C	21.714
618	75	LYS	CD	C	30.852
619	75	LYS	CE	C	39.419
620	75	LYS	H	H	7.756
621	75	LYS	HA	H	3.948
622	75	LYS	HB2	H	1.641
623	75	LYS	HB3	H	1.641
624	75	LYS	HG2	H	1.235
625	75	LYS	HG3	H	1.235
626	75	LYS	HD2	H	1.534
627	75	LYS	HD3	H	1.534
628	75	LYS	HE2	H	2.805
629	75	LYS	HE3	H	2.805
630	75	LYS	N	N	120.084
631	76	MET	CA	C	54.704
632	76	MET	CB	C	30.052
633	76	MET	CG	C	29.938
634	76	MET	H	H	7.985
635	76	MET	HA	H	4.168
636	76	MET	HB2	H	2.421
637	76	MET	HB3	H	2.421
638	76	MET	HG2	H	2.677
639	76	MET	HG3	H	2.677
640	76	MET	N	N	117.139
641	77	LYS	CA	C	53.184
642	77	LYS	CB	C	26.283
643	77	LYS	CG	C	21.828
644	77	LYS	CD	C	30.509
645	77	LYS	CE	C	39.419
646	77	LYS	H	H	7.275
647	77	LYS	HA	H	4.221
648	77	LYS	HB2	H	1.495
649	77	LYS	HB3	H	1.495
650	77	LYS	HG2	H	1.229
651	77	LYS	HG3	H	1.346
652	77	LYS	HD2	H	1.644
653	77	LYS	HD3	H	1.793
654	77	LYS	HE2	H	2.805
655	77	LYS	HE3	H	2.805
656	77	LYS	N	N	116.614
657	78	ASP	CA	C	51.732
658	78	ASP	CB	C	38.391
659	78	ASP	H	H	8.181
660	78	ASP	HA	H	4.451
661	78	ASP	HB2	H	2.335
662	78	ASP	HB3	H	2.506
663	78	ASP	N	N	123.187
664	79	THR	CA	C	61.322
665	79	THR	CB	C	66.147
666	79	THR	CG2	C	18.972
667	79	THR	H	H	8.377
668	79	THR	HA	H	4.034
669	79	THR	HB	H	4.151
670	79	THR	HG2	H	1.128
671	79	THR	N	N	114.325
672	80	ASP	CA	C	51.672
673	80	ASP	CB	C	37.591
674	80	ASP	H	H	8.223
675	80	ASP	HA	H	4.305
676	80	ASP	HB2	H	2.506
677	80	ASP	HB3	H	2.506
678	80	ASP	N	N	120.844
679	81	SER	CA	C	57.939
680	81	SER	CB	C	60.664
681	81	SER	H	H	7.785
682	81	SER	HA	H	3.911
683	81	SER	HB2	H	3.785
684	81	SER	HB3	H	3.913
685	81	SER	N	N	115.729
686	82	GLU	CA	C	56.829
687	82	GLU	CB	C	26.625
688	82	GLU	CG	C	33.479
689	82	GLU	H	H	8.208
690	82	GLU	HA	H	3.896
691	82	GLU	HB2	H	1.897
692	82	GLU	HB3	H	1.897
693	82	GLU	HG2	H	2.164
694	82	GLU	HG3	H	2.164
695	82	GLU	N	N	121.960

696 83 GLU CA C 55.945
697 83 GLU CB C 26.832
698 83 GLU CG C 33.593
699 83 GLU H H 7.898
700 83 GLU HA H 3.838
701 83 GLU HB2 H 1.761
702 83 GLU HB3 H 1.889
703 83 GLU HG2 H 2.166
704 83 GLU HG3 H 2.166
705 83 GLU N N 118.040
706 84 GLU CA C 54.758
707 84 GLU CB C 30.852
708 84 GLU CG C 36.791
709 84 GLU H H 8.154
710 84 GLU N N 118.825
711 85 ILE CA C 59.858
712 85 ILE CB C 35.649
713 85 ILE CG1 C 14.289
714 85 ILE CG2 C 24.798
715 85 ILE CD1 C 9.720
716 85 ILE H H 7.793
717 85 ILE HA H 3.767
718 85 ILE HB H 1.812
719 85 ILE HG12 H 0.947
720 85 ILE HG13 H 0.947
721 85 ILE HG2 H 1.513
722 85 ILE HD1 H 0.701
723 85 ILE N N 119.310
724 86 ARG CA C 57.265
725 86 ARG CB C 26.854
726 86 ARG CG C 24.569
727 86 ARG CD C 39.419
728 86 ARG H H 8.177
729 86 ARG HA H 3.925
730 86 ARG HB2 H 1.769
731 86 ARG HB3 H 1.876
732 86 ARG HG2 H 1.513
733 86 ARG HG3 H 1.513
734 86 ARG HD2 H 2.827
735 86 ARG HD3 H 2.827
736 86 ARG N N 120.640
737 87 GLU CA C 56.643
738 87 GLU CB C 26.054
739 87 GLU CG C 33.250
740 87 GLU H H 7.828
741 87 GLU HA H 3.852
742 87 GLU HB2 H 1.887
743 87 GLU HB3 H 1.759
744 87 GLU HG2 H 2.175
745 87 GLU HG3 H 2.175
746 87 GLU N N 119.448
747 88 ALA CA C 52.596
748 88 ALA CB C 14.632
749 88 ALA H H 8.283
750 88 ALA HA H 4.028
751 88 ALA HB H 1.609
752 88 ALA N N 122.592
753 89 PHE CA C 59.545
754 89 PHE CB C 36.335
755 89 PHE H H 8.423
756 89 PHE HA H 3.114
757 89 PHE HB2 H 2.219
758 89 PHE HB3 H 2.528
759 89 PHE N N 119.245
760 90 ARG CA C 56.313
761 90 ARG CB C 27.197
762 90 ARG CG C 25.141
763 90 ARG CD C 40.675
764 90 ARG H H 7.840
765 90 ARG HA H 3.849
766 90 ARG HB2 H 1.900
767 90 ARG HB3 H 1.761
768 90 ARG HG2 H 1.516
769 90 ARG HG3 H 1.516
770 90 ARG HD2 H 2.720
771 90 ARG HD3 H 3.039
772 90 ARG N N 117.455
773 91 VAL CA C 63.333
774 91 VAL CB C 28.110
775 91 VAL CG1 C 18.401
776 91 VAL CG2 C 20.229
777 91 VAL H H 7.262
778 91 VAL HA H 3.252
779 91 VAL HB H 2.070
780 91 VAL HG1 H 0.334
781 91 VAL HG2 H 0.760
782 91 VAL N N 118.698
783 92 PHE CA C 57.181
784 92 PHE CB C 39.419
785 92 PHE H H 6.693
786 92 PHE HA H 3.934
787 92 PHE N N 112.495
788 93 ASP CA C 49.781
789 93 ASP CB C 36.449
790 93 ASP H H 7.954
791 93 ASP HA H 4.434
792 93 ASP HB2 H 2.879
793 93 ASP HB3 H 2.485
794 93 ASP N N 117.214
795 94 LYS CA C 55.679
796 94 LYS CB C 29.595
797 94 LYS CG C 21.485

798 94 LYS CD C 25.483
799 94 LYS CE C 39.190
800 94 LYS H H 7.671
801 94 LYS HA H 3.779
802 94 LYS HB2 H 1.662
803 94 LYS HB3 H 1.662
804 94 LYS HG2 H 1.342
805 94 LYS HG3 H 1.247
806 94 LYS HD2 H 1.491
807 94 LYS HD3 H 1.491
808 94 LYS HE2 H 2.816
809 94 LYS HE3 H 2.816
810 94 LYS N N 125.565
811 95 ASP CA C 50.213
812 95 ASP CB C 36.563
813 95 ASP H H 7.944
814 95 ASP HA H 4.408
815 95 ASP HB2 H 2.890
816 95 ASP HB3 H 2.475
817 95 ASP N N 114.041
818 96 GLY CA C 44.199
819 96 GLY H H 7.529
820 96 GLY HA2 H 3.688
821 96 GLY HA3 H 3.688
822 96 GLY N N 108.849
823 97 ASN CA C 49.683
824 97 ASN CB C 36.563
825 97 ASN H H 8.234
826 97 ASN HA H 4.424
827 97 ASN HB2 H 2.879
828 97 ASN HB3 H 2.485
829 97 ASN N N 119.410
830 98 GLY CA C 42.176
831 98 GLY H H 10.298
832 98 GLY HA2 H 3.930
833 98 GLY HA3 H 3.930
834 98 GLY N N 112.073
835 99 TYR CA C 53.681
836 99 TYR CB C 39.875
837 99 TYR H H 7.497
838 99 TYR HA H 4.818
839 99 TYR HB2 H 2.326
840 99 TYR HB3 H 2.326
841 99 TYR HD1 H 6.770
842 99 TYR HD2 H 6.770
843 99 TYR N N 116.011
844 100 ILE CA C 58.629
845 100 ILE CB C 35.748
846 100 ILE CG1 C 24.006
847 100 ILE CG2 C 13.860
848 100 ILE CD1 C 12.264
849 100 ILE H H 9.833
850 100 ILE HA H 4.423
851 100 ILE HB H 1.656
852 100 ILE HG2 H 0.685
853 100 ILE N N 126.793
854 101 SER CA C 53.060
855 101 SER CB C 64.091
856 101 SER H H 8.870
857 101 SER HA H 4.657
858 101 SER HB2 H 3.774
859 101 SER HB3 H 3.774
860 101 SER N N 123.825
861 102 ALA CA C 53.050
862 102 ALA CB C 14.975
863 102 ALA H H 9.209
864 102 ALA HA H 3.764
865 102 ALA HB H 1.320
866 102 ALA N N 122.909
867 103 ALA CA C 52.485
868 103 ALA CB C 15.203
869 103 ALA H H 8.146
870 103 ALA HA H 3.874
871 103 ALA HB H 1.246
872 103 ALA N N 118.692
873 104 GLU CA C 56.575
874 104 GLU CB C 25.369
875 104 GLU CG C 33.593
876 104 GLU H H 7.832
877 104 GLU HA H 3.863
878 104 GLU HB2 H 1.897
879 104 GLU HB3 H 1.759
880 104 GLU HG2 H 2.250
881 104 GLU HG3 H 2.175
882 104 GLU N N 120.098
883 105 LEU CA C 55.696
884 105 LEU CB C 38.962
885 105 LEU CG C 23.770
886 105 LEU CD1 C 21.600
887 105 LEU H H 8.300
888 105 LEU HA H 4.116
889 105 LEU HB2 H 1.769
890 105 LEU HB3 H 1.769
891 105 LEU HG H 1.513
892 105 LEU HD1 H 0.643
893 105 LEU HD2 H 1.096
894 105 LEU N N 121.466
895 106 ARG CA C 57.434
896 106 ARG CB C 27.084
897 106 ARG CG C 25.260
898 106 ARG CD C 40.650
899 106 ARG H H 8.882

900 106 ARG HA H 3.852
901 106 ARG HB2 H 1.765
902 106 ARG HB3 H 1.882
903 106 ARG HG2 H 1.491
904 106 ARG HD2 H 2.731
905 106 ARG HD3 H 3.040
906 106 ARG N N 118.978
907 107 HIS CA C 56.825
908 107 HIS CB C 26.740
909 107 HIS H H 7.991
910 107 HIS HA H 4.200
911 107 HIS HB2 H 3.146
912 107 HIS HB3 H 3.146
913 107 HIS N N 118.543
914 108 VAL CA C 64.210
915 108 VAL CB C 28.910
916 108 VAL CG1 C 20.229
917 108 VAL CG2 C 17.716
918 108 VAL H H 7.425
919 108 VAL HA H 3.092
920 108 VAL HB H 1.644
921 108 VAL HG1 H 0.355
922 108 VAL HG2 H 0.600
923 108 VAL N N 118.687
924 109 MET CA C 55.212
925 109 MET CB C 27.425
926 109 MET CG C 31.080
927 109 MET H H 7.972
928 109 MET HA H 3.944
929 109 MET HB2 H 1.761
930 109 MET HB3 H 1.761
931 109 MET HG2 H 2.166
932 109 MET HG3 H 2.166
933 109 MET N N 115.725
934 110 THR CA C 63.918
935 110 THR CB C 65.844
936 110 THR CG2 C 18.762
937 110 THR H H 8.691
938 110 THR HA H 3.852
939 110 THR HB H 4.161
940 110 THR HG2 H 1.126
941 110 THR N N 116.999
942 111 ASN CA C 52.949
943 111 ASN CB C 34.964
944 111 ASN H H 7.911
945 111 ASN HA H 4.241
946 111 ASN HB2 H 2.827
947 111 ASN HB3 H 2.827
948 111 ASN N N 123.893
949 112 LEU CA C 52.901
950 112 LEU CB C 39.533
951 112 LEU CG C 23.541
952 112 LEU CD1 C 20.229
953 112 LEU CD2 C 21.828
954 112 LEU H H 7.618
955 112 LEU HA H 4.072
956 112 LEU HB2 H 1.782
957 112 LEU HB3 H 1.506
958 112 LEU HG H 1.506
959 112 LEU HD1 H 0.568
960 112 LEU N N 119.244
961 113 GLY CA C 42.437
962 113 GLY H H 7.743
963 113 GLY HA2 H 3.539
964 113 GLY HA3 H 4.092
965 113 GLY N N 107.263
966 114 GLU CA C 51.526
967 114 GLU CB C 27.539
968 114 GLU CG C 31.651
969 114 GLU H H 7.857
970 114 GLU HA H 4.290
971 114 GLU HB2 H 1.470
972 114 GLU HB3 H 1.470
973 114 GLU HG2 H 1.801
974 114 GLU HG3 H 1.801
975 114 GLU N N 120.073
976 115 LYS CA C 52.894
977 115 LYS CB C 29.481
978 115 LYS CG C 21.714
979 115 LYS CD C 26.283
980 115 LYS CE C 39.304
981 115 LYS H H 8.377
982 115 LYS HA H 4.220
983 115 LYS HB2 H 1.769
984 115 LYS HB3 H 1.769
985 115 LYS HG2 H 1.342
986 115 LYS HG3 H 1.224
987 115 LYS HD2 H 1.491
988 115 LYS HD3 H 1.491
989 115 LYS HE2 H 2.805
990 115 LYS HE3 H 2.805
991 115 LYS N N 124.142
992 116 LEU CA C 51.438
993 116 LEU CB C 40.675
994 116 LEU CG C 23.770
995 116 LEU CD1 C 20.800
996 116 LEU H H 8.002
997 116 LEU HA H 4.472
998 116 LEU HB2 H 1.534
999 116 LEU HB3 H 1.534
1000 116 LEU HG H 1.513
1001 116 LEU HD1 H 0.744

1002 116 LEU HD2 H 0.744
1003 116 LEU N N 125.240
1004 117 THR CA C 57.922
1005 117 THR CB C 68.352
1006 117 THR CG2 C 18.876
1007 117 THR H H 8.927
1008 117 THR N N 113.520
1009 118 ASP CA C 55.165
1010 118 ASP CB C 36.774
1011 118 ASP H H 8.754
1012 118 ASP HA H 4.043
1013 118 ASP HB2 H 2.414
1014 118 ASP HB3 H 2.414
1015 118 ASP N N 120.859
1016 119 GLU CA C 57.190
1017 119 GLU CB C 26.283
1018 119 GLU CG C 33.707
1019 119 GLU H H 8.507
1020 119 GLU HA H 3.927
1021 119 GLU HB2 H 1.759
1022 119 GLU HB3 H 1.876
1023 119 GLU HG2 H 2.175
1024 119 GLU HG3 H 2.175
1025 119 GLU N N 119.112
1026 120 GLU CA C 56.459
1027 120 GLU CB C 27.517
1028 120 GLU CG C 34.850
1029 120 GLU H H 7.809
1030 120 GLU HA H 3.858
1031 120 GLU HB2 H 2.198
1032 120 GLU HB3 H 2.198
1033 120 GLU HG2 H 2.208
1034 120 GLU HG3 H 2.208
1035 120 GLU N N 120.059
1036 121 VAL CA C 64.082
1037 121 VAL CB C 28.567
1038 121 VAL CG1 C 20.343
1039 121 VAL CG2 C 18.744
1040 121 VAL H H 7.898
1041 121 VAL HA H 3.472
1042 121 VAL HB H 2.058
1043 121 VAL HG1 H 0.835
1044 121 VAL HG2 H 0.338
1045 121 VAL N N 120.512
1046 122 ASP CA C 54.906
1047 122 ASP CB C 37.477
1048 122 ASP H H 7.897
1049 122 ASP HA H 4.168
1050 122 ASP HB2 H 2.453
1051 122 ASP HB3 H 2.603
1052 122 ASP N N 119.857
1053 123 GLU CA C 57.077
1054 123 GLU CB C 26.169
1055 123 GLU CG C 33.022
1056 123 GLU H H 7.963
1057 123 GLU HA H 3.838
1058 123 GLU HB2 H 1.887
1059 123 GLU HB3 H 1.759
1060 123 GLU HG2 H 2.175
1061 123 GLU HG3 H 2.175
1062 123 GLU N N 119.630
1063 124 MET CA C 56.508
1064 124 MET CB C 29.253
1065 124 MET CG C 31.080
1066 124 MET H H 7.631
1067 124 MET HA H 3.859
1068 124 MET HB2 H 1.921
1069 124 MET HB3 H 1.697
1070 124 MET HG2 H 2.240
1071 124 MET HG3 H 2.240
1072 124 MET N N 119.144
1073 125 ILE CA C 61.139
1074 125 ILE CB C 34.050
1075 125 ILE CG1 C 13.490
1076 125 ILE CG2 C 26.054
1077 125 ILE CD1 C 8.007
1078 125 ILE H H 7.669
1079 125 ILE HA H 3.284
1080 125 ILE HB H 1.900
1081 125 ILE HG12 H 0.579
1082 125 ILE HG13 H 0.515
1083 125 ILE HG2 H 1.026
1084 125 ILE HD1 H 0.547
1085 125 ILE N N 117.557
1086 126 ARG CA C 56.802
1087 126 ARG CB C 27.425
1088 126 ARG CG C 25.369
1089 126 ARG CD C 40.561
1090 126 ARG H H 7.952
1091 126 ARG HA H 3.858
1092 126 ARG HB2 H 1.751
1093 126 ARG HB3 H 1.889
1094 126 ARG HG2 H 1.484
1095 126 ARG HG3 H 1.484
1096 126 ARG HD2 H 3.039
1097 126 ARG HD3 H 3.039
1098 126 ARG N N 118.414
1099 127 GLU CA C 56.215
1100 127 GLU CB C 27.197
1101 127 GLU CG C 33.707
1102 127 GLU H H 7.294
1103 127 GLU HA H 3.858

1104 127 GLU HB2 H 1.889
1105 127 GLU HB3 H 1.775
1106 127 GLU HG2 H 2.166
1107 127 GLU HG3 H 2.166
1108 127 GLU N N 116.143
1109 128 ALA CA C 48.172
1110 128 ALA CB C 19.772
1111 128 ALA H H 7.110
1112 128 ALA HA H 4.453
1113 128 ALA HB H 1.244
1114 128 ALA N N 116.994
1115 129 ASP CA C 51.633
1116 129 ASP CB C 38.505
1117 129 ASP H H 7.508
1118 129 ASP HA H 4.442
1119 129 ASP HB2 H 2.326
1120 129 ASP HB3 H 2.326
1121 129 ASP N N 117.846
1122 130 ILE CA C 60.583
1123 130 ILE CB C 35.763
1124 130 ILE CG1 C 14.289
1125 130 ILE CG2 C 24.798
1126 130 ILE CD1 C 9.606
1127 130 ILE H H 8.168
1128 130 ILE HA H 3.750
1129 130 ILE HB H 1.803
1130 130 ILE HG12 H 0.744
1131 130 ILE HG13 H 0.744
1132 130 ILE HG2 H 1.513
1133 130 ILE HD1 H 0.690
1134 130 ILE N N 128.118
1135 131 ASP CA C 51.122
1136 131 ASP CB C 37.477
1137 131 ASP H H 8.136
1138 131 ASP HA H 4.296
1139 131 ASP HB3 H 2.251
1140 131 ASP N N 116.572
1141 132 GLY CA C 44.507
1142 132 GLY H H 7.460
1143 132 GLY HA2 H 3.668
1144 132 GLY HA3 H 3.691
1145 132 GLY N N 108.411
1146 133 ASP CA C 50.853
1147 133 ASP H H 8.177
1148 133 ASP HA H 4.296
1149 133 ASP HB2 H 2.315
1150 133 ASP HB3 H 2.315
1151 133 ASP N N 120.424
1152 134 GLY CA C 43.053
1153 134 GLY H H 10.043
1154 134 GLY HA2 H 3.869
1155 134 GLY HA3 H 3.243
1156 134 GLY N N 112.396
1157 135 GLN CA C 50.415
1158 135 GLN CB C 30.281
1159 135 GLN CG C 31.194
1160 135 GLN H H 7.866
1161 135 GLN HA H 4.804
1162 135 GLN HB2 H 1.633
1163 135 GLN HB3 H 1.633
1164 135 GLN HG2 H 1.804
1165 135 GLN HG3 H 1.804
1166 135 GLN N N 115.588
1167 136 VAL CA C 58.707
1168 136 VAL CB C 31.080
1169 136 VAL CG1 C 19.315
1170 136 VAL CG2 C 18.961
1171 136 VAL H H 8.856
1172 136 VAL HA H 4.999
1173 136 VAL HB H 2.027
1174 136 VAL HG1 H 1.037
1175 136 VAL HG2 H 0.676
1176 136 VAL N N 124.910
1177 137 ASN CA C 48.083
1178 137 ASN CB C 35.634
1179 137 ASN H H 9.390
1180 137 ASN HA H 5.173
1181 137 ASN HB2 H 2.958
1182 137 ASN HB3 H 2.958
1183 137 ASN N N 129.009
1184 138 TYR CA C 59.799
1185 138 TYR CB C 35.535
1186 138 TYR H H 8.075
1187 138 TYR HA H 4.478
1188 138 TYR HB2 H 3.275
1189 138 TYR HB3 H 3.393
1190 138 TYR HD1 H 6.770
1191 138 TYR N N 118.471
1192 139 GLU CA C 57.532
1193 139 GLU CB C 25.940
1194 139 GLU CG C 33.250
1195 139 GLU H H 7.925
1196 139 GLU HA H 3.838
1197 139 GLU HB2 H 1.876
1198 139 GLU HB3 H 1.876
1199 139 GLU HG2 H 2.177
1200 139 GLU HG3 H 2.177
1201 139 GLU N N 118.535
1202 140 GLU CA C 56.082
1203 140 GLU CB C 26.511
1204 140 GLU CG C 31.080
1205 140 GLU H H 8.664

1206 140 GLU HA H 3.849
1207 140 GLU HB2 H 1.769
1208 140 GLU HB3 H 1.940
1209 140 GLU HG2 H 2.218
1210 140 GLU HG3 H 2.218
1211 140 GLU N N 119.583
1212 141 PHE CA C 59.092
1213 141 PHE CB C 37.705
1214 141 PHE H H 8.395
1215 141 PHE HA H 3.721
1216 141 PHE HB2 H 3.252
1217 141 PHE HB3 H 2.901
1218 141 PHE N N 123.810
1219 142 VAL CA C 64.182
1220 142 VAL CB C 28.796
1221 142 VAL CG1 C 20.457
1222 142 VAL CG2 C 18.515
1223 142 VAL H H 8.484
1224 142 VAL HA H 3.092
1225 142 VAL HB H 1.644
1226 142 VAL HG1 H 0.600
1227 142 VAL HG2 H 0.355
1228 142 VAL N N 118.551
1229 143 GLN CA C 56.273
1230 143 GLN CB C 24.912
1231 143 GLN CG C 31.309
1232 143 GLN H H 7.803
1233 143 GLN HA H 3.838
1234 143 GLN HB2 H 1.932
1235 143 GLN HB3 H 1.932
1236 143 GLN HG2 H 2.240
1237 143 GLN HG3 H 2.240
1238 143 GLN N N 119.672
1239 144 MET CA C 55.387
1240 144 MET CB C 29.709
1241 144 MET CG C 30.509
1242 144 MET H H 7.322
1243 144 MET HA H 3.943
1244 144 MET HB2 H 1.655
1245 144 MET HB3 H 1.655
1246 144 MET HG2 H 1.644
1247 144 MET HG3 H 1.644
1248 144 MET N N 116.710
1249 145 MET CA C 53.291
1250 145 MET CB C 29.253
1251 145 MET CG C 30.052
1252 145 MET H H 7.467
1253 145 MET HA H 4.062
1254 145 MET HG2 H 1.804
1255 145 MET HG3 H 1.804
1256 145 MET N N 114.879
1257 146 THR CA C 59.201
1258 146 THR CB C 67.404
1259 146 THR CG2 C 18.401
1260 146 THR H H 7.551
1261 146 THR HA H 4.136
1262 146 THR HB H 4.104
1263 146 THR HG2 H 0.984
1264 146 THR N N 108.698
1265 147 ALA CA C 50.073
1266 147 ALA CB C 16.345
1267 147 ALA H H 7.596
1268 147 ALA HA H 4.145
1269 147 ALA HB H 1.247
1270 147 ALA N N 126.669
1271 148 LYS CA C 54.753
1272 148 LYS CB C 26.283
1273 148 LYS CG C 21.828
1274 148 LYS CD C 30.852
1275 148 LYS CE C 39.419
1276 148 LYS H H 7.805
1277 148 LYS HA H 3.964
1278 148 LYS HB2 H 1.523
1279 148 LYS HB3 H 1.523
1280 148 LYS HG2 H 1.217
1281 148 LYS HG3 H 1.217
1282 148 LYS HD2 H 1.641
1283 148 LYS HD3 H 1.641
1284 148 LYS HE2 H 2.816
1285 148 LYS HE3 H 2.816
1286 148 LYS N N 126.016

iNOS peptide assignments

1287 149 LEU CA C 55.533
1288 149 LEU H H 10.263
1289 149 LEU HA H 3.779
1290 149 LEU HB2 H 1.788
1291 149 LEU HB3 H 1.788
1292 149 LEU HG H 1.333
1293 149 LEU HD1 H 0.717
1294 149 LEU HD2 H 0.717
1295 149 LEU N N 128.585
1296 150 LYS CA C 56.947
1297 150 LYS H H 8.861
1298 150 LYS HA H 3.798
1299 150 LYS HB2 H 1.671
1300 150 LYS HB3 H 1.671
1301 150 LYS HG2 H 1.260
1302 150 LYS HG3 H 1.260
1303 150 LYS N N 115.210
1304 151 VAL CA C 63.221
1305 151 VAL H H 6.777
1306 151 VAL HA H 3.490

1307 151 VAL HB H 2.037
1308 151 VAL HG1 H 0.772
1309 151 VAL HG2 H 0.772
1310 151 VAL N N 117.710
1311 152 LEU CA C 55.392
1312 152 LEU H H 7.802
1313 152 LEU HA H 3.886
1314 152 LEU HB2 H 1.681
1315 152 LEU HB3 H 1.681
1316 152 LEU HG H 1.348
1317 152 LEU HD1 H 0.966
1318 152 LEU N N 120.709
1319 153 VAL CA C 64.212
1320 153 VAL H H 8.710
1321 153 VAL HA H 3.827
1322 153 VAL HB H 1.949
1323 153 VAL HG1 H 0.717
1324 153 VAL HG2 H 0.717
1325 153 VAL N N 111.964
1326 154 LYS CA C 57.786
1327 154 LYS H H 7.163
1328 154 LYS HA H 3.882
1329 154 LYS HB2 H 2.037
1330 154 LYS HB3 H 2.037
1331 154 LYS HG2 H 0.717
1332 154 LYS HG3 H 0.717
1333 154 LYS HD2 H 1.700
1334 154 LYS HD3 H 1.700
1335 154 LYS HZ H 2.392
1336 154 LYS N N 119.833
1337 155 ALA CA C 53.207
1338 155 ALA H H 7.803
1339 155 ALA HA H 4.395
1340 155 ALA HB H 1.700
1341 155 ALA N N 120.555
1342 156 VAL CA C 64.502
1343 156 VAL H H 8.295
1344 156 VAL HA H 3.578
1345 156 VAL HB H 2.331
1346 156 VAL HG1 H 0.996
1347 156 VAL HG2 H 0.996
1348 156 VAL N N 116.827
1349 157 LEU CA C 56.264
1350 157 LEU H H 8.910
1351 157 LEU HA H 4.003
1352 157 LEU HB2 H 1.685
1353 157 LEU HB3 H 1.685
1354 157 LEU HG H 1.667
1355 157 LEU HD1 H 0.952
1356 157 LEU HD2 H 0.952
1357 157 LEU N N 121.446
1358 158 PHE CA C 58.812
1359 158 PHE H H 7.935
1360 158 PHE HA H 4.165
1361 158 PHE HB2 H 3.402
1362 158 PHE HB3 H 3.402
1363 158 PHE HD1 H 6.776
1364 158 PHE HD2 H 6.776
1365 158 PHE N N 118.793
1366 159 ALA CA C 52.859
1367 159 ALA H H 7.687
1368 159 ALA HA H 3.636
1369 159 ALA HB H 1.612
1370 159 ALA N N 117.951
1371 160 CYS CA C 61.415
1372 160 CYS H H 8.557
1373 160 CYS HA H 4.077
1374 160 CYS HB2 H 3.035
1375 160 CYS HB3 H 3.035
1376 160 CYS N N 115.303
1377 161 MET CA C 56.156
1378 161 MET H H 8.502
1379 161 MET HA H 3.930
1380 161 MET HB2 H 1.979
1381 161 MET HB3 H 1.979
1382 161 MET HG2 H 2.712
1383 161 MET HG3 H 2.712
1384 161 MET HE H 2.291
1385 161 MET N N 120.601
1386 162 LEU CA C 52.975
1387 162 LEU H H 7.168
1388 162 LEU HA H 3.930
1389 162 LEU HB2 H 1.465
1390 162 LEU HB3 H 1.465
1391 162 LEU HG H 1.128
1392 162 LEU HD1 H 0.269
1393 162 LEU HD2 H 0.269
1394 162 LEU N N 118.166
1395 163 MET CA C 54.169
1396 163 MET H H 7.258
1397 163 MET HA H 4.032
1398 163 MET HB2 H 1.949
1399 163 MET HB3 H 1.949
1400 163 MET HG2 H 2.639
1401 163 MET HG3 H 2.639
1402 163 MET N N 117.255
1403 164 ARG CA C 53.310
1404 164 ARG H H 8.051
1405 164 ARG HA H 4.091
1406 164 ARG HB2 H 1.759
1407 164 ARG HB3 H 1.759
1408 164 ARG HG2 H 1.696

1409 164 ARG HG3 H 1.696
1410 164 ARG N N 122.437
1411 165 LYS CA C 54.802
1412 165 LYS H H 7.932
1413 165 LYS HA H 4.146
1414 165 LYS HB2 H 1.608
1415 165 LYS HB3 H 1.608
1416 165 LYS HG2 H 1.271
1417 165 LYS HG3 H 1.271
1418 165 LYS N N 128.142

Appendix C

CaM-eNOS Peptide Assigned Chemical Shifts

_Atom_shift_assign_ID
_Residue_seq_code
_Residue_label
_Atom_name
_Atom_type
_Chem_shift_value
_Chem_shift_value_error
_Chem_shift_ambiguity_code

1	2	ASP	CA	C	51.960		
2	2	ASP	H	H	8.502		
3	2	ASP	HA	H	4.585		
4	2	ASP	N	N	120.349		
5	3	GLN	CA	C	52.735		
6	3	GLN	CB	C	31.074		
7	3	GLN	CG	C	35.178		
8	3	GLN	H	H	8.200		
9	3	GLN	HA	H	4.212		
10	3	GLN	N	N	119.648		
11	4	LEU	CA	C	51.658		
12	4	LEU	CB	C	39.624		
13	4	LEU	CG	C	23.322		
14	4	LEU	CD1	C	20.016		
15	4	LEU	H	H	8.181		
16	4	LEU	HA	H	4.140		
17	4	LEU	HB2	H	1.584		
18	4	LEU	HB3	H	1.584		
19	4	LEU	HD1	H	0.751		
20	4	LEU	HD2	H	0.751		
21	4	LEU	N	N	123.025		
22	5	THR	CA	C	57.687		
23	5	THR	CB	C	68.580		
24	5	THR	CG2	C	18.990		
25	5	THR	H	H	8.615		
26	5	THR	HA	H	4.302		
27	5	THR	HB	H	4.625		
28	5	THR	HG2	H	1.169		
29	5	THR	N	N	112.894		
30	6	GLU	CA	C	57.247		
31	6	GLU	CB	C	29.136		
32	6	GLU	CG	C	33.696		
33	6	GLU	H	H	8.882		
34	6	GLU	HA	H	3.797		
35	6	GLU	HB2	H	1.880		
36	6	GLU	HB3	H	1.880		
37	6	GLU	HG2	H	2.219		
38	6	GLU	HG3	H	2.219		
39	6	GLU	N	N	120.209		
40	7	GLU	CA	C	57.198		
41	7	GLU	CB	C	26.274		
42	7	GLU	CG	C	33.696		
43	7	GLU	H	H	8.545		
44	7	GLU	HA	H	3.861		
45	7	GLU	HB2	H	1.846		
46	7	GLU	HB3	H	1.846		
47	7	GLU	HG2	H	2.178		
48	7	GLU	HG3	H	2.178		
49	7	GLU	N	N	119.415		
50	8	GLN	CA	C	55.976		
51	8	GLN	CB	C	26.400		
52	8	GLN	CG	C	33.582		
53	8	GLN	H	H	7.587		
54	8	GLN	HA	H	3.861		
55	8	GLN	HB2	H	1.920		
56	8	GLN	HB3	H	1.920		
57	8	GLN	HG2	H	2.175		
58	8	GLN	HG3	H	2.175		
59	8	GLN	N	N	119.809		
60	9	ILE	CA	C	63.796		
61	9	ILE	CB	C	35.178		
62	9	ILE	CG1	C	27.540		
63	9	ILE	CG2	C	14.772		
64	9	ILE	CD1	C	10.440		
65	9	ILE	H	H	8.268		
66	9	ILE	HA	H	3.553		
67	9	ILE	HB	H	1.773		
68	9	ILE	HG12	H	0.943		
69	9	ILE	HG13	H	0.943		
70	9	ILE	HD1	H	0.708		
71	9	ILE	N	N	119.415		
72	10	ALA	CA	C	52.702		
73	10	ALA	CB	C	15.114		
74	10	ALA	H	H	7.840		
75	10	ALA	HA	H	3.925		
76	10	ALA	HB	H	1.347		
77	10	ALA	N	N	121.044		
78	11	GLU	CA	C	56.563		
79	11	GLU	CB	C	26.400		
80	11	GLU	CG	C	33.468		
81	11	GLU	H	H	7.635		
82	11	GLU	HA	H	3.949		
83	11	GLU	HB2	H	1.899		

84	11	GLU	HB3	H	1.899
85	11	GLU	HG2	H	2.175
86	11	GLU	HG3	H	2.175
87	11	GLU	N	N	119.113
88	12	PHE	CA	C	56.954
89	12	PHE	CB	C	35.064
90	12	PHE	H	H	8.446
91	12	PHE	HA	H	4.777
92	12	PHE	HB2	H	3.350
93	12	PHE	N	N	119.662
94	13	LYS	CA	C	57.296
95	13	LYS	CB	C	29.592
96	13	LYS	CG	C	25.830
97	13	LYS	CD	C	33.696
98	13	LYS	H	H	9.107
99	13	LYS	HA	H	3.903
100	13	LYS	HB2	H	1.752
101	13	LYS	HB3	H	1.752
102	13	LYS	N	N	123.557
103	14	GLU	CA	C	56.465
104	14	GLU	CB	C	26.502
105	14	GLU	CG	C	33.584
106	14	GLU	H	H	7.652
107	14	GLU	HA	H	3.949
108	14	GLU	HB2	H	1.803
109	14	GLU	HB3	H	1.803
110	14	GLU	HG2	H	2.175
111	14	GLU	HG3	H	2.175
112	14	GLU	N	N	119.239
113	15	ALA	CA	C	52.751
114	15	ALA	CB	C	15.228
115	15	ALA	H	H	7.781
116	15	ALA	HA	H	3.993
117	15	ALA	HB	H	1.366
118	15	ALA	N	N	122.048
119	16	PHE	CA	C	59.544
120	16	PHE	CB	C	36.774
121	16	PHE	H	H	8.767
122	16	PHE	HA	H	3.095
123	16	PHE	HB2	H	2.669
124	16	PHE	HB3	H	2.669
125	16	PHE	HD1	H	6.477
126	16	PHE	HD2	H	6.477
127	16	PHE	HE1	H	6.903
128	16	PHE	HE2	H	6.903
129	16	PHE	HZ	H	7.035
130	16	PHE	N	N	118.962
131	17	SER	CA	C	58.567
132	17	SER	CB	C	60.600
133	17	SER	H	H	7.828
134	17	SER	HA	H	3.979
135	17	SER	HB2	H	3.883
136	17	SER	HB3	H	3.883
137	17	SER	N	N	111.534
138	18	LEU	CA	C	54.608
139	18	LEU	CB	C	39.638
140	18	LEU	CG	C	26.388
141	18	LEU	CD1	C	21.819
142	18	LEU	H	H	7.240
143	18	LEU	HA	H	3.920
144	18	LEU	HB2	H	1.499
145	18	LEU	HB3	H	1.499
146	18	LEU	HG	H	1.047
147	18	LEU	HD1	H	0.495
148	18	LEU	HD2	H	0.644
149	18	LEU	N	N	121.260
150	19	PHE	CA	C	57.247
151	19	PHE	CB	C	33.810
152	19	PHE	H	H	7.070
153	19	PHE	HA	H	3.963
154	19	PHE	HB2	H	2.218
155	19	PHE	HB3	H	2.218
156	19	PHE	HD1	H	6.977
157	19	PHE	HD2	H	6.977
158	19	PHE	N	N	114.235
159	20	ASP	CA	C	49.476
160	20	ASP	CB	C	36.782
161	20	ASP	H	H	7.667
162	20	ASP	HA	H	4.476
163	20	ASP	HB2	H	2.482
164	20	ASP	HB3	H	2.482
165	20	ASP	N	N	115.761
166	21	LYS	CA	C	56.025
167	21	LYS	CB	C	29.700
168	21	LYS	CG	C	21.476
169	21	LYS	CD	C	25.702
170	21	LYS	H	H	7.548
171	21	LYS	HA	H	3.786
172	21	LYS	HB2	H	1.688
173	21	LYS	HB3	H	1.688
174	21	LYS	HG2	H	1.369
175	21	LYS	HG3	H	1.283
176	21	LYS	HD2	H	1.560
177	21	LYS	HD3	H	1.560
178	21	LYS	HE2	H	2.881
179	21	LYS	HE3	H	2.881
180	21	LYS	N	N	124.906
181	22	ASP	CA	C	49.965
182	22	ASP	CB	C	36.774
183	22	ASP	H	H	7.952
184	22	ASP	HA	H	4.431
185	22	ASP	HB2	H	2.495

186 22 ASP HB3 H 2.943
187 22 ASP N N 113.609
188 23 GLY CA C 44.442
189 23 GLY H H 7.602
190 23 GLY HA2 H 3.686
191 23 GLY HA3 H 3.686
192 23 GLY N N 109.369
193 24 ASP CA C 51.040
194 24 ASP CB C 37.686
195 24 ASP H H 8.266
196 24 ASP HA H 4.329
197 24 ASP HB2 H 2.881
198 24 ASP HB3 H 2.881
199 24 ASP N N 120.643
200 25 GLY CA C 42.683
201 25 GLY H H 10.543
202 25 GLY HA2 H 3.582
203 25 GLY HA3 H 3.582
204 25 GLY N N 113.205
205 26 THR CA C 56.954
206 26 THR CB C 69.948
207 26 THR CG2 C 18.990
208 26 THR H H 8.020
209 26 THR HA H 5.140
210 26 THR HB H 3.688
211 26 THR HG2 H 0.876
212 26 THR N N 112.852
213 27 ILE CA C 57.931
214 27 ILE CB C 37.230
215 27 ILE CG1 C 24.120
216 27 ILE CG2 C 15.342
217 27 ILE CD1 C 12.948
218 27 ILE H H 9.689
219 27 ILE HA H 4.755
220 27 ILE HB H 1.859
221 27 ILE HG12 H 0.890
222 27 ILE HG13 H 0.890
223 27 ILE HD1 H 0.655
224 27 ILE N N 127.005
225 28 THR CA C 56.612
226 28 THR CB C 69.606
227 28 THR CG2 C 19.560
228 28 THR H H 8.275
229 28 THR HA H 4.753
230 28 THR HB H 4.727
231 28 THR HG2 H 0.718
232 28 THR N N 116.439
233 29 THR CA C 63.845
234 29 THR CB C 65.616
235 29 THR CG2 C 20.472
236 29 THR H H 9.057
237 29 THR HA H 3.612
238 29 THR HB H 4.015
239 29 THR HG2 H 1.102
240 29 THR N N 113.258
241 30 LYS CA C 56.465
242 30 LYS CB C 29.700
243 30 LYS CG C 21.705
244 30 LYS CD C 25.931
245 30 LYS H H 7.578
246 30 LYS HA H 4.003
247 30 LYS HB2 H 1.662
248 30 LYS HB3 H 1.662
249 30 LYS HG2 H 1.211
250 30 LYS HG3 H 1.211
251 30 LYS N N 121.230
252 31 GLU CA C 57.149
253 31 GLU CB C 26.058
254 31 GLU CG C 33.696
255 31 GLU H H 7.712
256 31 GLU HA H 3.880
257 31 GLU HB2 H 1.920
258 31 GLU HB3 H 1.920
259 31 GLU HG2 H 2.175
260 31 GLU HG3 H 2.175
261 31 GLU N N 122.002
262 32 LEU CA C 55.529
263 32 LEU CB C 39.981
264 32 LEU CG C 23.418
265 32 LEU CD1 C 21.133
266 32 LEU H H 8.520
267 32 LEU HA H 3.925
268 32 LEU HB2 H 1.764
269 32 LEU HB3 H 1.764
270 32 LEU HG H 1.386
271 32 LEU HD1 H 0.642
272 32 LEU N N 119.182
273 33 GLY CA C 45.664
274 33 GLY H H 8.384
275 33 GLY HA2 H 3.818
276 33 GLY HA3 H 3.392
277 33 GLY N N 103.688
278 34 THR CA C 64.285
279 34 THR CB C 66.186
280 34 THR CG2 C 18.648
281 34 THR H H 7.928
282 34 THR HA H 3.795
283 34 THR HB H 4.157
284 34 THR HG2 H 1.124
285 34 THR N N 117.399
286 35 VAL H H 7.091
287 35 VAL N N 120.256

288	36	MET	CA	C	57.101
289	36	MET	CB	C	29.929
290	36	MET	H	H	8.321
291	36	MET	HA	H	3.861
292	36	MET	HB2	H	1.715
293	36	MET	HB3	H	1.715
294	36	MET	HG2	H	1.978
295	36	MET	HG3	H	1.978
296	36	MET	N	N	117.757
297	37	ARG	CA	C	56.172
298	37	ARG	CB	C	27.084
299	37	ARG	CG	C	25.488
300	37	ARG	CD	C	40.878
301	37	ARG	H	H	8.236
302	37	ARG	HA	H	4.698
303	37	ARG	HB2	H	1.752
304	37	ARG	HB3	H	1.752
305	37	ARG	HG2	H	1.846
306	37	ARG	HG3	H	1.846
307	37	ARG	N	N	117.647
308	38	SER	CA	C	59.251
309	38	SER	CB	C	67.782
310	38	SER	H	H	7.874
311	38	SER	HA	H	4.140
312	38	SER	HB2	H	4.072
313	38	SER	HB3	H	4.072
314	38	SER	N	N	118.974
315	39	LEU	CA	C	51.333
316	39	LEU	CB	C	39.638
317	39	LEU	CG	C	23.190
318	39	LEU	CD1	C	20.791
319	39	LEU	H	H	7.258
320	39	LEU	HA	H	4.111
321	39	LEU	HB2	H	1.667
322	39	LEU	HB3	H	1.667
323	39	LEU	HG	H	1.584
324	39	LEU	HD1	H	0.517
325	39	LEU	HD2	H	0.517
326	39	LEU	N	N	118.804
327	40	GLY	CA	C	42.878
328	40	GLY	H	H	7.462
329	40	GLY	HA2	H	4.082
330	40	GLY	HA3	H	4.082
331	40	GLY	N	N	104.887
332	41	GLN	CA	C	51.187
333	41	GLN	CB	C	30.618
334	41	GLN	CG	C	37.116
335	41	GLN	H	H	7.860
336	41	GLN	HA	H	4.370
337	41	GLN	HB2	H	2.048
338	41	GLN	HB3	H	2.048
339	41	GLN	HG2	H	2.921
340	41	GLN	HG3	H	2.921
341	41	GLN	N	N	118.032
342	42	ASN	CA	C	48.694
343	42	ASN	CB	C	36.554
344	42	ASN	H	H	8.566
345	42	ASN	HA	H	5.094
346	42	ASN	HB2	H	2.348
347	42	ASN	HB3	H	2.348
348	42	ASN	N	N	115.627
349	43	PRO	HA	H	4.711
350	43	PRO	HD2	H	3.448
351	44	THR	CA	C	57.638
352	44	THR	CB	C	68.466
353	44	THR	CG2	C	18.990
354	44	THR	H	H	8.907
355	44	THR	HA	H	4.321
356	44	THR	HB	H	4.595
357	44	THR	HG2	H	1.162
358	44	THR	N	N	113.553
359	45	GLU	CA	C	57.101
360	45	GLU	CB	C	26.274
361	45	GLU	CG	C	33.696
362	45	GLU	H	H	8.654
363	45	GLU	HA	H	3.880
364	45	GLU	HB2	H	1.868
365	45	GLU	HB3	H	1.868
366	45	GLU	HG2	H	2.175
367	45	GLU	HG3	H	2.175
368	45	GLU	N	N	120.447
369	46	ALA	CA	C	52.311
370	46	ALA	CB	C	15.080
371	46	ALA	H	H	8.137
372	46	ALA	HA	H	3.925
373	46	ALA	HB	H	1.260
374	46	ALA	N	N	120.615
375	47	GLU	CA	C	56.270
376	47	GLU	CB	C	26.286
377	47	GLU	CG	C	33.468
378	47	GLU	H	H	7.589
379	47	GLU	HA	H	3.876
380	47	GLU	HB2	H	1.878
381	47	GLU	HB3	H	1.878
382	47	GLU	HG2	H	2.189
383	47	GLU	HG3	H	2.189
384	47	GLU	N	N	118.078
385	48	LEU	CA	C	55.048
386	48	LEU	CB	C	39.981
387	48	LEU	CG	C	23.532
388	48	LEU	CD1	C	20.562
389	48	LEU	H	H	7.868

390 48 LEU HA H 3.927
391 48 LEU HB2 H 1.636
392 48 LEU HB3 H 1.636
393 48 LEU HG H 1.602
394 48 LEU HD1 H 0.696
395 48 LEU HD2 H 1.277
396 48 LEU N N 120.241
397 49 GLN CA C 55.732
398 49 GLN CB C 27.882
399 49 GLN CG C 33.354
400 49 GLN H H 8.031
401 49 GLN HA H 3.901
402 49 GLN HB2 H 1.978
403 49 GLN HB3 H 1.978
404 49 GLN HG2 H 2.219
405 49 GLN HG3 H 2.219
406 49 GLN N N 117.939
407 50 ASP CA C 54.706
408 50 ASP CB C 37.572
409 50 ASP H H 8.010
410 50 ASP HA H 4.157
411 50 ASP HB2 H 2.517
412 50 ASP HB3 H 2.517
413 50 ASP N N 119.284
414 51 MET CA C 56.563
415 51 MET CB C 29.478
416 51 MET H H 7.609
417 51 MET HA H 3.923
418 51 MET HB2 H 1.728
419 51 MET HB3 H 1.728
420 51 MET N N 119.253
421 52 ILE CA C 61.890
422 52 ILE CB C 34.494
423 52 ILE CG1 C 26.058
424 52 ILE CG2 C 13.518
425 52 ILE CD1 C 9.984
426 52 ILE H H 7.514
427 52 ILE HA H 3.328
428 52 ILE HB H 1.786
429 52 ILE HG12 H 0.905
430 52 ILE HG13 H 0.905
431 52 ILE HG2 H 0.557
432 52 ILE HD1 H 0.554
433 52 ILE N N 117.584
434 53 ASN CA C 53.093
435 53 ASN CB C 35.292
436 53 ASN H H 8.418
437 53 ASN HA H 4.222
438 53 ASN HB2 H 2.815
439 53 ASN HB3 H 2.815
440 53 ASN N N 117.126
441 54 GLU CA C 56.123
442 54 GLU CB C 26.400
443 54 GLU CG C 33.582
444 54 GLU H H 7.460
445 54 GLU HA H 3.861
446 54 GLU HB2 H 1.956
447 54 GLU HB3 H 1.956
448 54 GLU HG2 H 2.241
449 54 GLU HG3 H 2.241
450 54 GLU N N 116.395
451 55 VAL CA C 58.176
452 55 VAL CB C 30.162
453 55 VAL CG1 C 18.990
454 55 VAL CG2 C 16.824
455 55 VAL H H 7.044
456 55 VAL HA H 4.272
457 55 VAL HB H 1.912
458 55 VAL HG1 H 0.729
459 55 VAL HG2 H 0.729
460 55 VAL N N 108.622
461 56 ASP CA C 50.991
462 56 ASP CB C 36.896
463 56 ASP H H 7.560
464 56 ASP HA H 4.390
465 56 ASP HB2 H 2.943
466 56 ASP HB3 H 2.503
467 56 ASP N N 121.492
468 57 ALA CA C 51.480
469 57 ALA CB C 16.793
470 57 ALA H H 8.359
471 57 ALA HA H 4.053
472 57 ALA HB H 1.369
473 57 ALA N N 131.811
474 58 ASP CA C 49.916
475 58 ASP CB C 36.774
476 58 ASP H H 7.978
477 58 ASP HA H 4.453
478 58 ASP HB2 H 2.921
479 58 ASP HB3 H 2.517
480 58 ASP N N 113.609
481 59 GLY CA C 44.491
482 59 GLY H H 7.424
483 59 GLY HA2 H 3.688
484 59 GLY HA3 H 3.688
485 59 GLY N N 108.143
486 60 ASN CA C 49.769
487 60 ASN CB C 36.554
488 60 ASN H H 7.916
489 60 ASN HA H 4.455
490 60 ASN HB2 H 2.517
491 60 ASN HB3 H 2.517

492 60 ASN N N 118.109
493 61 GLY CA C 42.878
494 61 GLY H H 10.485
495 61 GLY HA2 H 4.050
496 61 GLY HA3 H 4.050
497 61 GLY N N 113.247
498 62 THR CA C 56.661
499 62 THR H H 7.511
500 62 THR HA H 4.580
501 62 THR HB H 3.788
502 62 THR HG2 H 0.948
503 62 THR N N 108.699
504 63 ILE CA C 57.101
505 63 ILE CB C 37.344
506 63 ILE CG1 C 24.462
507 63 ILE CG2 C 15.684
508 63 ILE CD1 C 10.554
509 63 ILE H H 8.732
510 63 ILE HA H 5.054
511 63 ILE HB H 1.859
512 63 ILE HG12 H 1.059
513 63 ILE HG13 H 1.059
514 63 ILE HG2 H 0.910
515 63 ILE HD1 H 0.590
516 63 ILE N N 122.717
517 64 ASP CA C 49.378
518 64 ASP CB C 36.782
519 64 ASP H H 8.707
520 64 ASP HA H 5.075
521 64 ASP HB2 H 2.668
522 64 ASP HB3 H 2.945
523 64 ASP N N 127.818
524 65 PHE CA C 60.717
525 65 PHE CB C 33.126
526 65 PHE H H 8.847
527 65 PHE HA H 3.861
528 65 PHE HB2 H 1.824
529 65 PHE HB3 H 1.824
530 65 PHE HD1 H 6.590
531 65 PHE HD2 H 6.590
532 65 PHE HZ H 7.035
533 65 PHE N N 118.653
534 67 GLU CA C 56.337
535 67 GLU CB C 26.045
536 67 GLU CG C 33.470
537 67 GLU H H 7.948
538 67 GLU HA H 3.861
539 67 GLU HB2 H 1.868
540 67 GLU HB3 H 1.868
541 67 GLU HG2 H 2.321
542 67 GLU HG3 H 2.321
543 67 GLU N N 117.690
544 68 PHE CA C 58.727
545 68 PHE CB C 37.572
546 68 PHE H H 8.760
547 68 PHE HA H 3.840
548 68 PHE HB2 H 3.371
549 68 PHE HB3 H 3.371
550 68 PHE HD1 H 6.844
551 68 PHE HD2 H 6.844
552 68 PHE HE1 H 6.502
553 68 PHE HE2 H 6.502
554 68 PHE HZ H 7.001
555 68 PHE N N 123.348
556 69 LEU CA C 55.158
557 69 LEU CB C 38.256
558 69 LEU CG C 22.752
559 69 LEU CD1 C 21.270
560 69 LEU CD2 C 22.752
561 69 LEU H H 8.400
562 69 LEU HA H 3.245
563 69 LEU HB2 H 1.361
564 69 LEU HB3 H 1.361
565 69 LEU HG H 1.026
566 69 LEU HD1 H 0.514
567 69 LEU N N 118.822
568 70 THR CA C 63.843
569 70 THR CB C 65.502
570 70 THR CG2 C 19.192
571 70 THR H H 7.540
572 70 THR HA H 3.624
573 70 THR HB H 4.168
574 70 THR HG2 H 1.068
575 70 THR N N 116.379
576 71 MET CA C 56.303
577 71 MET CB C 29.706
578 71 MET H H 7.721
579 71 MET HA H 3.752
580 71 MET HB2 H 1.707
581 71 MET HB3 H 1.707
582 71 MET HG2 H 2.197
583 71 MET HG3 H 2.197
584 71 MET N N 121.678
585 72 MET CA C 53.307
586 72 MET CB C 28.787
587 72 MET CG C 28.787
588 72 MET CE C 15.194
589 72 MET H H 7.969
590 72 MET HA H 3.773
591 72 MET HB2 H 1.750
592 72 MET HB3 H 1.750
593 72 MET HG2 H 2.065

594	72	MET	HG3	H	2.065
595	72	MET	N	N	116.476
596	73	ALA	CA	C	52.095
597	73	ALA	CB	C	15.342
598	73	ALA	H	H	8.059
599	73	ALA	HA	H	3.880
600	73	ALA	HB	H	1.252
601	73	ALA	N	N	121.540
602	74	ARG	CA	C	55.731
603	74	ARG	CB	C	27.987
604	74	ARG	H	H	7.353
605	74	ARG	HA	H	3.883
606	74	ARG	HB2	H	1.671
607	74	ARG	HB3	H	1.671
608	74	ARG	HD2	H	2.963
609	74	ARG	HD3	H	2.963
610	74	ARG	N	N	115.761
611	75	LYS	CA	C	53.947
612	75	LYS	CB	C	26.400
613	75	LYS	CG	C	22.068
614	75	LYS	CD	C	30.960
615	75	LYS	CE	C	39.738
616	75	LYS	H	H	7.621
617	75	LYS	HA	H	3.949
618	75	LYS	HB2	H	1.587
619	75	LYS	HB3	H	1.587
620	75	LYS	HG2	H	1.277
621	75	LYS	HG3	H	1.277
622	75	LYS	HD2	H	1.540
623	75	LYS	HD3	H	1.540
624	75	LYS	HE2	H	2.898
625	75	LYS	HE3	H	2.898
626	75	LYS	N	N	117.213
627	76	MET	CA	C	53.947
628	76	MET	CB	C	29.478
629	76	MET	CG	C	29.815
630	76	MET	H	H	7.779
631	76	MET	HA	H	4.242
632	76	MET	HB2	H	2.027
633	76	MET	HB3	H	2.027
634	76	MET	HG2	H	2.591
635	76	MET	HG3	H	2.591
636	76	MET	N	N	117.986
637	77	LYS	CA	C	54.283
638	77	LYS	CB	C	29.478
639	77	LYS	CG	C	26.400
640	77	LYS	H	H	7.646
641	77	LYS	HA	H	4.140
642	77	LYS	HB2	H	1.690
643	77	LYS	HB3	H	1.690
644	77	LYS	HG2	H	1.470
645	77	LYS	HG3	H	1.470
646	77	LYS	HD2	H	1.693
647	77	LYS	HD3	H	1.693
648	77	LYS	N	N	119.979
649	78	ASP	CA	C	52.061
650	78	ASP	H	H	8.007
651	78	ASP	HA	H	4.243
652	78	ASP	HB2	H	2.547
653	78	ASP	HB3	H	2.547
654	78	ASP	N	N	119.333
655	79	THR	CA	C	59.030
656	79	THR	CB	C	67.668
657	79	THR	CG2	C	18.534
658	79	THR	H	H	7.590
659	79	THR	HA	H	4.170
660	79	THR	HB	H	4.096
661	79	THR	HG2	H	1.080
662	79	THR	N	N	112.721
663	80	ASP	CA	C	50.850
664	80	ASP	CB	C	37.353
665	80	ASP	H	H	8.349
666	80	ASP	HA	H	4.683
667	80	ASP	HB2	H	2.585
668	80	ASP	HB3	H	2.585
669	80	ASP	N	N	122.829
670	81	SER	CA	C	57.717
671	81	SER	CB	C	60.884
672	81	SER	H	H	8.235
673	81	SER	HA	H	4.140
674	81	SER	HB2	H	3.796
675	81	SER	HB3	H	3.796
676	81	SER	N	N	117.571
677	82	GLU	CA	C	56.707
678	82	GLU	CB	C	29.592
679	82	GLU	CG	C	33.468
680	82	GLU	H	H	8.372
681	82	GLU	HA	H	3.883
682	82	GLU	HB2	H	1.965
683	82	GLU	HG2	H	2.175
684	82	GLU	N	N	121.904
685	83	GLU	CA	C	56.606
686	83	GLU	CB	C	29.364
687	83	GLU	CG	C	33.582
688	83	GLU	H	H	8.036
689	83	GLU	HA	H	3.883
690	83	GLU	HB2	H	1.956
691	83	GLU	HB3	H	1.956
692	83	GLU	HG2	H	2.219
693	83	GLU	HG3	H	2.219
694	83	GLU	N	N	119.340
695	84	GLU	CA	C	56.606

696	84	GLU	CB	C	25.817
697	84	GLU	CG	C	33.470
698	84	GLU	H	H	8.153
699	84	GLU	HA	H	3.871
700	84	GLU	HB2	H	1.917
701	84	GLU	HB3	H	1.917
702	84	GLU	HG2	H	2.226
703	84	GLU	HG3	H	2.226
704	84	GLU	N	N	118.279
705	85	ILE	CA	C	63.439
706	85	ILE	CB	C	34.608
707	85	ILE	CG1	C	27.654
708	85	ILE	CG2	C	15.912
709	85	ILE	CD1	C	10.212
710	85	ILE	H	H	7.910
711	85	ILE	HA	H	3.612
712	85	ILE	HB	H	1.778
713	85	ILE	HG12	H	0.919
714	85	ILE	HG13	H	0.919
715	85	ILE	HG2	H	0.983
716	85	ILE	HD1	H	0.686
717	85	ILE	N	N	120.905
718	86	ARG	CA	C	57.515
719	86	ARG	CB	C	26.856
720	86	ARG	CG	C	24.690
721	86	ARG	CD	C	40.536
722	86	ARG	H	H	8.227
723	86	ARG	HA	H	4.008
724	86	ARG	HB2	H	1.899
725	86	ARG	HB3	H	1.899
726	86	ARG	HG2	H	1.496
727	86	ARG	HG3	H	1.496
728	86	ARG	HD2	H	2.810
729	86	ARG	HD3	H	2.810
730	86	ARG	N	N	121.722
731	87	GLU	CA	C	56.606
732	87	GLU	CB	C	25.817
733	87	GLU	CG	C	33.698
734	87	GLU	H	H	8.156
735	87	GLU	HA	H	3.861
736	87	GLU	HB2	H	1.890
737	87	GLU	HB3	H	1.890
738	87	GLU	HG2	H	2.175
739	87	GLU	HG3	H	2.175
740	87	GLU	N	N	118.369
741	88	ALA	CA	C	52.263
742	88	ALA	CB	C	15.080
743	88	ALA	H	H	7.884
744	88	ALA	HA	H	3.949
745	88	ALA	HB	H	1.605
746	88	ALA	N	N	120.389
747	89	PHE	CA	C	59.703
748	89	PHE	CB	C	36.774
749	89	PHE	H	H	8.446
750	89	PHE	HA	H	3.115
751	89	PHE	HB2	H	2.815
752	89	PHE	HB3	H	2.815
753	89	PHE	HD1	H	6.478
754	89	PHE	HD2	H	6.478
755	89	PHE	HE1	H	7.054
756	89	PHE	HE2	H	7.054
757	89	PHE	N	N	118.191
758	90	ARG	CA	C	56.168
759	90	ARG	CB	C	27.654
760	90	ARG	CG	C	25.716
761	90	ARG	CD	C	40.764
762	90	ARG	H	H	7.762
763	90	ARG	HA	H	3.905
764	90	ARG	HB2	H	1.803
765	90	ARG	HB3	H	1.803
766	90	ARG	HG2	H	1.562
767	90	ARG	HG3	H	1.562
768	90	ARG	HD2	H	3.073
769	90	ARG	HD3	H	3.073
770	90	ARG	N	N	116.070
771	91	VAL	CA	C	63.357
772	91	VAL	CB	C	28.444
773	91	VAL	CG1	C	18.164
774	91	VAL	CG2	C	19.877
775	91	VAL	H	H	7.229
776	91	VAL	HA	H	3.243
777	91	VAL	HB	H	1.901
778	91	VAL	HG1	H	0.346
779	91	VAL	HG2	H	0.815
780	91	VAL	N	N	118.202
781	92	PHE	CA	C	58.029
782	92	PHE	CB	C	38.838
783	92	PHE	H	H	6.690
784	92	PHE	HA	H	3.967
785	92	PHE	HD1	H	6.373
786	92	PHE	HD2	H	6.373
787	92	PHE	N	N	113.143
788	93	ASP	CA	C	49.525
789	93	ASP	CB	C	35.183
790	93	ASP	H	H	7.860
791	93	ASP	HA	H	4.476
792	93	ASP	HB2	H	2.517
793	93	ASP	HB3	H	2.517
794	93	ASP	N	N	116.549
795	94	LYS	CA	C	55.976
796	94	LYS	CB	C	31.414
797	94	LYS	CG	C	25.246

798 94 LYS CD C 27.644
799 94 LYS CE C 40.764
800 94 LYS H H 7.595
801 94 LYS HA H 3.700
802 94 LYS HB2 H 1.667
803 94 LYS HB3 H 1.667
804 94 LYS HG2 H 1.369
805 94 LYS HG3 H 1.283
806 94 LYS HD2 H 1.560
807 94 LYS HD3 H 1.560
808 94 LYS N N 125.339
809 95 ASP CA C 50.307
810 95 ASP CB C 36.774
811 95 ASP H H 8.091
812 95 ASP HA H 4.415
813 95 ASP HB2 H 2.924
814 95 ASP HB3 H 2.498
815 95 ASP N N 114.015
816 96 GLY CA C 44.344
817 96 GLY H H 7.659
818 96 GLY HA2 H 3.686
819 96 GLY HA3 H 3.686
820 96 GLY N N 109.044
821 97 ASN CA C 49.916
822 97 ASN CB C 35.183
823 97 ASN H H 8.243
824 97 ASN HA H 4.500
825 97 ASN HB2 H 3.271
826 97 ASN HB3 H 3.271
827 97 ASN N N 119.575
828 98 GLY CA C 42.292
829 98 GLY H H 10.445
830 98 GLY HA2 H 3.986
831 98 GLY HA3 H 3.986
832 98 GLY N N 112.392
833 99 TYR CA C 53.582
834 99 TYR CB C 39.981
835 99 TYR H H 7.568
836 99 TYR HA H 4.841
837 99 TYR HB2 H 2.412
838 99 TYR HB3 H 2.412
839 99 TYR HD1 H 6.736
840 99 TYR HD2 H 6.736
841 99 TYR N N 116.256
842 100 ILE CA C 58.616
843 100 ILE CB C 36.432
844 100 ILE CG1 C 24.234
845 100 ILE CG2 C 14.316
846 100 ILE CD1 C 13.632
847 100 ILE H H 9.957
848 100 ILE HA H 4.457
849 100 ILE HB H 1.731
850 100 ILE HG2 H 0.751
851 100 ILE HD1 H 1.197
852 100 ILE N N 127.103
853 101 SER CA C 52.897
854 101 SER CB C 64.134
855 101 SER H H 8.845
856 101 SER HA H 4.711
857 101 SER HB2 H 3.818
858 101 SER HB3 H 3.818
859 101 SER N N 123.768
860 102 ALA CA C 53.093
861 102 ALA CB C 15.114
862 102 ALA H H 9.185
863 102 ALA HA H 3.669
864 102 ALA HB H 1.305
865 102 ALA N N 122.940
866 103 ALA CA C 52.409
867 103 ALA CB C 15.456
868 103 ALA H H 8.132
869 103 ALA HA H 3.861
870 103 ALA HB H 1.262
871 103 ALA N N 118.443
872 104 GLU CA C 56.563
873 104 GLU CB C 26.400
874 104 GLU CG C 33.582
875 104 GLU H H 7.782
876 104 GLU HA H 3.839
877 104 GLU HB2 H 1.917
878 104 GLU HB3 H 1.917
879 104 GLU HG2 H 2.260
880 104 GLU HG3 H 2.260
881 104 GLU N N 120.268
882 105 LEU CA C 55.732
883 105 LEU CB C 40.209
884 105 LEU CG C 23.532
885 105 LEU CD1 C 20.791
886 105 LEU H H 8.231
887 105 LEU HA H 3.962
888 105 LEU HB2 H 1.743
889 105 LEU HB3 H 1.743
890 105 LEU HG H 1.577
891 105 LEU HD1 H 0.773
892 105 LEU HD2 H 1.036
893 105 LEU N N 121.501
894 106 ARG CA C 57.345
895 106 ARG CB C 30.390
896 106 ARG CG C 25.944
897 106 ARG CD C 39.054
898 106 ARG H H 8.774
899 106 ARG HA H 3.861

900 106 ARG HB2 H 1.686
901 106 ARG HB3 H 1.686
902 106 ARG HG2 H 1.452
903 106 ARG HG3 H 1.452
904 106 ARG HD2 H 3.076
905 106 ARG HD3 H 3.076
906 106 ARG N N 118.625
907 107 HIS CA C 56.807
908 107 HIS CB C 27.198
909 107 HIS H H 7.946
910 107 HIS HA H 3.876
911 107 HIS HB2 H 1.837
912 107 HIS HB3 H 1.837
913 107 HIS N N 119.052
914 108 VAL CA C 64.285
915 108 VAL CB C 28.908
916 108 VAL CG1 C 18.078
917 108 VAL CG2 C 20.700
918 108 VAL H H 7.713
919 108 VAL HA H 3.442
920 108 VAL HB H 2.027
921 108 VAL HG1 H 0.466
922 108 VAL HG2 H 0.861
923 108 VAL N N 119.160
924 109 MET CA C 54.461
925 109 MET CB C 29.706
926 109 MET H H 8.130
927 109 MET HA H 4.139
928 109 MET HB2 H 1.781
929 109 MET HB3 H 1.781
930 109 MET HG2 H 2.038
931 109 MET HG3 H 2.038
932 109 MET N N 115.318
933 110 THR CA C 63.845
934 110 THR CB C 66.072
935 110 THR CG2 C 18.876
936 110 THR H H 8.515
937 110 THR HA H 3.935
938 110 THR HB H 4.168
939 110 THR HG2 H 1.080
940 110 THR N N 116.846
941 111 ASN CA C 53.093
942 111 ASN CB C 35.292
943 111 ASN H H 7.877
944 111 ASN HA H 4.242
945 111 ASN HB2 H 2.689
946 111 ASN HB3 H 2.815
947 111 ASN N N 123.887
948 112 LEU CA C 52.653
949 112 LEU CB C 39.738
950 112 LEU CG C 23.094
951 112 LEU CD1 C 20.244
952 112 LEU H H 7.672
953 112 LEU HA H 4.093
954 112 LEU HB2 H 1.750
955 112 LEU HB3 H 1.750
956 112 LEU HG H 1.643
957 112 LEU HD1 H 0.621
958 112 LEU HD2 H 0.621
959 112 LEU N N 118.372
960 113 GLY CA C 42.536
961 113 GLY H H 7.704
962 113 GLY HA2 H 4.124
963 113 GLY HA3 H 4.124
964 113 GLY N N 106.860
965 114 GLU CA C 52.067
966 114 GLU CB C 26.616
967 114 GLU CG C 31.071
968 114 GLU H H 7.871
969 114 GLU HA H 4.242
970 114 GLU HB2 H 1.518
971 114 GLU HB3 H 1.518
972 114 GLU HG2 H 1.803
973 114 GLU HG3 H 1.803
974 114 GLU N N 120.133
975 115 LYS CA C 52.848
976 115 LYS CB C 30.957
977 115 LYS CG C 26.502
978 115 LYS CD C 21.933
979 115 LYS H H 8.494
980 115 LYS HA H 4.223
981 115 LYS HB2 H 1.773
982 115 LYS HB3 H 1.773
983 115 LYS HG2 H 1.198
984 115 LYS HG3 H 1.198
985 115 LYS HD2 H 1.496
986 115 LYS HD3 H 1.496
987 115 LYS N N 124.987
988 116 LEU CA C 51.089
989 116 LEU CB C 42.588
990 116 LEU CG C 24.804
991 116 LEU CD1 C 21.384
992 116 LEU CD2 C 16.482
993 116 LEU H H 7.978
994 116 LEU HA H 4.712
995 116 LEU HB2 H 1.473
996 116 LEU HB3 H 1.473
997 116 LEU HG H 1.433
998 116 LEU HD1 H 0.663
999 116 LEU N N 124.868
1000 117 THR CA C 57.834
1001 117 THR CB C 68.580

1002 117 THR CG2 C 18.990
1003 117 THR H H 9.129
1004 117 THR HA H 4.302
1005 117 THR HB H 4.647
1006 117 THR HG2 H 1.153
1007 117 THR N N 114.337
1008 118 ASP CA C 55.243
1009 118 ASP CB C 37.002
1010 118 ASP H H 8.767
1011 118 ASP HA H 4.031
1012 118 ASP HB2 H 2.412
1013 118 ASP HB3 H 2.412
1014 118 ASP N N 120.881
1015 119 GLU CA C 57.149
1016 119 GLU CB C 25.931
1017 119 GLU CG C 33.812
1018 119 GLU H H 8.521
1019 119 GLU HA H 3.927
1020 119 GLU HB2 H 1.837
1021 119 GLU HB3 H 1.837
1022 119 GLU HG2 H 2.203
1023 119 GLU HG3 H 2.203
1024 119 GLU N N 119.298
1025 120 GLU CA C 56.319
1026 120 GLU CB C 25.830
1027 120 GLU CG C 33.696
1028 120 GLU H H 7.577
1029 120 GLU HA H 3.847
1030 120 GLU HB2 H 1.878
1031 120 GLU HB3 H 1.878
1032 120 GLU HG2 H 2.176
1033 120 GLU HG3 H 2.176
1034 120 GLU N N 120.118
1035 121 VAL CA C 64.090
1036 121 VAL CB C 28.680
1037 121 VAL CG1 C 20.700
1038 121 VAL CG2 C 18.078
1039 121 VAL H H 7.852
1040 121 VAL HA H 3.423
1041 121 VAL HB H 1.899
1042 121 VAL HG1 H 0.749
1043 121 VAL HG2 H 0.174
1044 121 VAL N N 122.079
1045 122 ASP CA C 54.901
1046 122 ASP CB C 37.572
1047 122 ASP H H 7.882
1048 122 ASP HA H 4.157
1049 122 ASP HB2 H 2.623
1050 122 ASP HB3 H 2.623
1051 122 ASP N N 120.225
1052 123 GLU CA C 56.612
1053 123 GLU CB C 26.172
1054 123 GLU CG C 33.468
1055 123 GLU H H 7.814
1056 123 GLU HA H 3.880
1057 123 GLU HB2 H 1.978
1058 123 GLU HB3 H 1.978
1059 123 GLU HG2 H 2.175
1060 123 GLU HG3 H 2.175
1061 123 GLU N N 119.175
1062 124 MET CA C 56.905
1063 124 MET CB C 29.250
1064 124 MET H H 7.431
1065 124 MET HA H 3.818
1066 124 MET HB2 H 1.707
1067 124 MET HB3 H 1.707
1068 124 MET HG2 H 2.109
1069 124 MET HG3 H 2.109
1070 124 MET N N 119.067
1071 125 ILE CA C 60.131
1072 125 ILE CB C 33.240
1073 125 ILE CG1 C 13.595
1074 125 ILE CG2 C 24.789
1075 125 ILE CD1 C 6.906
1076 125 ILE H H 7.710
1077 125 ILE HA H 3.380
1078 125 ILE HB H 2.086
1079 125 ILE HG12 H 0.554
1080 125 ILE HG13 H 0.554
1081 125 ILE HG2 H 1.233
1082 125 ILE HD1 H 0.408
1083 125 ILE N N 118.171
1084 126 ARG CA C 56.673
1085 126 ARG CB C 29.478
1086 126 ARG CG C 26.058
1087 126 ARG CD C 40.992
1088 126 ARG H H 7.951
1089 126 ARG HA H 3.883
1090 126 ARG HB2 H 1.707
1091 126 ARG HB3 H 1.707
1092 126 ARG N N 117.910
1093 127 GLU CA C 56.319
1094 127 GLU CB C 26.286
1095 127 GLU CG C 33.696
1096 127 GLU H H 7.600
1097 127 GLU HA H 3.861
1098 127 GLU HB2 H 1.878
1099 127 GLU HB3 H 1.878
1100 127 GLU HG2 H 2.175
1101 127 GLU HG3 H 2.175
1102 127 GLU N N 117.507
1103 128 ALA CA C 48.205

1104 128 ALA CB C 20.105
1105 128 ALA H H 7.171
1106 128 ALA HA H 4.500
1107 128 ALA HB H 1.337
1108 128 ALA N N 116.595
1109 129 ASP CA C 51.822
1110 129 ASP CB C 37.686
1111 129 ASP H H 7.830
1112 129 ASP HA H 4.351
1113 129 ASP HB2 H 2.517
1114 129 ASP HB3 H 2.517
1115 129 ASP N N 118.048
1116 130 ILE CA C 60.522
1117 130 ILE CB C 36.090
1118 130 ILE CG1 C 25.032
1119 130 ILE CG2 C 14.430
1120 130 ILE CD1 C 9.756
1121 130 ILE H H 8.140
1122 130 ILE HA H 3.797
1123 130 ILE HB H 1.837
1124 130 ILE HG12 H 0.751
1125 130 ILE HG13 H 0.751
1126 130 ILE HG2 H 1.518
1127 130 ILE HD1 H 0.708
1128 130 ILE N N 128.000
1129 131 ASP CA C 51.187
1130 131 ASP CB C 37.468
1131 131 ASP H H 8.188
1132 131 ASP HA H 4.343
1133 131 ASP HB2 H 2.900
1134 131 ASP HB3 H 2.900
1135 131 ASP N N 116.678
1136 132 GLY CA C 44.638
1137 132 GLY H H 7.551
1138 132 GLY HA2 H 3.690
1139 132 GLY HA3 H 3.690
1140 132 GLY N N 108.469
1141 133 ASP CA C 50.942
1142 133 ASP CB C 37.458
1143 133 ASP H H 8.211
1144 133 ASP HA H 4.329
1145 133 ASP HB2 H 2.879
1146 133 ASP HB3 H 2.879
1147 133 ASP N N 120.377
1148 134 GLY CA C 43.122
1149 134 GLY H H 9.933
1150 134 GLY HA2 H 3.253
1151 134 GLY HA3 H 3.253
1152 134 GLY N N 112.182
1153 135 GLN CA C 50.454
1154 135 GLN CB C 30.614
1155 135 GLN CG C 30.614
1156 135 GLN H H 7.840
1157 135 GLN HA H 4.844
1158 135 GLN HB2 H 1.617
1159 135 GLN HB3 H 1.617
1160 135 GLN HG2 H 1.808
1161 135 GLN HG3 H 1.808
1162 135 GLN N N 115.288
1163 136 VAL CA C 58.713
1164 136 VAL CB C 31.416
1165 136 VAL CG1 C 20.358
1166 136 VAL CG2 C 19.104
1167 136 VAL H H 8.977
1168 136 VAL HA H 5.096
1169 136 VAL HB H 2.168
1170 136 VAL HG1 H 0.948
1171 136 VAL HG2 H 0.358
1172 136 VAL N N 125.238
1173 137 ASN CA C 48.352
1174 137 ASN CB C 35.640
1175 137 ASN H H 9.391
1176 137 ASN HA H 5.226
1177 137 ASN HB2 H 2.964
1178 137 ASN HB3 H 2.964
1179 137 ASN N N 129.014
1180 138 TYR CA C 59.669
1181 138 TYR CB C 37.572
1182 138 TYR H H 8.153
1183 138 TYR HA H 3.603
1184 138 TYR HB2 H 3.177
1185 138 TYR HB3 H 3.177
1186 138 TYR HD1 H 6.865
1187 138 TYR HD2 H 6.865
1188 138 TYR N N 118.562
1189 139 GLU CA C 57.540
1190 139 GLU CB C 26.274
1191 139 GLU CG C 33.812
1192 139 GLU H H 7.985
1193 139 GLU HA H 3.511
1194 139 GLU HB2 H 1.890
1195 139 GLU HB3 H 1.890
1196 139 GLU HG2 H 2.219
1197 139 GLU HG3 H 2.219
1198 139 GLU N N 118.555
1199 140 GLU CA C 56.025
1200 140 GLU CB C 26.274
1201 140 GLU CG C 33.240
1202 140 GLU H H 8.665
1203 140 GLU HA H 3.880
1204 140 GLU HB2 H 1.846
1205 140 GLU HB3 H 1.846

1206 140 GLU HG2 H 2.197
1207 140 GLU HG3 H 2.197
1208 140 GLU N N 119.774
1209 141 PHE CA C 59.447
1210 141 PHE CB C 37.686
1211 141 PHE H H 8.520
1212 141 PHE HA H 3.627
1213 141 PHE HB2 H 3.147
1214 141 PHE HB3 H 2.945
1215 141 PHE HD1 H 6.630
1216 141 PHE HD2 H 6.630
1217 141 PHE HE1 H 6.990
1218 141 PHE HE2 H 6.990
1219 141 PHE HZ H 6.390
1220 141 PHE N N 124.147
1221 142 VAL CA C 64.432
1222 142 VAL CB C 28.908
1223 142 VAL CG1 C 18.762
1224 142 VAL CG2 C 20.586
1225 142 VAL H H 8.642
1226 142 VAL HA H 2.947
1227 142 VAL HB H 1.601
1228 142 VAL HG1 H 0.576
1229 142 VAL HG2 H 0.291
1230 142 VAL N N 119.144
1231 143 GLN CA C 56.514
1232 143 GLN CB C 25.246
1233 143 GLN CG C 31.414
1234 143 GLN H H 7.795
1235 143 GLN HA H 3.671
1236 143 GLN HB2 H 1.912
1237 143 GLN HB3 H 1.912
1238 143 GLN HG2 H 2.219
1239 143 GLN HG3 H 2.219
1240 143 GLN N N 120.173
1241 144 MET CA C 55.683
1242 144 MET CB C 28.110
1243 144 MET H H 7.401
1244 144 MET HA H 3.832
1245 144 MET HB2 H 1.781
1246 144 MET HB3 H 1.781
1247 144 MET HG2 H 1.781
1248 144 MET HG3 H 1.781
1249 144 MET N N 118.573
1250 145 MET CA C 53.630
1251 145 MET CB C 29.592
1252 145 MET H H 7.531
1253 145 MET HA H 3.905
1254 145 MET HB2 H 1.672
1255 145 MET HB3 H 1.672
1256 145 MET HG2 H 1.672
1257 145 MET HG3 H 1.672
1258 145 MET N N 114.177
1259 146 THR CA C 59.251
1260 146 THR CB C 67.896
1261 146 THR CG2 C 18.534
1262 146 THR H H 7.587
1263 146 THR HA H 4.140
1264 146 THR HB H 4.103
1265 146 THR HG2 H 0.964
1266 146 THR N N 109.158
1267 147 ALA CA C 50.307
1268 147 ALA CB C 16.336
1269 147 ALA H H 7.381
1270 147 ALA HA H 4.095
1271 147 ALA HB H 1.241
1272 147 ALA N N 126.868
1273 148 LYS CA C 54.803
1274 148 LYS CB C 30.843
1275 148 LYS CG C 21.933
1276 148 LYS CD C 26.388
1277 148 LYS CE C 39.852
1278 148 LYS H H 7.854
1279 148 LYS HA H 3.920
1280 148 LYS HB2 H 1.515
1281 148 LYS HB3 H 1.515
1282 148 LYS HG2 H 1.220
1283 148 LYS HG3 H 1.220
1284 148 LYS N N 126.436

Appendix D

CaM Y99E-eNOS Peptide Assigned Chemical Shift

_Atom_shift_assign_ID	_Residue_seq_code	_Residue_label	_Atom_name	_Atom_type	_Chem_shift_value	_Chem_shift_value_error	_Chem_shift_ambiguity_code
1	2	ASP	H	H	8.493		
2	2	ASP	N	N	120.229		
3	3	GLN	H	H	8.207		
4	3	GLN	N	N	119.571		
5	4	LEU	H	H	8.177		
6	4	LEU	N	N	122.970		
7	5	THR	H	H	8.611		
8	5	THR	N	N	112.923		
9	6	GLU	H	H	8.875		
10	6	GLU	N	N	120.083		
11	7	GLU	H	H	8.532		
12	7	GLU	N	N	119.246		
13	8	GLN	H	H	7.586		
14	8	GLN	N	N	119.770		
15	9	ILE	H	H	8.271		
16	9	ILE	N	N	119.252		
17	10	ALA	H	H	7.840		
18	10	ALA	N	N	120.938		
19	11	GLU	H	H	7.637		
20	11	GLU	N	N	118.880		
21	12	PHE	H	H	8.449		
22	12	PHE	N	N	119.525		
23	13	LYS	H	H	9.106		
24	13	LYS	N	N	123.495		
25	14	GLU	H	H	7.653		
26	14	GLU	N	N	119.053		
27	15	ALA	H	H	7.789		
28	15	ALA	N	N	121.934		
29	16	PHE	H	H	8.766		
30	16	PHE	N	N	118.861		
31	17	SER	H	H	7.826		
32	17	SER	N	N	111.507		
33	18	LEU	H	H	7.237		
34	18	LEU	N	N	121.142		
35	19	PHE	H	H	7.071		
36	19	PHE	N	N	114.305		
37	20	ASP	H	H	7.664		
38	20	ASP	N	N	115.786		
39	21	LYS	H	H	7.550		
40	21	LYS	N	N	124.882		
41	22	ASP	H	H	7.962		
42	22	ASP	N	N	113.582		
43	23	GLY	H	H	7.599		
44	23	GLY	N	N	109.251		
45	24	ASP	H	H	8.254		
46	24	ASP	N	N	120.421		
47	25	GLY	H	H	10.560		
48	25	GLY	N	N	113.190		
49	26	THR	H	H	8.021		
50	26	THR	N	N	112.893		
51	27	ILE	H	H	9.682		
52	27	ILE	N	N	127.001		
53	28	THR	H	H	8.264		
54	28	THR	N	N	116.659		
55	29	THR	H	H	9.056		
56	29	THR	N	N	113.245		
57	30	LYS	H	H	7.575		
58	30	LYS	N	N	121.098		
59	31	GLU	H	H	7.710		
60	31	GLU	N	N	122.001		
61	33	GLY	H	H	8.383		
62	33	GLY	N	N	103.650		
63	34	THR	H	H	7.928		
64	34	THR	N	N	117.566		
65	35	VAL	H	H	7.091		
66	35	VAL	N	N	120.234		
67	36	MET	H	H	8.323		
68	36	MET	N	N	117.714		
69	37	ARG	H	H	8.230		
70	37	ARG	N	N	117.626		
71	38	SER	H	H	7.879		
72	38	SER	N	N	118.880		
73	39	LEU	H	H	7.258		
74	39	LEU	N	N	118.681		
75	40	GLY	H	H	7.460		
76	40	GLY	N	N	104.808		
77	41	GLN	H	H	7.869		
78	41	GLN	N	N	117.938		
79	42	ASN	H	H	8.557		
80	42	ASN	N	N	115.663		
81	44	THR	H	H	8.894		
82	44	THR	N	N	113.567		
83	45	GLU	H	H	8.654		
84	45	GLU	N	N	120.295		
85	46	ALA	H	H	8.137		
86	46	ALA	N	N	120.487		
87	47	GLU	H	H	7.591		

88	47	GLU	N	N	118.007
89	48	LEU	H	H	7.853
90	48	LEU	N	N	120.152
91	49	GLN	H	H	8.028
92	49	GLN	N	N	117.871
93	50	ASP	H	H	8.011
94	50	ASP	N	N	119.212
95	51	MET	H	H	7.616
96	51	MET	N	N	119.106
97	52	ILE	H	H	7.511
98	52	ILE	N	N	117.539
99	53	ASN	H	H	8.415
100	53	ASN	N	N	117.128
101	54	GLU	H	H	7.465
102	54	GLU	N	N	116.411
103	55	VAL	H	H	7.039
104	55	VAL	N	N	108.519
105	56	ASP	H	H	7.557
106	56	ASP	N	N	121.284
107	57	ALA	H	H	8.359
108	57	ALA	N	N	131.832
109	58	ASP	H	H	7.988
110	58	ASP	N	N	113.582
111	59	GLY	H	H	7.424
112	59	GLY	N	N	108.085
113	60	ASN	H	H	7.918
114	60	ASN	N	N	117.926
115	61	GLY	H	H	10.485
116	61	GLY	N	N	113.230
117	62	THR	H	H	7.507
118	62	THR	N	N	108.615
119	63	ILE	H	H	8.730
120	63	ILE	N	N	122.672
121	64	ASP	H	H	8.706
122	64	ASP	N	N	127.837
123	65	PHE	H	H	8.845
124	65	PHE	N	N	118.569
125	67	GLU	H	H	7.952
126	67	GLU	N	N	117.588
127	68	PHE	H	H	8.765
128	68	PHE	N	N	123.283
129	69	LEU	H	H	8.405
130	69	LEU	N	N	118.741
131	70	THR	H	H	7.542
132	70	THR	N	N	116.411
133	71	MET	H	H	7.720
134	71	MET	N	N	121.576
135	72	MET	H	H	7.977
136	72	MET	N	N	116.517
137	73	ALA	H	H	8.061
138	73	ALA	N	N	121.465
139	74	ARG	H	H	7.354
140	74	ARG	N	N	115.794
141	75	LYS	H	H	7.636
142	75	LYS	N	N	117.245
143	76	MET	H	H	7.792
144	76	MET	N	N	117.911
145	77	LYS	H	H	7.627
146	77	LYS	N	N	119.836
147	78	ASP	H	H	8.009
148	78	ASP	N	N	119.273
149	79	THR	H	H	7.597
150	79	THR	N	N	112.709
151	80	ASP	H	H	8.341
152	80	ASP	N	N	122.718
153	81	SER	H	H	8.233
154	81	SER	N	N	117.456
155	82	GLU	H	H	8.375
156	82	GLU	N	N	121.788
157	83	GLU	H	H	8.044
158	83	GLU	N	N	119.225
159	84	GLU	H	H	8.159
160	84	GLU	N	N	118.203
161	85	ILE	H	H	7.937
162	85	ILE	N	N	120.792
163	86	ARG	H	H	8.231
164	86	ARG	N	N	121.538
165	87	GLU	H	H	8.161
166	87	GLU	N	N	118.379
167	88	ALA	H	H	7.882
168	88	ALA	N	N	120.239
169	89	PHE	H	H	8.449
170	89	PHE	N	N	118.117
171	90	ARG	H	H	7.775
172	90	ARG	N	N	116.079
173	91	VAL	H	H	7.230
174	91	VAL	N	N	118.183
175	92	PHE	H	H	6.688
176	92	PHE	N	N	113.127
177	93	ASP	H	H	7.819
178	93	ASP	N	N	116.503
179	94	LYS	H	H	7.602
180	94	LYS	N	N	125.373
181	95	ASP	H	H	8.070
182	95	ASP	N	N	114.036
183	96	GLY	H	H	7.613
184	96	GLY	N	N	108.687
185	97	ASN	H	H	8.172
186	97	ASN	N	N	119.358
187	98	GLY	H	H	10.540
188	98	GLY	N	N	113.216
189	100	ILE	H	H	9.928

190	100	ILE	N	N 127.731
191	101	SER	H	H 8.782
192	101	SER	N	N 123.256
193	102	ALA	H	H 9.162
194	102	ALA	N	N 122.818
195	103	ALA	H	H 8.117
196	103	ALA	N	N 118.189
197	104	GLU	H	H 7.787
198	104	GLU	N	N 120.128
199	105	LEU	H	H 8.231
200	105	LEU	N	N 121.366
201	106	ARG	H	H 8.787
202	106	ARG	N	N 118.502
203	107	HIS	H	H 7.957
204	107	HIS	N	N 118.774
205	108	VAL	H	H 7.685
206	108	VAL	N	N 119.066
207	109	MET	H	H 8.110
208	109	MET	N	N 115.413
209	110	THR	H	H 8.529
210	110	THR	N	N 116.879
211	111	ASN	H	H 7.870
212	111	ASN	N	N 123.846
213	112	LEU	H	H 7.667
214	112	LEU	N	N 118.323
215	113	GLY	H	H 7.699
216	113	GLY	N	N 106.760
217	114	GLU	H	H 7.864
218	114	GLU	N	N 119.971
219	115	LYS	H	H 8.490
220	115	LYS	N	N 124.969
221	116	LEU	H	H 7.985
222	116	LEU	N	N 124.895
223	117	THR	H	H 9.119
224	117	THR	N	N 114.373
225	118	ASP	H	H 8.763
226	118	ASP	N	N 120.773
227	119	GLU	H	H 8.514
228	119	GLU	N	N 119.166
229	120	GLU	H	H 7.568
230	120	GLU	N	N 119.969
231	121	VAL	H	H 7.858
232	121	VAL	N	N 122.014
233	122	ASP	H	H 7.879
234	122	ASP	N	N 120.064
235	123	GLU	H	H 7.809
236	123	GLU	N	N 119.053
237	124	MET	H	H 7.427
238	124	MET	N	N 118.974
239	125	ILE	H	H 7.707
240	125	ILE	N	N 118.137
241	126	ARG	H	H 7.962
242	126	ARG	N	N 117.749
243	127	GLU	H	H 7.593
244	127	GLU	N	N 117.582
245	128	ALA	H	H 7.167
246	128	ALA	N	N 116.600
247	130	ILE	H	H 8.162
248	130	ILE	N	N 128.314
249	131	ASP	H	H 8.300
250	131	ASP	N	N 118.314
251	132	GLY	H	H 7.555
252	132	GLY	N	N 108.507
253	133	ASP	H	H 8.072
254	133	ASP	N	N 120.492
255	134	GLY	H	H 9.977
256	134	GLY	N	N 112.410
257	135	GLN	H	H 7.715
258	135	GLN	N	N 115.893
259	136	VAL	H	H 8.887
260	136	VAL	N	N 124.770
261	137	ASN	H	H 9.267
262	137	ASN	N	N 128.023
263	138	TYR	H	H 8.120
264	138	TYR	N	N 118.376
265	139	GLU	H	H 8.002
266	139	GLU	N	N 118.503
267	141	PHE	H	H 8.654
268	141	PHE	N	N 124.119
269	142	VAL	H	H 8.677
270	142	VAL	N	N 119.140
271	143	GLN	H	H 7.793
272	143	GLN	N	N 120.240
273	144	MET	H	H 7.391
274	144	MET	N	N 118.549
275	145	MET	H	H 7.544
276	145	MET	N	N 114.271
277	146	THR	H	H 7.591
278	146	THR	N	N 109.129
279	147	ALA	H	H 7.371
280	147	ALA	N	N 126.868
281	148	LYS	H	H 7.855
282	148	LYS	N	N 126.436

Appendix E

Relaxation data for CaM-iNOS peptide

Res #	T1(ms)	T2 (ms)	NOE	S^2
2				
3	675.676	234.192		0.800
4		95.602	0.742	
5	840.336	80.775	0.711	0.851
6	819.672	90.253	0.905	0.966
7	763.359	83.264	0.791	0.888
8	884.956	79.554	0.779	0.770
9	819.672	77.280	0.804	0.892
10	869.565	81.699	0.827	0.845
11	1010.101	77.882	0.840	0.710
12	884.956	69.204	0.871	0.742
13	862.069	87.489	0.863	0.822
14		81.766	0.867	
15	813.008	86.957	0.876	0.851
16	869.565	81.301	0.894	0.773
17	884.956	69.493	0.905	0.822
18	854.701	87.642	0.851	0.824
19	869.565	69.784	0.862	0.783
20	980.392	75.245	0.889	0.756
21	909.091	76.687	0.842	0.853
22	840.336	73.964	0.872	0.904
23		99.602	0.955	
24	793.651	83.403	0.911	0.880
25	869.565	65.359	0.926	0.755
26	671.141	62.814	0.947	0.913
27	934.579	87.108	0.974	0.880
28	840.336	72.993	0.783	0.911
29	892.857	72.202	0.826	0.763
30	917.431	88.574	0.818	0.728
31	925.926	74.516	0.929	0.707
32	925.926	78.989	0.901	0.984
33	980.392	62.854	0.828	0.709
34	787.402	63.694	0.856	0.822
35	869.565	79.428	0.923	0.774
36	763.359	62.150	0.863	0.914
37	854.701	69.348	0.945	0.797
38	806.452	71.073	0.793	0.794
39	862.069	63.371	0.824	0.830
40	840.336	103.093	0.883	0.602
41	862.069	75.700	0.832	0.882
42	757.576	88.968	0.794	0.716
44	892.857	74.627	0.887	0.870
45	769.231	85.543	0.883	0.882
46	847.458	89.767	0.826	0.818
47	847.458	74.460	0.833	0.801
48	840.336	84.317	0.839	0.847
49	833.333	70.522	0.834	0.818
50	952.381	83.472	0.818	0.678
51	970.874	86.655	0.842	0.699
52	813.008	68.776	0.982	0.841
53	793.651	69.348	0.835	0.838
54	909.091	71.736	0.795	0.741
55	900.901	78.186	0.805	0.744
56	943.396	96.899	0.956	0.871
57				
58	1063.830	76.046	0.908	0.659

59	854.701	90.334	0.905	0.731
60	869.565	78.802	0.934	0.889
61	819.672	70.323	0.947	0.860
62	719.424	77.459	0.854	0.960
63	884.956	89.445	0.815	0.803
64	854.701	75.188	0.922	0.890
65	787.402	68.918	0.870	0.966
67	833.333	80.710	0.799	0.868
68	943.396	87.566	0.964	0.813
69		84.104	0.921	
70	775.194	69.156	0.913	0.972
71	793.651	73.529	0.860	0.932
72	892.857	72.780	0.845	0.878
73	833.333	81.235	0.916	0.867
74	1000.000	95.511	0.780	0.730
75	877.193	87.336	0.857	0.812
76	877.193	61.013	0.851	0.803
77	854.701	68.634	0.720	0.834
78	909.091	138.313	0.202	0.482
79	598.802	82.305	0.733	0.792
80	724.638	105.597	0.764	0.654
81	684.932	84.890	0.736	0.924
82	751.880	91.659	0.741	0.718
83	952.381	69.638	0.847	0.699
84	806.452	73.206	0.840	0.842
85				
86	925.926	80.128	0.895	0.763
87		91.743	0.910	
88	806.452	86.730	0.889	0.855
89	925.926	79.051	0.806	0.834
90	847.458	66.756	0.901	0.822
91	781.250	78.678	0.841	0.909
92	840.336	69.013	0.867	0.931
93	806.452	66.711	0.851	0.879
94	943.396	87.796	0.864	0.781
95	819.672	72.307	0.932	0.926
96		86.059	0.940	
97	869.565	82.034	0.908	0.974
98	1010.101	70.771	1.000	0.989
99	793.651	75.301	0.940	0.917
100	925.926	81.367	0.915	0.988
101	735.294	77.220	0.869	0.945
102	952.381	79.681	0.822	0.811
103		76.161	0.890	
104	757.576	85.985	0.848	0.738
105	884.956	75.358	0.896	0.868
106	934.579	71.531	0.834	0.743
107	826.446		0.898	
108	1000.000	74.738	0.895	0.733
109	877.193	66.979	0.901	0.789
110	787.402	64.226	0.829	0.989
111	787.402	75.930	0.841	0.921
112	1075.269	82.781	0.803	0.689
113	884.956	92.081	0.887	0.791
114	1041.667		0.945	
115	934.579	101.523	0.537	0.707
116	961.538	119.904	0.495	0.582
117	826.446	74.963	0.814	0.781
118	757.576	96.993	0.910	0.662
119	892.857	81.037	0.775	0.838
120		77.882	0.841	
121	800.000	83.195	0.888	0.877
122	952.381	83.195	0.868	0.801
123	900.901	81.833	0.822	0.829
124	813.008	83.056	0.884	0.993
125	925.926	68.166	0.888	0.800
126	847.458	70.373	0.921	0.920
127	909.091	79.618	0.874	0.754

128	862.069	64.977	0.876	0.807
129	943.396	69.444	0.763	0.808
130	1388.889	110.742	0.824	0.573
131	970.874	70.472	0.918	0.850
132	1190.476	84.746	0.873	0.579
133	900.901	87.413	0.883	0.806
134	833.333	68.776	0.867	0.773
135	862.069	69.444	0.936	0.911
136	1219.512	84.602	0.779	0.585
137	877.193	76.220	0.906	0.996
138	826.446	67.340	0.935	0.810

139	952.381	77.220	0.847	0.690
140		76.453	0.891	
141	925.926		0.924	
142	746.269	70.472	0.893	0.909
143	892.857	80.775	0.837	0.734
144	787.402		0.692	
145	781.250	74.738	0.915	0.931
146	751.880	88.496	0.813	0.879
147	709.220	115.741	0.619	0.592
148	847.458	182.482	0.118	0.322

Appendix F

Relaxation data for CaM-eNOS peptide

Res #	T1 (ms)	T2 (ms)	NOE	S^2
2	342.466	200.401		
3	628.931	239.808		
4	628.931	138.504	0.175	0.586
5	666.667	84.388	0.803	0.938
6	636.943	92.251	0.774	0.920
7	757.576	85.543	0.762	0.793
8	719.424	85.179	0.885	0.812
9	793.651	83.682	0.867	0.703
10	800.000	82.102	0.869	0.700
11	787.402	86.430	0.863	0.854
12	763.359	84.531	0.879	0.808
13	793.651	81.833	0.862	0.663
14	632.911	82.372	0.872	0.982
15	813.008	85.543	0.903	0.842
16	781.250	78.740	0.800	0.755
17	757.576	79.554	0.949	0.796
18	724.638	83.056	0.813	0.898
19	847.458	77.101	0.914	0.985
20	800.000	74.129	0.943	0.729
21	840.336	74.627	0.833	0.617
22	840.336	77.280		
23	746.269	82.713	0.912	0.890
24	806.452	85.324	0.964	0.862
25	746.269	72.622	0.910	0.833
26	675.676	70.077	0.946	0.994
27	806.452	75.415	0.890	0.901
28	719.424	64.725	0.886	0.877
29	826.446	70.028	0.885	0.664
30	729.927	76.628	0.875	0.939
31	763.359	75.019	0.704	0.830
32	833.333	67.340	0.902	0.691
33	793.651	69.784	0.943	0.719
34	694.444	70.423	0.875	1.000
35				
36	884.956	72.464	0.908	0.648
37			0.817	
38	709.220	72.833	0.864	0.913
39	826.446	74.239	0.867	0.669
40	757.576	72.098	0.851	0.869
41	598.802	80.128	0.926	1.000
42	598.802	93.371	0.756	0.692
44	751.880	80.000	0.880	0.906
45	781.250	84.674	0.942	0.978
46	606.061	81.967	0.877	0.850
47	757.576	77.459	0.838	0.917
48		75.301		
49	714.286	78.864	0.885	0.860
50				
51	819.672	88.106	0.845	0.824
52	704.225	81.103	0.880	0.935
53	769.231	75.700	0.905	0.922
54	862.069	77.942	0.835	0.788
55	826.446	84.317	0.926	0.834
56	751.880	92.851	0.887	0.723
57				
58	826.446	77.042	0.922	0.784
59	854.701	89.445	0.846	0.655
60	724.638	77.220	0.898	0.736

61	724.638	77.340	0.826	0.939
62	781.250	76.746	0.887	0.762
63	854.701	83.333	0.960	0.931
64	833.333	73.368	0.896	0.739
65	751.880	79.936	0.946	0.911
67	666.667	77.580	0.820	0.974
68	775.194	83.752	0.900	0.987
69	757.576	80.064	0.908	0.901
70	662.252	72.411	0.963	0.950
71	746.269	83.195	0.897	0.892
72	699.301	71.174	0.872	0.994
73	769.231	84.890	0.931	0.990
74	793.651	80.515	0.874	0.786
75	735.294	84.746	0.814	0.890
76	781.250	83.472	0.754	0.869
77	645.161	104.822	0.720	0.643
78	666.667		0.326	
79	581.395	106.270	0.644	0.897
80	625.000	116.686	0.744	0.504
81			0.869	
82	671.141	85.543	0.871	0.937
83	694.444	85.837	0.789	0.919
84			0.741	
85	751.880	79.051	0.849	0.913
86	787.402	80.000	0.913	0.735
87				
88	729.927	79.302	0.868	0.919
89	769.231	76.046	0.907	0.991
90	781.250	73.046	0.905	0.928
91	775.194	78.247	0.901	0.905
92	826.446	76.923	0.855	0.883
93	793.651	72.464	0.890	0.835
94	800.000	78.493	0.914	0.677
95	787.402	76.687	0.992	0.744

96	793.651	86.655	0.953	0.865
97	819.672	73.746		
98	763.359	74.571	0.961	0.697
99	704.225	73.314	0.940	0.996
100	769.231	76.805	0.959	0.949
101	735.294	77.399	0.959	0.997
102	813.008	74.627	0.822	0.631
103	833.333	76.278	0.907	0.712
104			0.700	
105	769.231	72.202	0.838	0.678
106	689.655	74.184	0.936	0.902
107	781.250	57.971	0.842	0.794
108	900.901	71.327	0.823	0.582
109	847.458	69.252	0.881	0.634
110	735.294	69.061	0.911	0.876
111	699.301	75.700	0.999	0.907
112	892.857	77.519	0.902	0.576
113	787.402	88.574	0.871	0.843
114	763.359	84.890	0.734	0.861
115	719.424	100.200	0.438	0.673
116	877.193	107.759	0.526	0.566
117	649.351	75.758	0.837	0.838
118	689.655	80.775	0.900	0.946
119		84.246	0.887	
120	763.359	81.433	0.898	0.727
121	787.402	75.358	0.836	0.913
122	961.538	90.744	0.786	0.752
123	694.444	82.645	0.835	0.849
124	826.446	85.911	0.906	0.732
125	840.336	80.257	0.864	0.855
126	763.359	77.220	0.851	0.914
127	800.000	79.302	0.840	0.708
128	775.194	75.873	0.840	0.914
129		83.195	0.854	

130	1136.364	111.857	0.889	0.452
131	840.336	75.358	0.888	0.667
132	925.926	87.566	0.944	0.998
133	833.333	78.247	0.961	0.739
134	751.880	79.936	0.947	0.910
135	704.225	71.225	0.926	0.847
136	862.069	72.464	0.906	0.675
137	806.452	71.480	0.983	0.794
138	740.741	83.472	0.881	0.818
139	869.565	79.618	0.875	0.757

140	800.000	80.580	0.875	0.876
141	724.638	76.805	0.971	0.959
142	793.651	76.982	0.927	0.971
143		96.432	0.919	
144	781.250	82.988	0.901	0.810
145	719.424	71.942	0.876	0.975
146	689.655	80.064	0.894	0.788
147	675.676	100.402	0.705	0.728
148	854.701	171.233		0.517

Appendix G

Relaxation data for CaM Y99E-eNOS peptide

Res #	T1(ms)	T2(ms)	NOE	S^2
2	452.489	146.843		
3	714.286	234.192	0.351	0.255
4	917.431	130.039	0.204	0.596
5	751.880	78.003	0.671	0.907
6	763.359	87.260	0.692	0.771
7	800.000	78.493	0.728	0.889
8	793.651	95.147	0.886	0.822
9	591.716	68.074	1.000	0.971
10	854.701	87.108	0.714	0.707
11		74.405	0.819	
12	735.294	77.821	0.877	0.817
13	793.651	84.388	0.810	0.747
14		87.566	0.706	
15	819.672	84.674	0.950	0.815
16	704.225	77.399	0.771	0.903
17	781.250	70.721	0.831	0.866
18	763.359	83.056	0.746	0.894
19	869.565	76.278	0.908	0.998
20	724.638	60.938	0.741	0.872
21	751.880	80.257	0.783	0.910
22	877.193	78.186	0.806	0.703
23	806.452	92.593	0.741	0.733
24	653.595	85.324	0.826	0.959
25	609.756	72.833	0.918	0.882
26	657.895	63.131	0.816	1.000
27	775.194	78.864	0.859	0.911
28	854.701	66.269	0.831	0.747
29	793.651	65.189	0.855	0.831
30	714.286	74.349	0.750	0.974
31	813.008	85.251	0.841	0.854
32				
33		78.927	0.663	
34	729.927	56.148	0.886	0.987
35				
36	869.565	66.445	0.952	0.776
37		83.333	0.697	
38	746.269	70.225	0.762	0.983
39	787.402	78.493	0.830	0.899
40	840.336	84.034	0.708	0.769
41	800.000	84.746	0.771	0.798
42	826.446	97.371	0.820	0.797
44	662.252	66.934	0.843	0.960
45	854.701	88.028	0.813	0.821
46	793.651	82.102	0.780	0.880
47	787.402	75.529	0.778	0.924
48	840.336	91.324	0.831	0.813
49	671.141	76.394	0.824	0.997
50	787.402	86.430	0.713	0.846
51	781.250	85.837	0.817	0.865
52	952.381	75.131	0.891	0.703
53	826.446	76.687	0.809	0.894
54	892.857	67.340	0.784	0.790
55	840.336	80.515	0.794	0.865
56	729.927	85.616	0.800	0.772
57				
58	769.231	74.294	0.940	0.982
59	862.069	92.081	0.868	0.796
60	714.286	78.003	0.830	0.854

61	763.359	78.247	0.693	0.906
62	704.225	78.186	0.893	0.961
63	598.802	64.185	0.947	0.791
64		66.138	0.796	
65	781.250	72.674	0.679	0.824
67	724.638	80.515	0.899	0.933
68	666.667	83.472	0.873	0.957
69	653.595	78.802	0.739	0.993
70	709.220	65.402	0.971	0.959
71	671.141	82.440	0.777	0.951
72	609.756	60.643	0.933	0.983
73	625.000	78.740	0.842	1.000
74	740.741	76.046	0.880	0.946
75	709.220	70.126	0.943	0.869
76	719.424	84.674	0.750	0.838
77	735.294	96.339	0.653	0.737
78	602.410	93.284	0.699	0.830
79	606.061	90.580	0.597	0.907
80	595.238	118.483	0.610	0.550
81	775.194	70.126	0.796	0.964
82	735.294	78.802	0.670	0.862
83	769.231	85.397	0.708	0.867
84		67.522	0.939	
85	892.857	79.554	0.801	0.731
86	847.458	81.500	0.613	0.700
87		64.185	0.863	
88	813.008	82.305	0.722	0.859
89	763.359	68.540	0.819	0.848
90	833.333	63.251	0.725	0.839
91	746.269	73.746	0.896	0.959
92	833.333	74.294	0.888	0.901
93	769.231	71.124	0.740	0.837
94	787.402	84.890	0.750	0.720
95	819.672	73.314	0.995	0.706
96	769.231	82.850	0.753	0.891
97	719.424	79.428	0.882	0.941
98	877.193	62.657	0.849	0.750
99				
100	925.926	78.370	0.677	0.705
101		84.531	0.709	
102	952.381	73.475	0.736	0.671
103				
104		90.909	0.871	
105	900.901	72.359	0.941	0.698
106	833.333	76.687	0.972	0.988
107	769.231	65.876	0.883	0.906
108	653.595	80.515	0.980	0.985
109	833.333	59.277	0.628	0.744
110	763.359	72.833		
111	653.595	71.378	0.785	1.000
112	862.069	76.570	0.757	0.708
113	854.701	89.606	0.801	0.813
114	735.294	83.333	0.898	0.909
115	862.069	100.200	0.334	0.716
116	970.874	104.275	0.457	0.542
117	806.452	75.643	0.714	0.691
118	653.595	84.962	0.824	0.955
119	793.651	75.873	0.813	0.829
120	709.220	86.430	0.771	0.911
121	787.402	86.505	0.723	0.851
122	694.444	90.580	0.768	0.791
123	763.359	81.235	0.682	0.885
124	724.638	81.037	0.774	0.931
125	757.576	75.586	0.761	0.940
126	666.667	73.099	0.708	0.961
127	826.446	74.129	0.859	0.800
128	763.359	69.930	0.803	0.970
129				

130	1123.596	100.806	0.761	0.511
131	813.008	73.046	0.859	0.755
132	900.901	90.171	0.922	0.906
133				
134	719.424	78.186	0.938	0.869
135	787.402	68.074	0.955	0.821
136	769.231	65.789	0.885	0.854
137	925.926	82.102	0.978	0.678
138	584.795	72.780	0.829	0.757
139	806.452	77.882	0.895	0.897

140				
141	862.069	80.064	0.943	0.887
142	719.424	76.687	0.881	0.956
143		85.690	0.807	
144	666.667	79.114	0.830	0.971
145	934.579	66.800	0.803	0.761
146	680.272	77.942	0.741	0.928
147	775.194	99.502	0.674	0.673
148	909.091	179.856		

Appendix H

Percent assignment of CaM-iNOS

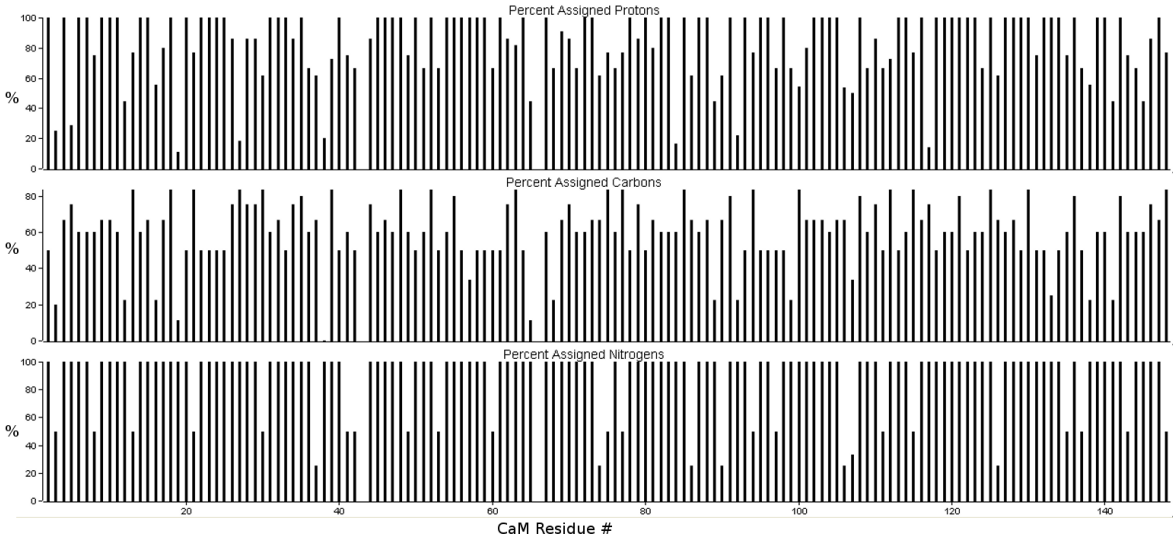

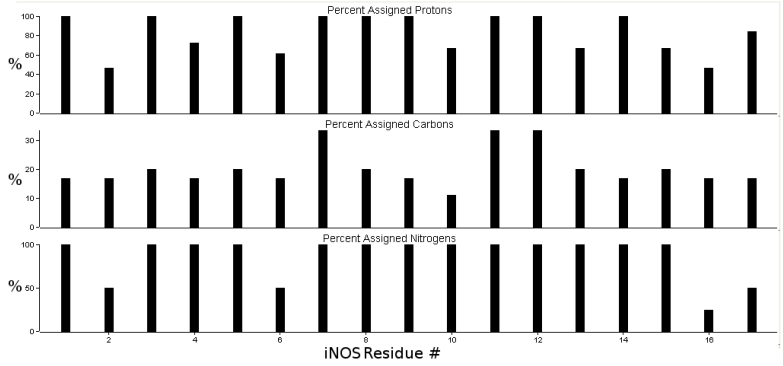

Appendix I

Percent assignment of CaM-eNOS

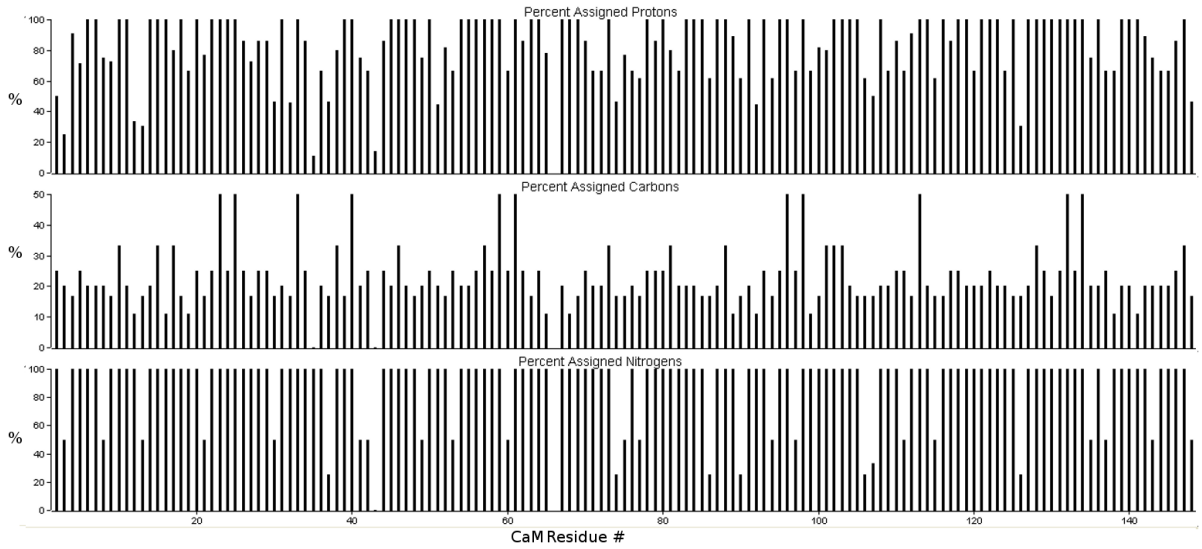

Permissions

Dear Michael,

Permission is granted for you to use the material requested for your thesis/dissertation subject to the usual acknowledgements and on the understanding that you will reapply for permission if you wish to distribute or publish your thesis/dissertation commercially.

Permission is granted solely for use in conjunction with the thesis, and the article may not be posted online separately.

Any third party material is expressly excluded from this permission. If any material appears within the article with credit to another source, authorisation from that source must be obtained.

Best Wishes

Verity Butler
Permissions Assistant
John Wiley & Sons Ltd.

Bibliography

Abu-Soud H. M., Stuehr D. J. (1993) Nitric oxide synthases reveal a role for calmodulin in controlling electron transfer. *Proc. Natl. Acad. Sci. U. S. A.* **90,** 10769-10772.

Afshar M., Caves L. S. D., Guimard L., Hubbard R. E., Calas B., Grassy G. & Haiech J. (1994) Investigating the high affinity and low sequence specificity of calmodulin binding to its targets. *J. Mol. Biol.* **244,** 554-571.

Alderton W. K., Cooper C. E. & Knowles R. G. (2001) Nitric oxide synthases: Structure, function and inhibition. *Biochem. J.* **357,** 593-615.

Andrew P. J., Mayer B. (1999) Enzymatic function of nitric oxide synthases. *Cardiovasc. Res.* **43,** 521-531.

Aoyagi M., Arvai A. S., Tainer J. A. & Getzoff E. D. (2003) Structural basis for endothelial nitric oxide synthase binding to calmodulin. *EMBO J.* **22,** 766-775.

Barbato, G., Ikura, M., Kay, L. E., Pastor, R. W., & Bax, A. (1992) Backbone Dynamics of Calmodulin Studied by N-15 Relaxation Using Inverse Detected 2-Dimensional Nmr Spectroscopy - the Central Helix Is Flexible. *Biochemistry* **31**, 5269-5278.

Bax, A., Clore, G. M., & Gronenborn, A. M. (1990) ^{1}H-^{1}H correlation via isotropic mixing of ^{13}C magnetization, a new three-dimensional approach for assigning ^{1}H and ^{13}C spectra of ^{13}C-enriched proteins. *J. Magn. Reson.* **88**, 425-431.

Benaim G., Villalobo A. (2002) Phosphorylation of calmodulin: Functional implications. *European Journal of Biochemistry* **269,** 3619-3631.

Berjanskii M, Tang P, Liang J, Cruz JA, Zhou J, Zhou Y, Bassett E, MacDonell C, Lu P, Lin G, Wishart DS. (2009) GeNMR: a web server for rapid NMR-based protein structure determination. *Nucleic Acids Res*. 37(Web server issue):W670-W677

Berridge M. J., Bootman M. D. & Lipp P. (1998) Calcium - A life and death signal. *Nature* **395,** 645-648.

Bertini, I., Kursula, P., Luchinat, C., Parigi, G., Vahokoski, J., Wilmanns, M., & Yuan, J. (2009) Accurate Solution Structures of Proteins from X-ray Data and a Minimal Set of NMR Data: Calmodulin-Peptide Complexes As Examples. *Journal of the American Chemical Society* **131**, 5134-5144.

Bisaglia M., Trolio A., Tessari I., Bubacco L., Mammi S. & Bergantino E. (2005) Cloning, expression, purification, and spectroscopic analysis of the fragment 57-102 of human alpha-synuclein. *Protein Expr. Purif.*, **39**, 90-96.

Brunger, A., Adams, P., Clore, G., DeLano, W., Gros, P., Grosse-Kunstleve, R., Jiang, J., Kuszewski, J., Nilges, M., Pannu, N., Read, R., Rice, L., Simonson, T., & Warren, G. (1998) Crystallography & NMR system: A new software suite for macromolecular structure determination. *Acta Crystallographica Section D-Biological Crystallography* **54**, 905-921.

Cavanagh, J., Fairbrother, W. J., Palmer, A. G., III, & Skelton, N. J. (1996) *Protein NMR Spectroscopy: Principles and Practice*, Academic Press, Inc., San Diego.

Censarek P., Beyermann M. & Koch K. - W. (2004) Thermodynamics of apocalmodulin and nitric oxide synthase II peptide interaction. *FEBS Lett.* **577,** 465-468.

Chien Y. H., David I. B. (1984) Isolation and characterization of calmodulin genes from Xenopus laevis. *Mol. Cell. Biol.* **4,** 507-513.

Cho H. J., Martin E., Xie Q.-W., Sassa S. & Nathan C. (1995) Inducible nitric oxide synthase: Identification of amino acid residues essential for dimerization and binding of tetrahydrobiopterin. *Proc. Natl. Acad. Sci. U. S. A.* **92,** 11514-11518.

Cho H. J., Xie Q. -., Calaycay J., Mumford R. A., Swiderek K. M., Lee T. D. & Nathan C. (1992) Calmodulin is a subunit of nitric oxide synthase from macrophages. *J. Exp. Med.* **176,** 599-604.

Clore, G. M., & Gronenborn, A. M. (1991) Applications of 3-dimensional and 4-dimensional heteronuclear NMR spectroscopy to protein structure determination.*Prog. Nucl. Magn. Reson. Spectrsc.* **23**, 43-92.

Corti C., L'Hostis E. L., Quadroni M., Schmid H., Durussel I., Cox J., Hatt P. D., James P. & Carafoli E. (1999) Tyrosine phosphorylation modulates the interaction of calmodulin with its target proteins. *European Journal of Biochemistry* **262,** 790-802.

Crivici A., Ikura M. (1995) Molecular and structural basis of target recognition by calmodulin. *Annu. Rev. Biophys. Biomol. Struct.* **24,** 85-116.

Crouch T. H., Klee C. B. (1980) Positive cooperative binding of calcium to bovine brain calmodulin. *Biochemistry (N. Y.)* **19,** 3692-3698.

Cunningham, F., and Deber, C. M. (2007) Optimizing synthesis and expression of transmembrane peptides and proteins. *Methods* **41**, 370-380.

Daff S. (2010) NO synthase: Structures and mechanisms. *Nitric oxide*, **23**, 1-11.

Drum, C., Yan, S., Bard, J., Shen, Y., Lu, D., Soelalman, S., Grabarek, Z., Bohm, A., & Tang, W. (2002) Structural basis for the activation of anthrax adenylyl cyclase exotoxin by calmodulin. *Nature* **415**, 396-402.

Evans, J. N. S. (1995). Biomolecular NMR spectroscopy. Oxford University Press Inc, New York.

Fallon J. L., Quiocho F. A. (2003) A closed compact structure of native Ca^{2+}-calmodulin. *Structure* **11,** 1303-1307.

Fesik, S. W., & Zuiderweg, E. R. P. (1990) Heteronuclear 3-Dimensional Nmr Spectroscopy Of Isotopically Labeled Biological Macromolecules. *Quart. Rev. Biophys.* **23**, 97-131.

Fischmann T. O., Hruza A., Niu X. D., Fossetta J. D., Lunn C. A., Dolphin E., Prongay A. J., Reichert P., Lundell D. J., Narula S. K. & Weber P. C. (1999) Structural characterization of nitric oxide synthase isoforms reveals striking active-site conservation. *Nat. Struct. Biol.* **6,** 233-242.

Friedberg F. (1990) Species comparison of calmodulin sequences. *Protein Seq. Data Anal.* **3,** 335-337.

Garcin E. D., Bruns C. M., Lloyd S. J., Hosfield D. J., Tiso M., Gachhui R., Stuehr D. J., Tainer J. A. & Getzoff E. D. (2004) Structural basis for isozyme-specific regulation of electron transfer in nitric-oxide synthase. *J. Biol. Chem.* **279,** 37918-37927.

Gellman S. H. (1991) On the role of methionine residues in the sequence-independent recognition of nonpolar protein surfaces. *Biochemistry (N. Y.)* **30,** 6633-6636.

Ghosh D., Salerno J. (2003) Nitric oxide synthases: domain structure and alignment in enzyme function and control. *Front. Biosci.* 8, 193-209.

Greif D. M., Sacks D. B. & Michel T. (2004) Calmodulin phosphorylation and modulation of endothelial nitric oxide synthase catalysis. *Proc. Natl. Acad. Sci. U. S. A.* **101,** 1165-1170.

Gribovskaja I., Brownlow K. C., Dennis S. J., Rosko A. J., Marletta M. A. & Stevens-Truss R. (2005) Calcium-binding sites of calmodulin and electron transfer by inducible nitric oxide synthase. *Biochemistry (N. Y.)* **44,** 7593-7601.

Grzesiek, S., & Bax, A. (1992) Correlating Backbone Amide and Side Chain Resonances in Larger Proteins By Multiple Relayed Triple Resonance NMR. *J. Am. Chem. Soc.* **114**, 6291-6293.

Guan Z. -., Kamatani D., Kimura S. & Iyanagi T. (2003) Mechanistic studies on the intramolecular one-electron transfer between the two flavins in the human neuronal nitric-oxide synthase and inducible nitric-oxide synthase flavin domains. *J. Biol. Chem.* **278,** 30859-30868.

Guo, C., Li, Z., Shi, Y., Xu, M., Wise, J., Trommer, W., and Yuan, J. (2004) Intein-mediated fusion expression, high efficient refolding, and one-step purification of gelonin toxin. *Protein Expr Purif* **37**, 361-367.

Hoffman, D. W., and Spicer, L. D. (1991) Isotopic Labeling of Specific Amino-Acid Types as an Aid to Nmr-Spectrum Assignment of the Methionine Repressor Protein. *Techniques in Protein Chemistry Ii*, 409-416.

Houdusse A., Gaucher J. -., Krementsova E., Mui S., Trybus K. M. & Cohen C. (2006) Crystal structure of apo-calmodulin bound to the first two IQ motifs of myosin V reveals essential recognition features. *Proc. Natl. Acad. Sci. U. S. A.* **103,** 19326-19331.

Ikura M., Ames J. B. (2006) Genetic polymorphism and protein conformational plasticity in the calmodulin superfamily: Two ways to promote multifunctionality. *Proc. Natl. Acad. Sci. U. S. A.* **103,** 1159-1164.

Ikura M., Clore G. M., Gronenborn A. M., Zhu G., Klee C. B. & Bax A. (1992) Solution structure of a calmodulin-target peptide complex by multidimensional NMR. *Science* **256,** 632-638.

Ikura, M., Kay, L.E. and Bax, A. (1990) A novel approach for sequential assignment of ^{1}H, ^{13}C, and ^{15}N spectra of proteins: heteronuclear triple-resonance three-dimensional NMR spectroscopy. Application to calmodulin. *Biochemistry 29*, 4659-67.

Igumenova, T., Lee, A., & Wand, A. (2005) Backbone and side chain dynamics of mutant calmodulin-peptide complexes. *Biochemistry* **44**, 12627-12639.

Jang, D., Guo, M., & Wang, D. (2007) Proteomic and biochemical studies of calcium- and phosphorylation-dependent calmodulin complexes in mammalian cells. *Journal of Proteome Research* **6**, 3718-3728.

James, T. L., Oppenheimer, N. J. (1994) Methods in Enzymology. Volume 239. Nuclear Magnetic Resonance Part C. Academic Press, San Diego, California.

Jelesarov I., Bosshard H. R. (1999) Isothermal titration calorimetry and differential scanning calorimetry as complementary tools to investigate the energetics of biomolecular recognition. *Journal of Molecular Recognition* **12,** 3-18.

Jones R.J, Smith S. M. E, Gao Y. T., DeMay B. S., Mann K.J., Salerno K. M., Salerno J. C., (2004) The function of the small insertion in the hinge subdomain in the control of constitutive mammalian nitric-oxide synthases, *J. Biol. Chem*. **279** 36876–36883.

Jurado L. A., Chockalingam P. S. & Jarrett H. W. (1999) Apocalmodulin. *Physiol. Rev.* **79,** 661-682.

Keller, R. (2004). The Computer Aided Resonance Assignment Tutorial, 1st Ed., CANTINA Verlag.

Keller, R. (2005) Optimizing the Process of Nuclear Magnetic Resonance Spectrum Analysis and Computer Aided Resonance Assignment. Swiss Federal Institute of Technology, Zurich.

Kilhoffer M. -., Kubina M., Travers F. & Haiech J. (1992) Use of engineered proteins with internal tryptophan reporter groups and pertubation techniques to probe the mechanism of ligand-protein interactions: Investigation of the mechanism of calcium binding to calmodulin. *Biochemistry (N. Y.)* **31,** 8098-8106.

Knudsen G. M., Nishida C. R., Mooney S. D. & Ortiz de Montellano P. R. (2003) Nitric-oxide synthase (NOS) reductase domain models suggest a new control element in endothelial NOS that attenuates calmodulin-dependent activity. *J. Biol. Chem.* **278,** 31814-31824.

Kortvely E., Gulya K. (2004) Calmodulin, and various ways to regulate its activity. *Life Sci.* **74,** 1065-1070.

Kuboniwa H., Tjandra N., Grzesiek S., Ren H., Klee C. B. & Bax A. (1995) Solution structure of calcium-free calmodulin. *Nat. Struct. Biol.* **2,** 768-776.

Kurokawa H., Osawa M., Kurihara H., Katayama N., Tokumitsu H., Swindells M. B., Kainosho M. & Ikura M. (2001) Target-induced conformational adaptation of calmodulin revealed by the crystal structure of a complex with nematode Ca(2+)/calmodulin-dependent kinase kinase peptide. *J. Mol. Biol.* **312,** 59-68. 10.1006/jmbi.2001.4822.

Li H., Poulos T. L. (2005) Structure-function studies on nitric oxide synthases. *J. Inorg. Biochem.* **99,** 293-305.

Li H., Raman C. S., Martásek P., Masters B. S. S. & Poulos T. L. (2001) Crystallographic studies on endothelial nitric oxide synthase complexed with nitric oxide and mechanism-based inhibitors. *Biochemistry (N. Y.)* **40,** 5399-5406.

Lipari, G., and Szabo, A. (1982) A model free approach to the interpretation of nuclear magnetic resonance relaxation in macromolecules. *J. Am. Chem. Soc.* **104**, 4546-4559.

Malhotra, A. (2009) Tagging for protein expression. *Methods Enzymol* **463**, 239-258.

Marlow M. S., Wand A. J. (2006) Conformational dynamics of calmodulin in complex with the calmodulin-dependent kinase kinase α calmodulin-binding domain. *Biochemistry (N. Y.)* **45,** 8732-8741.

Martin S. R., Andersson Teleman A. & Bayley P. M. (1985) Kinetics of calcium dissociation from calmodulin and its tryptic fragments. A stopped-flow fluorescence study using Quin 2 reveals a two-domain structure. *European Journal of Biochemistry* **151,** 543-550.

Matsubara M., Hayashi N., Titani K. & Taniguchi H. (1997) Circular dichroism and 1H NMR studies on the structures of peptides derived from the calmodulin-binding domains of inducible and endothelial nitric-oxide synthase in solution and in complex with calmodulin: Nascent α- helical structures are stabilized by calmodulin both in the presence and absence of Ca2+. *J. Biol. Chem.* **272,** 23050-23056.

Matter H., Kumar H. S. A., Fedorov R., Frey A., Kotsonis P., Hartmann E., Fröhlich L. G., Reif A., Pfleiderer W., Scheurer P., Ghosh D. K., Schlichting I. & Schmidt H. H. H. W. (2005) Structural analysis of isoform-specific inhibitors targeting the tetrahydrobiopterin binding site of human nitric oxide synthases. *J. Med. Chem.* **48,** 4783-4792.

Mishra, O., Ashraf, Q., & Delivoria-Papadopoulos, M. (2009) Tyrosine phosphorylation of neuronal nitric oxide synthase (nNOS) during hypoxia in the cerebral cortex of newborn piglets: The role of nitric oxide. *Neuroscience Letters* **462**, 64-67.

Montgomery H. J., Romanov V. & Guillemette J. G. (2000) Removal of a putative inhibitory element reduces the calcium-dependent calmodulin activation of neuronal nitric-oxide synthase. *J. Biol. Chem.* **275,** 5052-5958.

Muhandiram, D. R., & Kay, L. E. (1994) Gradient-enhanced triple-resonance 3-dimensional NMR experiments with improved sensitivity. *J. Magn. Reson.* **103**, 203-216.

Nahrevanian H., Dascombe M. J. (2003) The role of nitric oxide and its up/downstream molecules in malaria: cytotoxic or preventive? *Southeast Asian J. Trop. Med. Public Health* **34 Suppl 2,** 44-50.

Newman, E., Spratt, D., Mosher, J., Cheyne, B., Montgomery, H., Wilson, D., Weinberg, J., Smith, S., Salerno, J., Ghosh, D., and Guillemette, J. (2004) Differential activation of nitric-oxide synthase isozymes by calmodulin-troponin C chimeras. *Journal of Biological Chemistry*, 33547-33557.

Ng H.L., Greenstein A., Marletta M., Wand A.J., Alber T. (PDB 3GOF) Structural diversity in calmodulin recognition of nitric oxide synthases.

Olwin B. B., Storm D. R. (1985) Calcium binding to complexes of calmodulin and calmodulin binding proteins. *Biochemistry (N. Y.)* **24,** 8081-8086.

O'Neil K. T., DeGrado W. F. (1990) How calmodulin binds its targets: sequence independent recognition of amphiphilic α-helices. *Trends Biochem. Sci.* **15,** 59-64.

Palfi A., Kortvely E., Fekete E., Kovacs B., Varszegi S. & Gulya K. (2002) Differential calmodulin gene expression in the rodent brain. *Life Sci.* **70,** 2829-2855.

Persechini A., Kretsinger R. H. (1988) The central helix of calmodulin functions as a flexible tether. *J. Biol. Chem.* **263,** 12175-12178.

Pettersen, E. F., Goddard, T. D., Huang, C. C., Couch, G. S., Greenblatt, D. M., Meng, E. C., & Ferrin, T. E. (2004) UCSF chimera - A visualization system for exploratory research and analysis. *J. Comput. Chem.* **25**, 1605-1612.

Pierce M. M., Raman C. S. & Nall B. T. (1999) Isothermal titration calorimetry of protein-protein interactions. *Methods: A Companion to Methods in Enzymology* **19,** 213-221.

Quadroni M., James P. & Carafoli E. (1994) Isolation of phosphorylated calmodulin from rat liver and identification of the in vivo phosphorylation sites. *J. Biol. Chem.* **269,** 16116-16122.

Quadroni M., L'Hostis E. L., Corti C., Myagkikh I., Durussel I., Cox J., James P. & Carafoli E. (1998) Phosphorylation of calmodulin alters its potency as an activator of target enzymes. *Biochemistry (N. Y.)* **37,** 6523-6532.

Rhoads A. R., Friedberg F. (1997) Sequence motifs for calmodulin recognition. *FASEB Journal* **11,** 331-340.

Roman L. J., Martásek P. & Masters B. S. S. (2002) Intrinsic and extrinsic modulation of nitric oxide synthase activity. *Chem. Rev.* **102,** 1179-1189.

Salerno J. C., Harris D. E., Irizarry K., Patelf B., Morales A. J., Smith S. M. E., Martasek P., Roman L. J., Masters B. S. S., Jones C. L., Weissman B. A., Lane P., Liu Q. & Gross S. S. (1997) An autoinhibitory control element defines calcium-regulated isoforms of nitric oxide synthase. *J. Biol. Chem.* **272,** 29769-29777.

Schägger, H., and von Jagow, G. (1987) Tricine-sodium dodecyl sulfate-polyacrylamide gel electrophoresis for the separation of proteins in the range from 1 to 100 kDa.. *Anal Biochem* **166**, 368-379.

Shen, Y., Delaglio, F., Cornilescu, G., & Bax, A. (2009) TALOS plus : a hybrid method for predicting protein backbone torsion angles from NMR chemical shifts. *Journal of Biomolecular Nmr* **44**, 213-223.

Shen X., Valencia C. A., Szostak J., Dong B. & Liu R. (2005) Scanning the human proteome for calmodulin-binding proteins. *Proc. Natl. Acad. Sci. U. S. A.* **102,** 5969-5974.

Spratt, D. E. (2008). Calmodulin Binding and Activation of Mammalian Nitric Oxide Synthase. *Chemistry*. (p. 369). Waterloo: University of Waterloo.

Spratt D. E., Duangkham, Y., Taiakina, V., & Guillemette, J. G. (2011) Mapping the binding and CaM-dependent activation of NOS isozymes. *The Open Nitric Oxide J*.

Spratt D. E., Israel O. K., Taiakina V. & Guillemette J. G. (2008) Regulation of mammalian nitric oxide synthases by electrostatic interactions in the linker region of calmodulin. *Biochimica Et Biophysica Acta - Proteins and Proteomics* **1784,** 2065-2070.

Spratt D. E., Newman E., Mosher J., Ghosh D. K., Salerno J. C. & Guillemette J. G. (2006) Binding and activation of nitric oxide synthase isozymes by calmodulin EF hand pairs. *FEBS Journal* **273,** 1759-1771.

Spratt D. E., Taiakina V., Palmer M. & Guillemette J. G. (2007) Differential binding of calmodulin domains to constitutive and inducible nitric oxide synthase enzymes. *Biochemistry (N. Y.)* **46,** 8288-8300.

Strynadka N. C. J., James M. N. G. (1989) Crystal structures of the helix-loop-helix calcium-binding proteins. *Annu. Rev. Biochem.* **58,** 951-998.

Sudhakar Babu Y., Bugg C. E. & Cook W. J. (1988) Structure of calmodulin refined at 2.2 Å resolution. *J. Mol. Biol.* **204,** 191-204.

Venema R., Sayegh H., Kent J., & Harrison D. (1996) Identification, characterization, and comparison of the calmodulin-binding domains of the endothelial and inducible nitric oxide synthases. *Journal of Biological Chemistry* **271**, 6435-6440.

Vetter S. W., Leclerc E. (2003) Novel aspects of calmodulin target recognition and activation. *European Journal of Biochemistry* **270,** 404-414.

Vorherr T., Knopfel L., Hofmann F., Mollner S., Pfeuffer T., & Carafoli E. (1993) The calmodulin binding domain of nitric oxide synthase and adenylyl cyclase. *Biochemistry* **32**, 6081-6088.

Wang W., Malcolm B. (1999) Two-stage PCR protocol allowing introduction of multiple mutations, deletions and insertions using QuikChange (TM) site-directed mutagenesis. *Biotechniques* **26**, 680-682.

Wang, T., Frederick, K., Igumenova, T., Wand, A., & Zuiderweg, E. (2005) Changes in calmodulin main-chain dynamics upon ligand binding revealed by cross-correlated NMR relaxation measurements. *Journal of the American Chemical Society* **127**, 828-829.

Welland A., Daff S. (2010) Conformation-dependent hydride transfer in neuronal nitric oxide synthase reductase domain. *Febs Journal* **277**, 3833-3843.

Wüthrich, K. (1986). NMR of proteins and nucleic acids. Wiley, Toronto, ON.

Wu G., Berka V., & Tsai A. L. (2011) Binding kinetics of calmodulin with target peptides of three nitric oxide synthase isozymes. *Journal of Inorganic Chemistry* **105**, 1226-1237.

Xia C., Misra I., Iyanagi T. & Kim J. -. P. (2009) Regulation of interdomain interactions by calmodulin in inducible nitric-oxide synthase. *J. Biol. Chem.* **284,** 30708-30717.

Xie Q., Nathan C. (1994) The high-output nitric oxide pathway: Role and regulation. *J. Leukoc. Biol.* **56,** 576-582.

Xiong L-W., Kleerekoper Q. K., Wang X., & Putkey J. A. (2010) Intra- and Interdomain Effects due to Mutation of Calcium-Binding Sites in Calmodulin. *J. Biol. Chem.* **285**. 8094-103.

Yamniuk A. P., Ishida H., Lippert D. & Vogel H. J. (2009) Thermodynamic effects of noncoded and coded methionine substitutions in calmodulin. *Biophys. J.* **96,** 1495-1507.

Yamniuk A. P., Vogel H. J. (2004) Calmodulin's flexibility allows for promiscuity in its interactions with target proteins and peptides. *Applied Biochemistry and Biotechnology - Part B Molecular Biotechnology* **27,** 35-57.

Yap K. L., Kim J., Truong K., Sherman M., Yuan T. & Ikura M. (2000) Calmodulin target database. *Journal of Structural and Functional Genomics* **1,** 8-14.

Zhang J., Martàsek P., Paschke R., Shea T., Masters B. S. S. & Kim J. -. P. (2001) Crystal structure of the FAD/NADPH-binding domain of rat neuronal nitric-oxide synthase: Comparisons with NADPH-cytochrome P450 oxidoreductase. *J. Biol. Chem.* **276,** 37506-37513.

Zhang M., Tanaka T. & Ikura M. (1995) Calcium-induced conformational transition revealed by the solution structure of apo calmodulin. *Nat. Struct. Biol.* **2,** 758-767.

Zhang W., Kuncewicz T., Yu Z. -., Zou L., Xu X. & Kone B. C. (2003) Protein-protein interactions involving inducible nitric oxide synthase. *Acta Physiol. Scand.* **179,** 137-142.

Zoche M., Bienert M., Beyermann M., Koch K. W. (1996) Distinct molecular recognition of calmodulin-binding sites in the neuronal and macrophage nitric oxide synthases: a surface plasmon resonance study. *Biochemistry* **35**, 8742-8747.